

Seismic Response of Building Frames Controlled using Semi Active Multiple Tuned Mass Dampers

Alireza Torkaman Rashid

A Thesis

in

The Department

of

Building, Civil & Environmental Engineering

Presented in Partial Fulfilment of the Requirements

For the Degree of Master of Applied Science (Civil Engineering) at

Concordia University

Montréal, Québec, Canada

Octobre 2019

© Alireza Torkaman Rashid, 2019

Concordia University
School of Graduate Studies

This is to certify that the thesis prepared

By: Alireza Torkaman Rashid
Entitled: Seismic Response of Building Frames Controlled using Semi Active
Multiple Tuned Mass Dampers

and submitted in partial fulfillment of the requirements for the degree of

Master of Applied Science (Civil Engineering)

Complies with the regulations of the University and meets the accepted standards with respect to originality and quality.

Signed by the final examining committee:

_____ Chair

Dr. Anjan Bhowmick

_____ Examiner

Dr. Ramin Sedaghati

_____ Examiner

Dr. Emre Erkmen

_____ Thesis Supervisor

Dr. Ashutosh Bagchi

Approved by

Graduate Program Director: Dr. Michelle Nokken

Dr. Amir Asif, Dean, Gina Cody School of Engineering and Computer Science.

Date October 2019

Abstract

Seismic Response of Building Frames Controlled using Semi Active Multiple Tuned Mass Dampers

Alireza Torkaman Rashid

Earthquakes induce lateral forces on buildings that could result in damage and potential for collapse of the structures. Therefore, it is necessary to control and design the structures for resisting the forces due to ground motions. Various energy dissipating systems have been developed and used in the past. The application of the Tuned Mass Damper (TMD) has been proven to be effective in tall buildings for the control of vibrations due to wind or earthquake. In this research, for better performance of buildings, Multiple Tuned Mass Damper (MTMD) distributed in different floors of a building has been used and the seismic performance of the building has been studied. A modal analysis has been conducted and the TMDs were placed in a structure and tuned based on its dominant modes. Furthermore, the influence of the distribution of the mass on different levels of a structure has been studied. It is found the MTMDs are very effective in controlling the vibration of a building and compared to a single TMD placed at the top floor. To further improve the performance of a building frame with MTMDs, multiple Magnetorheological dampers (MR dampers) have been paired with each of the MTMDs to create a semi-active system of Semi-Active Multiple Tuned Mass Damper (SAMTMD). While application of MTMDs were explored by other researchers, the use of SAMTMD is a novel concept introduced in this thesis. The seismic demands of the structure including displacement, velocity, acceleration, and the energy dissipating capacity of the structure have been significantly improved with the SAMTMD system.

Acknowledgment

I would like to take this opportunity to express my immense gratitude to all those persons who have given their invaluable support and assistance.

I would like to express my utmost gratitude to my research supervisor, Dr. Ashutosh Bagchi, for his sincere and selfless support, prompt and useful advice during my research. He gives me a lifetime unforgettable memory of his benevolence, patience, intelligence, diligence, and erudition.

Last, but definitely not the least, I am greatly indebted to my family. It was my parents' and sister's unconditional love, care and tolerance which made the hardship of writing the thesis worthwhile. Without their support, I do not think that I could overcome the difficulties during these years.

Table of Contents

List of Figures	x
List of Tables	xv
Chapter 1: Introduction.....	1
1.1. Background and motivation	1
1.2. Problem Statement	6
1.3. Research Objectives	7
1.4. Organization of thesis.....	7
Chapter 2: Literature review.....	9
2.1. Introduction	9
2.2. Building with common lateral resisting load systems.....	9
2.2.1. Moment resisting Structures	9
2.2.2. Simply Braced Frames	10
2.2.3. Shear wall buildings.....	11
2.3. Building with Passive Energy Dissipating Systems.....	12
2.3.1. Base Isolation Systems	12
2.3.2. Friction Dampers	13
2.3.3. Tuned Mass Damper	14

2.3.4.	Tuned Liquid Damper	16
2.3.5.	Metallic Damper	17
2.3.6.	Viscoelastic Damper	18
2.3.7.	Viscous Fluid Damper	20
2.4.	Building with Semi Active Energy Dissipating Systems.....	22
2.4.1.	Semi Active Viscous Fluid Damper	23
2.4.2.	Semi Active Stiffness Control Device	24
2.4.3.	Semi Active Tuned Mass Damper	25
2.4.4.	MR Damper	25
2.5.	Building with Active Energy Dissipating Systems	25
2.5.1.	Active Tendon System	26
2.5.2.	Active Brace System.....	27
2.5.3.	Active Mass Damper.....	28
2.5.4.	Pulse Generation System	29
2.6.	Summery	30
Chapter 3:	Modeling of Tuned Mass Dampers.....	31
3.1.	Introduction	31
3.2.	Properties of Tuned Mass Damper.....	31
3.3.	Equation of Motion	34

3.3.1.	Assembling of Mass, Stiffness, and Damping Coefficient Matrix	35
3.3.2.	Formulation of the equation of motion	39
3.4.	Summary	40
Chapter 4:	Modeling of MR Damper.....	42
4.1.	Introduction	42
4.2.	Modeling of MR Damper.....	45
4.2.1.	Bingham Model	45
4.2.2.	Extended Bingham Model	46
4.2.3.	Bouc-Wen Model.....	47
4.2.4.	Modified Bouc-Wen Model.....	49
4.3.	Large-Scale MR Damper	50
4.4.	Summary	53
Chapter 5:	Modeling of Semi-Active Multiple Tuned Mass Damper	54
5.1.	Introduction	54
5.2.	State Space Equations	54
5.3.	LQR Control Algorithm.....	56
5.4.	Case Study of a Structure with Multiple Tuned Mass Dampers Integrated with MR Dampers	57
5.5.	Sensitivity Analysis.....	61

5.6.	Analytical Results	73
5.6.1.	Analytical results for the modelled structure exposed to Capemendocino Earthquake:	74
5.6.2.	Analytical results for the modelled structure exposed to Duzce Earthquake:	76
5.6.3.	Analytical results for the modelled structure exposed to Hector Mine Earthquake: 77	
5.6.4.	Analytical results for the modelled structure exposed to Imperial Valley Earthquake:	79
5.6.5.	Analytical results for the modelled structure exposed to Kobe Earthquake:	80
5.6.6.	Analytical results for the modelled structure exposed to Northridge Earthquake: ..	82
5.6.7.	Analytical results for the modelled structure exposed to Chi-Chi Earthquake:	83
5.6.8.	Analytical results for the modelled structure exposed to Kocaeli Earthquake:	85
5.6.9.	Analytical results for the modelled structure exposed to LomaPrieta Earthquake:	86
5.6.10.	Analytical results for the modelled structure exposed to Manjil Earthquake:	88
5.6.11.	Energy Dissipation.....	91
5.7.	Summary	93
Chapter 6:	Summary and Conclusion.....	94
6.1.	Summary	94
6.2.	Conclusions	95

6.3. Scope for Future Work.....	96
Reference	97
Appendix I: Analytical Results of the Structure on Floors of Existing Dampers.....	101
Appendix II: Analytical Results of the Structure on Different Floors	111

List of Figures

Figure 2-1 Typical Bracing configurations in Concentrically Braced Frames. a) Diagonal Bracing b) X Bracing c) Inverted V Bracing d) V Bracing e) Two-story X Bracing (Cheng et al., 2008)..	11
Figure 2-2 Friction Damper-Typical braced bay (Vezina. et al 1992)	14
Figure 2-3 Tuned Mass damper configuration (Cheng et al., 2008).....	15
Figure 2-4 The vibration model of a Tuned Liquid (Malekghasemi et al., 2015)	17
Figure 2-5 The installation of metal yield damper in a V-shape beam and bracing connection (left). Behavior of the metal damper in a V-shape beam and bracing connection (right) (Teruna et al. 2015).	18
Figure 2-6 Typical Viscoelastic Damper (left), and configuration (right). Source: (Castaldo, P. 2014)	19
Figure 2-7 Viscous Fluid damper Installation. Source: https://www.engineering-society.com/2018/03/fluid-viscous-dampers-and-structural.html	21
Figure 2-8 Installation of Fluid Viscous Dampers: (a) diagonal; (b) chevron; (c) toggle; (d) scissor. Source: (Guo, Tong, et al. 2014).....	21
Figure 2-9 Semi Active Viscous Fluid Damper (Cheng et al., 2008).....	23
Figure 2-10 Semi-Active Stiffness Damper (Cheng et al., 2008).....	24
Figure 2-11 The schematic diagram of active tendon (Cheng et al., 2008).....	26
Figure 2-12 Active Bracing System with hydraulic actuator (Cheng et al., 2008).....	28
Figure 2-13 The schematic of active mass damper (Yamamoto & Sone, 2014)	29
Figure 3-1 Schematic of a structure with TMD (Matta & De Stefano, 2009).....	32

Figure 4-1 Mono Tube MR Damper	43
Figure 4-2 Twin Tube MR Damper	44
Figure 4-3 Double Ended MR Damper (Poynor, 2001)	44
Figure 4-4 The Schematic of Bingham Model (R Stanway et al., 1985; RSJL Stanway et al., 1987)	46
Figure 4-5 The Extended Bingham Model (Gamota & Filisko, 1991).....	47
Figure 4-6 The Schematic of Bouc-Wen Model (Spencer Jr et al., 1997).....	48
Figure 4-7 Modified Bouc-Wen Model (Spencer Jr et al., 1997).....	50
Figure 4-8 Schematic of the 20 ton MR Fluid Damper made by LORD company (Yang et al., 2002)	51
Figure 5-1 The 2D Model of The Modelled Structure.....	58
Figure 5-2 First 3 Mode Shapes of the Modelled Structure.....	59
Figure 5-3 The Comparison of the Location of the TMDs.....	60
Figure 5-4 Response of the Structure with and without TMDs	61
Figure 5-5 Sensitivity of the Mass Distribution.....	62
Figure 5-6 Ground Motion Acceleration of Capemendocino Earthquake.....	64
Figure 5-7 Ground Motion Acceleration of Duzce Earthquake.....	64
Figure 5-8 Ground Motion Acceleration of Hector Mine Earthquake	65
Figure 5-9 Ground Motion Acceleration of Imperial Valley Earthquake.....	65
Figure 5-10 Ground Motion Acceleration of Kobe Earthquake	66
Figure 5-11 Ground Motion Acceleration of Northridge Earthquake	66
Figure 5-12 Ground Motion Acceleration of Chi-Chi Earthquake.....	67

Figure 5-13 Ground Motion Acceleration of Kocaeli Earthquake	67
Figure 5-14 Ground Motion Acceleration of Loma Prieta Earthquake	68
Figure 5-15 Ground Motion Acceleration of Manjil Earthquake	68
Figure 5-16 Unscaled and Scaled Spectrum	69
Figure 5-17 The Placement of the Dampers in the Modelled Structure	69
Figure 5-18 The Schematic Block Diagram of the Modelled System Including the Structure and Dampers	70
Figure 5-19 The details of the Block Diagram of the Modelled System in Simulink Software...	71
Figure 5-20 The Schematic Block Diagram of the Modelled System Including the Structure and Dampers in Simulink Software	72
Figure 5-21 The Applied Electricity Current and Adaptive Resistance Force of the MR Damper for Capemendocino Earthquake.....	74
Figure 5-22 Response of the 15th floor under the Capmendocino Excitation.....	75
Figure 5-23 The Applied Electricity Current and Adaptive Resistance Force of the MR Damper for Duzce Earthquake	76
Figure 5-24 Response of the 15th floor under the Duzce Excitation.....	76
Figure 5-25 The Applied Electricity Current and Adaptive Resistance Force of the MR Damper for Hector Mine Earthquake	77
Figure 5-26 Response of the 15th floor under the Hector Mine Excitation.....	78
Figure 5-27 The Applied Electricity Current and Adaptive Resistance Force of the MR Damper for Imperial Valley Earthquake	79
Figure 5-28 Response of the 15th floor under the Imperial Valley Excitation.....	79

Figure 5-29 The Applied Electricity Current and Adaptive Resistance Force of the MR Damper for Kobe Earthquake	80
Figure 5-30 Response of the 15th floor under the Kobe Excitation	81
Figure 5-31 The Applied Electricity Current and Adaptive Resistance Force of the MR Damper for Northridge Earthquake	82
Figure 5-32-Response of the 15th floor under the Northridge Excitation	82
Figure 5-33 The Applied Electricity Current and Adaptive Resistance Force of the MR Damper for Chi-Chi Earthquake.....	83
Figure 5-34 Response of the 15th floor under the Chi-Chi Excitation.....	84
Figure 5-35 The Applied Electricity Current and Adaptive Resistance Force of the MR Damper for Kocaeli Earthquake	85
Figure 5-36- Response of the 15th floor under the Kocaeli Excitation	85
Figure 5-37 The Applied Electricity Current and Adaptive Resistance Force of the MR Damper for Loma Prieta Earthquake	86
Figure 5-38 Response of the 15th floor under the Loma Prieta Excitation	87
Figure 5-39 The Applied Electricity Current and Adaptive Resistance Force of the MR Damper for Manjil Earthquake.....	88
Figure 5-40- Response of the 15th floor under the Manjil Excitation.....	88
Figure 5-41 Displacement of the Structure.....	89
Figure 5-42 Mean Displacement of the Structure of the 10 Earthquake Records	90
Figure 5-43 Standard Deviation of the Displacement of the Structure of the 10 Earthquake Records	91

Figure 5-44 The Seismic Energy of the Structure in the Top Floor	92
Figure 6-1 -Response of the 10th floor under the Capmendocino Excitation	101
Figure 6-2- Response of the 10th floor under the Duzce Excitation	101
Figure 6-3- Response of the 10th floor under the Hector Mine Excitation	102
Figure 6-4- Response of the 10th floor under the Imperial Valley Excitation	102
Figure 6-5- Response of the 10th floor under the Kobe Excitation	103
Figure 6-6- Response of the 10th floor under the Northridge Excitation	103
Figure 6-7- Response of the 10th floor under the Chi-Chi Excitation.....	104
Figure 6-8- Response of the 10th floor under the Kocaeli Excitation	104
Figure 6-9- Response of the 10th floor under the Loma Prieta Excitation.....	105
Figure 6-10- Response of the 10th floor under the Manjil Excitation	105
Figure 6-11- Response of the 5th floor under the Capmendocino Excitation	106
Figure 6-12- Response of the 5th floor under the Duzce Excitation	106
Figure 6-13- Response of the 5th floor under the Hector Mine Excitation	107
Figure 6-14- Response of the 5th floor under the Imperial Valley Excitation	107
Figure 6-15- Response of the 5th floor under the Kobe Excitation	108
Figure 6-16- Response of the 5th floor under the Northridge Excitation	108
Figure 6-17- Response of the 5th floor under the Chi-Chi Excitation.....	109
Figure 6-18- Response of the 5th floor under the Kocaeli Excitation	109
Figure 6-19- Response of the 5th floor under the Loma Prieta Excitation.....	110
Figure 6-20- Response of the 5th floor under the Manjil Excitation	110

List of Tables

Table 4-1 The Details of the properties of MDR-9000 MR damper (Yang et al., 2002)	52
Table 5-1 Frequencies and Periods of the Structure	60
Table 5-2 Earthquake Records.....	63
Table 5-3- The Stroke Length of TMDs	75
Table 5-4- The Stroke Length of TMDs.....	77
Table 5-5- The Stroke Length of TMDs	78
Table 5-6- The Stroke Length of TMDs	80
Table 5-7- The Stroke Length of TMDs	81
Table 5-8- The Stroke Length of TMDs	83
Table 5-9- The Stroke Length of TMDs.....	84
Table 5-10- The Stroke Length of TMDs	86
Table 5-11- The Stroke Length of TMDs.....	87
Table 5-12- The Stroke Length of TMDs.....	89
Table 5-13 Mean and Standard Deviation of the Base Shear of the Structure	91
Table 6-1-Maximum Displacement of Structure under the Capmendocino Earthquake.....	111
Table 6-2- Maximum Displacement of Structure under the Duzce Earthquake.....	112
Table 6-3- Maximum Displacement of Structure under the Hector Mine Earthquake.....	112
Table 6-4- Maximum Displacement of Structure under the Imperial Valley Earthquake.....	113
Table 6-5- Maximum Displacement of Structure under the Kobe Earthquake	113
Table 6-6- Maximum Displacement of Structure under the Northridge Earthquake	114
Table 6-7- Maximum Displacement of Structure under the Chi-Chi Earthquake	114

Table 6-8- Maximum Displacement of Structure under the Kocaeli Earthquake	115
Table 6-9- Maximum Displacement of Structure under the Loma Prieta Earthquake	115
Table 6-10- Maximum Displacement of Structure under the Manjil Earthquake	116
Table 6-11- Maximum Velocity of Structure under the Capemendocino Earthquake	117
Table 6-12- Maximum Velocity of Structure under the Duzce Earthquake	117
Table 6-13- Maximum Velocity of Structure under the Hector Mine Earthquake.....	118
Table 6-14- Maximum Velocity of Structure under the Imperial Valley Earthquake	118
Table 6-15- Maximum Velocity of Structure under the Kobe Earthquake	119
Table 6-16- Maximum Velocity of Structure under the Northridge Earthquake.....	119
Table 6-17- Maximum Velocity of Structure under the Chi-Chi Earthquake	120
Table 6-18- Maximum Velocity of Structure under the Kocaeli Earthquake.....	120
Table 6-19- Maximum Velocity of Structure under the Loma Prieta Earthquake	121
Table 6-20- Maximum Velocity of Structure under the Manjil Earthquake	121
Table 6-21- Maximum Acceleration of Structure under the Capemendocino Earthquake	122
Table 6-22- Maximum Acceleration of Structure under the Duzce Earthquake	123
Table 6-23- Maximum Acceleration of Structure under the Hector Mine Earthquake	123
Table 6-24- Maximum Acceleration of Structure under the Imperial Valley Earthquake	124
Table 6-25- Maximum Acceleration of Structure under the Kobe Earthquake.....	124
Table 6-26- Maximum Acceleration of Structure under the Northridge Earthquake.....	125
Table 6-27- Maximum Acceleration of Structure under the Chi-Chi Earthquake.....	125
Table 6-28- Maximum Acceleration of Structure under the Kocaeli Earthquake	126
Table 6-29- Maximum Acceleration of Structure under the Loma Prieta Earthquake.....	126

Table 6-30- Maximum Acceleration of Structure under the Manjil Earthquake..... 127

Chapter 1: Introduction

1.1. Background and motivation

Earthquake-induced force has been one of the most important considerations in the design of structure during recent decades. Most earthquakes occur when the two segments of the earth's crust move in relation to one another or collide. The surfaces that move against one another is called fault. While the fault starts moving, the earth will release energy in form of strain and causes seismic wave to propagate. The waves emitting from the fault make the ground to shake violently. The main concern of a structural engineer is how to control these movements and to design the structure to resist the ground motions. Inadequate consideration of earthquake effects in the design of a structure can cause catastrophic damage and loss of life. For example, in January 1994 an earthquake with the magnitude of 6.7 in the San Fernando Valley region of Los Angeles, California, USA occurred (Langenheim et al., 2011). The duration of the earthquake was approximately 10 to 20 seconds. The estimated death toll is 57, with more than 8,700 injured. The costs of the damage to the properties is estimated to be about \$13 to \$50 billion. Another example, the Great Hanshin Earthquake or Kobe Earthquake happened on January 1995 with the magnitude of 6.9 (Toda et al., 1998). The victims of this earthquake have been estimated as 4,571 dead, 2 persons missing, and 14,678 injured. This earthquake caused the complete collapse of 67,421 and partial collapse of 55,145 structures. Another Earthquake occurred in Northern California on October 1989 with the magnitude of 6.9 (Nolen-Hoeksema & Morrow, 1991). The Loma Prieta Earthquake caused the death of 63 people and 3,757 injured. The damage to the properties was

estimated to be about \$6 billion. The Tohoku Earthquake and Tsunami occurred on the March 2011 with the magnitude of 9.1 (Duputel et al., 2012). This earthquake caused the death of 15,896, 6,157 injured, and 2,537 missing people. The earthquake triggered a tsunami with the height of 40.5 meters. The damage was estimated to be about \$14.5 to \$34.6 billion. The Southern Peru Earthquake occurred on June 2001 (Duputel et al., 2012). The magnitude of the earthquake was recorded as 8.4. The death toll recorded was at least 74 people. 2,687 people were injured due to the earthquake and 17,510 properties were destroyed and 35,549 homes were damaged. On March of 1964 an earthquake with the magnitude of 9.2 happened in south central Alaska (Kanamori & Anderson, 1975). This earthquake is known as the Good Friday Earthquake or Great Alaska Earthquake. The estimation of the life lost due to the earthquake are believed to be 139 people. On May 1960 the most powerful earthquake was recorded in Chile (Kanamori & Anderson, 1975). This earthquake is known as The Great Chilean Earthquake or Valdivia Earthquake. The earthquake killed about 1,700 people. The estimated damage to the properties was about 550\$ million. Another earthquake happened on December 2003 in Bam, Kerman, Iran (Doocy et al., 2013). The recorded magnitude for this earthquake was 6.6 and caused the death of 26,271, and injuring about 30,000 people. More than 85% of the building were damaged, with 70% of the homes completely destroyed. An earthquake with the magnitude of 7.4 occurred in the northern of Iran on June 1990 (Berberian et al., 1992). The death toll recorded for this earthquake was more than 40,000 people, and it has cause the destruction of 700 villages. This earthquake left approximately 500,000 people homeless.

Earthquake is a natural phenomenon that cannot be predicted and anticipated. In order to prevent the damages caused by earthquakes, civil engineers have studied many ways to make the design

of the structure robust and resistant to earthquakes. During recent years, they have discovered many methods to mitigate the vibration of the structure due to ground motions. Some of the methods have been implemented in the design of the structure to make them more resilient to lateral forces applied. Furthermore, many types of devices have been developed to dissipate the energy of the applied earthquake to the structure.

The traditional methods for the seismic design of structures has been mainly based on the combination of the strength and ductility of the structure. The main idea in this method is that the structure would remain in its elastic range and it would not reach the yield stress of the material under minor earthquakes. However, when the structure is subjected to a major earthquake, it would dissipate the energy through inelastic deformation and damage. In this case, the structural design depends on the ductility of the structure. This method has been adopted to contemporary seismic design codes consisting of equivalent static lateral force method and inelastic design response spectrum (Constantinou et al., 1998).

Meanwhile, considering the nature and behavior of the dynamic loads more sophisticated devices have been developed to improve the response of the structure due to seismic activities. The following approaches have been developed to dissipate the energy in a structure subjected to dynamic forces, which include Passive Energy Dissipation, Semi-Active Energy Dissipation, and Active Energy Dissipation. The Passive Energy Dissipation systems are the most common types of methods used for mitigation the vibration of the structure. In this method, the dissipating system reacts to the vibration of the structure, and based on that, it applies a passive force to control the deformation in the structure. The design of such systems is simple, cost-effective, and efficient. However, the drawbacks of this system consist of not adapting to the varying dynamic forces in a

structure. Friction Dampers is an example of the Passive System. Another benefit of this system is that there is no need for an external power source to control the structure. Hence, a passive system is considered more reliable and stable as compared to an active system.

During recent years, more sophisticated methods has been developed for the seismic design of the structure called semi-active, and active system. Active system consists of sensors and actuators that are installed on the structure. During seismic activities on the structure these sensors record the magnitude of the vibration. Then, the system would calculate an appropriate counter force for the disturbances. Subsequently, these forces will be applied on the structure using the actuators. The advantage of this system is that the applied force on the structure during a vibration is adjusted specifically for the disturbance. Hence, it would mitigate the vibration more efficiently and have a better performance. However, since providing the energy for the actuators require an external source and a large power supply, this would not be a very dependable system especially considering the power outages during an earthquake. Furthermore, if the control system is not perfectly designed, the applied force might result in instability in the structure.

Meanwhile, the concept of semi-active system is to change the characteristics of system vibration to match the seismic response of the structure. There are many devices that have been developed based on this system such as variable stiffness devices, controllable fluid dampers, friction control devices, fluid viscous damper. Unlike the active system, semi-active system functions with a small power source and since the semi-active system does not produce external force, hence, the structure would be stable. In another word, the semi-active controllers have the reliability of the passive dampers, while maintaining the versatility of the active dampers.

The utilization of a mass for mitigating of the structure's vibration have been used for many years. The system that would use a mass with a stiffness for the reduction of ground motion effects on the structure is called Tuned Mass Damper (TMD). This system consists of a mass with a damping and stiffness. Many studies have been conducted for designing the optimum characteristics of a mass damper (K. Xu & Igusa, 1992). Primarily, structure with a tuned mass damper located at the top floor have been studied. They have been designed in such a way that could have the best response due to the fundamental vibration mode of the structure. Meanwhile, many optimization methods have been used for determining the efficient parameters of TMD (Singh et al., 2002). The effects of Multiple Tuned Mass Dampers (MTMD) for a one degree of freedom structure have been studied in (K. Xu & Igusa, 1992). It has been determined that a structure with MTMD tuned to distributed frequencies has better response than a single TMD at the top of the structure. Furthermore, the modelling and design of single active and semi-active Tuned Mass Dampers have been studied by a number of researchers (Esteki et al., 2011; Han & Li, 2006; Li & Zhu, 2007; P. Lin et al., 2005). It has been proven that the utilization of a semi-active TMD would be more beneficial in the aspect of saving energy and the resilience of the structure.

In order to change the damping system of Tuned Mass Dampers from passive to semi-active mitigating system, either the movement of the mass or the stiffness of the TMD should be controlled. These types of systems are called semi-active TMD or Hybrid TMD. One of the method to control the applied force from the movement of the mass to the structure is the utilization of Magneto-Rheological (MR) dampers.

A semi-active MR damper consists of two parts, the magnetorheological fluid and an electromagnet to generate the magnetic field. There are some magnetic particles in the carrier oil

of the magnetorheological fluid. While these particles are subjected to the magnetic field they would cause a change in the viscosity of the magnetorheological fluid resulting in a change in the damper force. Subsequently, with the change of the current applied to the damper the force of the damper would change.

The utilization of semi-active TMD controlled with MR dampers would have the reliability of the passive dampers while having the versatility and adaptability of the active dampers with optimized amount of use of exterior power supplies.

1.2. Problem Statement

In this research the response of buildings integrated with Multiple Semi-Active Tuned Mass Damper has been analyzed. The utilization of one huge mass on the top of a building would occupy a lot of space. The distribution of this mass on different levels of the structure would decrease the space usage and distribute this occupied space on different floors. Meanwhile, it could also result in to a better response of the structure due to lateral excitations. The purpose of this thesis is to analyze the optimal locations of the Tuned Mass dampers. Furthermore, a method to model and tune the TMDs would be defined.

There is an importance for prediction of the response of the structure installed with MTMD that are controlled with the use of MR dampers. The study of the MR damper so far is limited to the experiments that have been done in small scales, and the numerical models that have been provided

is limited to one or two MR dampers in the structure. In previous studies such as (Bathaei et al., 2018; Esteki et al., 2011) the combination of TMD and MR damper is utilized to provide the structure with an adaptive energy dissipation system. In this research multiple tuned mass dampers are integrated with multiple controllable MR dampers in order to provide better response of the structure due to the distribution of mass dampers in the building. Moreover, by utilizing multiple tuned mass dampers the structure is sturdy to different frequencies of different modes. Furthermore by combining the TMDs with controllable MR dampers further stability would be provided.

1.3. Research Objectives

The current research has the following objectives:

- Study of the response of structure instrumented with multiple distributed tuned mass dampers.
- Study effect of the location of TMDs and the distribution of the mass of the dampers on the response of the structure.
- Study of the effectiveness of multiple tuned mass dampers controlled with magnetorheological dampers.

1.4. Organization of thesis

This thesis consists of six chapters. In chapter one the motivation, objectives, and the organization of the thesis is explained. Chapter two explains the different types of dissipating

systems that are designed and used in structures. Chapter three covers the modelling of tuned mass dampers and the method of the tuning of multiple TMD. Chapter four contains the explanation of the numerical modelling of MR dampers and semi-active tuned mass dampers. Chapter five presents the response of a structure with MSATMD and a comparison between the results. Chapter six gives a summary of the thesis and the acquired results and the potential future works.

Chapter 2: Literature review

2.1. Introduction

The literature review performed in this chapter aimed to present the core of supplementary damping systems used in structures and their physical response to the structure's movement. The types of supplementary damping systems which could be used in structures are divided to three category based on the dissipation of the energy as follows: passive, semi active, and active energy dissipation systems. This chapter provide a holistic information about each particular damping system and the application of them. The common lateral load resisting systems which used in buildings is presented then, the mechanism of supplementary damping systems and modeling techniques are discussed respectively.

2.2. Building with common lateral resisting load systems

2.2.1. Moment resisting Structures

Moment Resisting Frames carry lateral loads occurred due to any external forces such as earthquake or wind. Steel moment resisting frames contain columns and beams which are mostly connected by bolting or welding. The main purpose of using reinforced concrete (RC) frames is to transfer moment by beam-column joints. The objective for the design of a building's lateral resistance system would be to provide adequate flexural and shear capacity in both columns and beams. It is also important to ensure adequate ductility in the literal load resisting system

depending on the levels of ductility desired. Furthermore, the formation of plastic hinge in beams should be considered in the connection's design of the moment-resistance frames. The required energy for dissipation mechanism provided by the beam's plastic hinge. In the ductile design of the moment-resistance frames, the formation of the plastic hinge in the beams and columns is governed by the *Capacity Design* principle where beams at a joint should tie before the columns. The structural stability due to non-adherence of capacity design can jeopardize the safety and trigger collapse. Although, there is an exception for columns located at bottom of the ground floor. Also, plastic hinge leads to damage and destroy of the connections.

2.2.2. Simply Braced Frames

Concentrically Braced Frames (CBFs) are a class of structures resisting lateral loads. Providing high strength and stiffness due to wind and earthquake loads in steel frame buildings would be other purpose of using these frames. One of the advantages of the correctly designed brace is providing plastic deformations and dissipate hysteretic energy in a supported way with the help of sequential buckling in compression and yielding in tension.

The most important part in designing area would be to ensure that plastic deformation only occur in braces, leaving the columns, beams, and connection elastic. It is possible to design braces as a member for only tension or both tension and compression. One of the differences in tension-compression braces is the size of the hysteresis loop. Basically, a majority of the vibration energy can be dissipated due to larger hysteresis loop in these braces. The arrangement of braces vary and

adaptable but, their installation between beams and columns is most common among them. The figure below illustrate different installation of braces between beam and column (**Figure 2-1**).

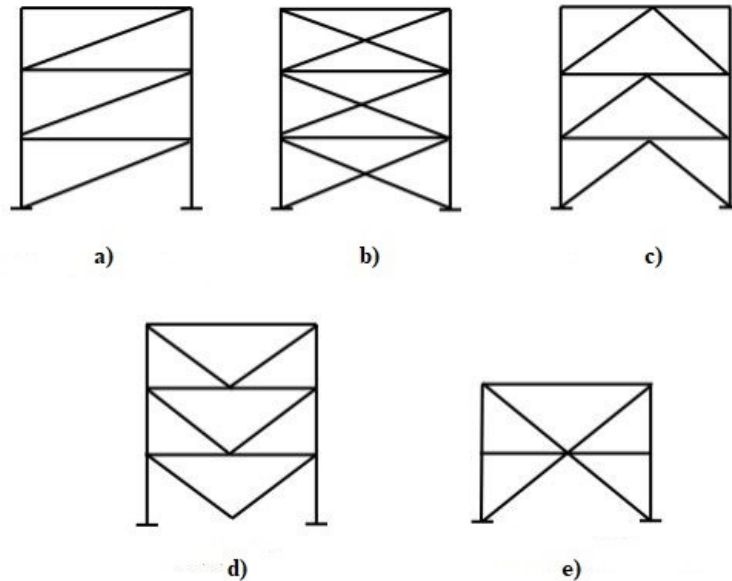


Figure 2-1 Typical Bracing configurations in Concentrically Braced Frames. a) Diagonal Bracing b) X Bracing c) Inverted V Bracing d) V Bracing e) Two-story X Bracing (Cheng et al., 2008)

2.2.3. Shear wall buildings

Shear wall is a vertical panel which is used in building structures in order to resist lateral loads. Basically, these elements transfer lateral loads from upper floors to lower floor and then to building foundations. There are two types of shear walls based on their materials; concrete and steel. These elements have much higher lateral stiffness in comparison to other structural elements. Hence, the lateral forces caused by wind or seismic loads can be absorb by shear walls. In medium to high rise concrete structures, shear walls mostly considered as a primary resistance system. The level

of concrete walls ductility directly affects the amount of energy which can be dissipated by shear walls.

2.3. Building with Passive Energy Dissipating Systems

The building with passive energy dissipating systems have external add-on damping devices. These devices are used in order to dissipate the vibration energy of the buildings, and no external power sources are necessary for their operation. In other words, the buildings with passive energy dissipating systems suppress the reaction of the structure to vibration and reduce deformation. For instance, different dissipation devices such as Base Isolation Systems, Friction Dampers, Tuned Mass Damper, Tuned Liquid Damper, Metallic Damper, Viscoelastic Damper, and Viscous Fluid Damper are introduced briefly below.

2.3.1. Base Isolation Systems

Base isolation or seismic base isolation is one of the common yet powerful tools in passive structural vibration control techniques which is used to protect structures against seismic loads. This device is installed between the foundation and the base of the buildings. By using a base isolation system, the base of the building becomes flexible, which increases the first period of the structure in comparison to the corresponding fixed-base building. Basically, the larger time periods of the building causes lower seismic forces in a building. Furthermore, the nonlinear behavior of

base isolation device and by considering the hysteresis loop, using this device helps to dissipate a majority of induced energy.

Base isolation is an effective device in order to protect structures since it is altering the fundamental period of a structure. It is clear that low and mid-rise structures have high frequencies hence, such devices would be efficient to control the vibration of buildings from seismic events. Base isolation systems are divided to friction bearing system and elastomeric bearing system which are introduced briefly below.

2.3.2. Friction Dampers

Friction dampers are one of the most efficient devices for dissipating seismic energy. This type of dampers is dependent on friction developed between two sliding solid faces hence, the structural vibration dissipates when two solid interfaces start to sliding. In other words, when the parts slide over each other, they create friction which uses some of the energy from the earthquake that goes into the building. Basically, during a severe earthquake a friction damper with a predefined slip load starts to slide, and dissipates the seismic energy by friction. The hysteresis loop is of large rectangular shape in friction dampers which give them the capacity to dissipate large amount of energy.

These types of dampers have some particular features. For example, the design of them avoid slippage due to wind force. Also, the performance of them is completely dependent on velocity and temperature. Energy dissipated during sliding increases the temperature of the damper. Furthermore, the friction dampers are inexpensive but still reliable, and there is no need for regular

maintenance and repair. The figure below illustrate the friction damper installation and corresponding details (**Figure 2-2**).

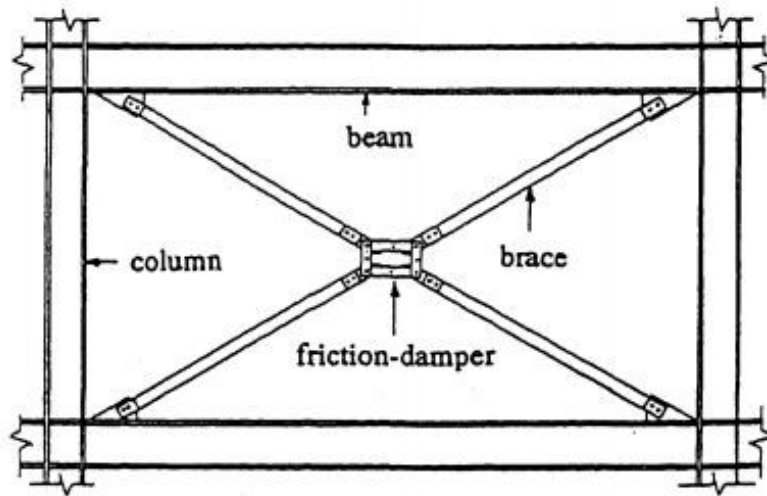


Figure 2-2 Friction Damper-Typical braced bay (Vezina. et al 1992)

2.3.3. Tuned Mass Damper

Tuned mass damper (TMD) is a device which installed in a specific location of the structures to reduce the amplitude of vibration from lateral forces such as earthquake and wind. TMD consist of spring, mass, and damper (**Figure 3**). Due to the reduction of a structure's dynamic response they are mostly connected to the main structure. These type of dampers are also called harmonic absorbers, and they are generally divided in to Horizontal TMD's and Vertical TMD's. The horizontal TMD is applied in slender buildings and towers, on the other hand the vertical is found in the walkways and bridges.

Basically, the frequency of TMDs is tuned to the fundamental frequency of the structure. When the lateral forces hit a building, the structure is excited at the frequency close to its fundamental frequency then, TMD acts as a damper to dissipate the vibration energy and controls the effect of any resonance. In other words, TMD acts as a counteragent in a vibrating structure. As a result, the building will stop oscillating within a shorter time frame and will stabilize faster. It should be considered that, one of the effects of using TMDs would be to increase the overall damping ratio of a structure.

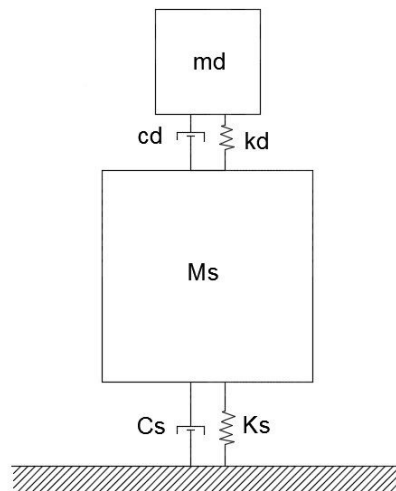


Figure 2-3 Tuned Mass damper configuration (Cheng et al., 2008)

The vertical TMDs which mostly used in buildings are divided into different types such as pendulums, dashpots, and viscoelastic. In the pendulums types, the sets of spring and bearing shape (or gravity load) can produced the restoring force. On the other hand, the damping force is generated by dashpot and viscoelastic material such as rubber. One of the advantages of using these dampers would be their response to small level of excitation. Also they are not dependent on

the external power source for their operation. On the other hand, as it mentioned earlier that the frequency of the TMDs are tuned to first natural frequency, hence this device would work well as first mode is usually the dominant one. Furthermore a large mass or a large space is needed for their installation. In order to increase the control efficiency of tuned mass dampers to different frequencies the utilization of multiple dampers have been introduced(C.-C. Lin et al., 2017). Several researches have been conducted in order to determine the parameters of the TMD (stiffness, mass, and damping coefficient of the dampers). They have calculated these parameters with different optimization methods such as artificial ant colony (Bozer & Özsarııldız, 2018), genetic algorithm (Z.-D. Xu et al., 2019).

2.3.4. Tuned Liquid Damper

The origin of the tuned liquid dampers comes from tuned mass damper. Tuned liquid damper is water confined in a tank which is used to reduce the vibrations of the structures. The sloshing energy of the water leads to reduction of the dynamic response of the structure due to excitation (**Figure 4**). Because of the friction between water and container and also the turbulence of flow, the dynamic energy of water is converted to heat, and the vibration energy of the structures is dissipated. Fundamental mode frequency of liquid sloshing is tuned to the natural frequency of the structure, and the damping ratio of the sloshing mode is set to an optimal value.

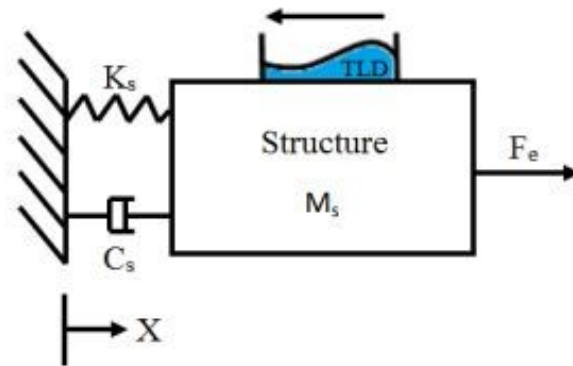


Figure 2-4 The vibration model of a Tuned Liquid (Malekghasemi et al., 2015)

The attractiveness of TLDs lies in their low cost, low maintenance requirements, and simple design compared to other vibration dampers. Moreover, TLDs can be used as water tanks for building, either to be used for regular water supply or for fire fighting emergencies. However, unlike TMDs, the response of a TLD is in general highly nonlinear and naturally complex due to the liquid sloshing motion.

2.3.5. Metallic Damper

This type of dampers are passive energy dissipation devices which are mainly made from steel. The concept of the using these dampers is based on plastic deformation behavior of the steel. Basically, the main functional part of these dampers made from metal or alloy metal. Hence, the inelastic deformation of metal would be effective mechanism in order to dissipating the earthquake energy. The metallic dampers yield and dissipate the seismic energy easily when, structure suffered by seismic events. Furthermore, because of the high elastic stiffness of metal (steel), they can

prevent the primary structural damage sufficiently due to seismic events. Hence, the structural response can be simply reduced when subjected to lateral forces. The advantages of these dampers would be their effectiveness and low cost. The installation of the typical metal damper in a chevron is illustrated below (Figure 5).

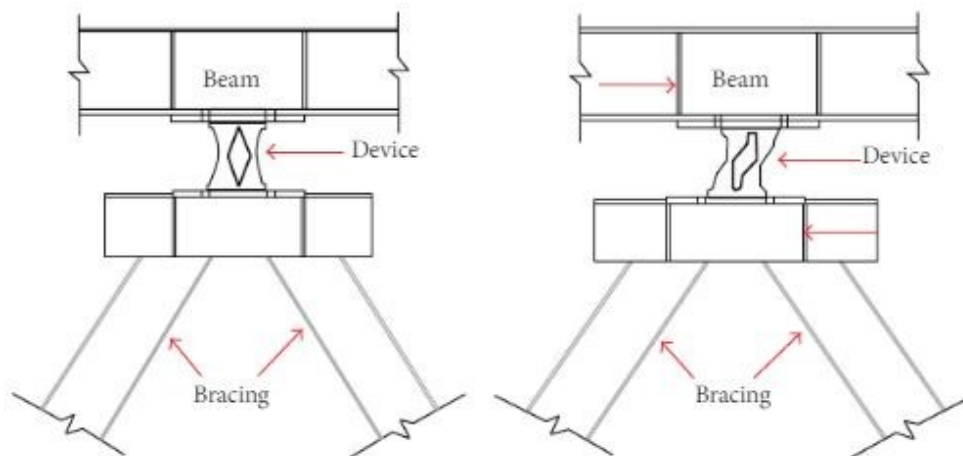


Figure 2-5 The installation of metal yield damper in a V-shape beam and bracing connection (left).

Behavior of the metal damper in a V-shape beam and bracing connection (right) (Teruna et al. 2015).

2.3.6. Viscoelastic Damper

One of the earliest type of passive dampers are viscoelastic dampers which are installed in many of tall building in order to reduction vibration and the acceleration occurring due to lateral forces such as wind and earthquake forces. The portion of mechanical energy converted to heat by viscoelastic dampers. These dampers also known for providing restoring forces. The viscoelastic

materials have both viscous and elastic behavior simultaneously. The elastic material stores all the energy during the loading, then recover when the loads removed. On the other hand, the viscous material returns the stored energy of loading phase with a delay. These type of dampers are influenced by several parameters such as, temperature, frequency, dynamic strain rate, and some other time also irreversible effects. Typical VE dampers are consist of a VE material which simply bounded in a steel plate (**Figure 2-6**). Hence, the steel part of VE dampers attached to the structure by a bracing. The installation of the viscoelastic dampers is shown in figure below:

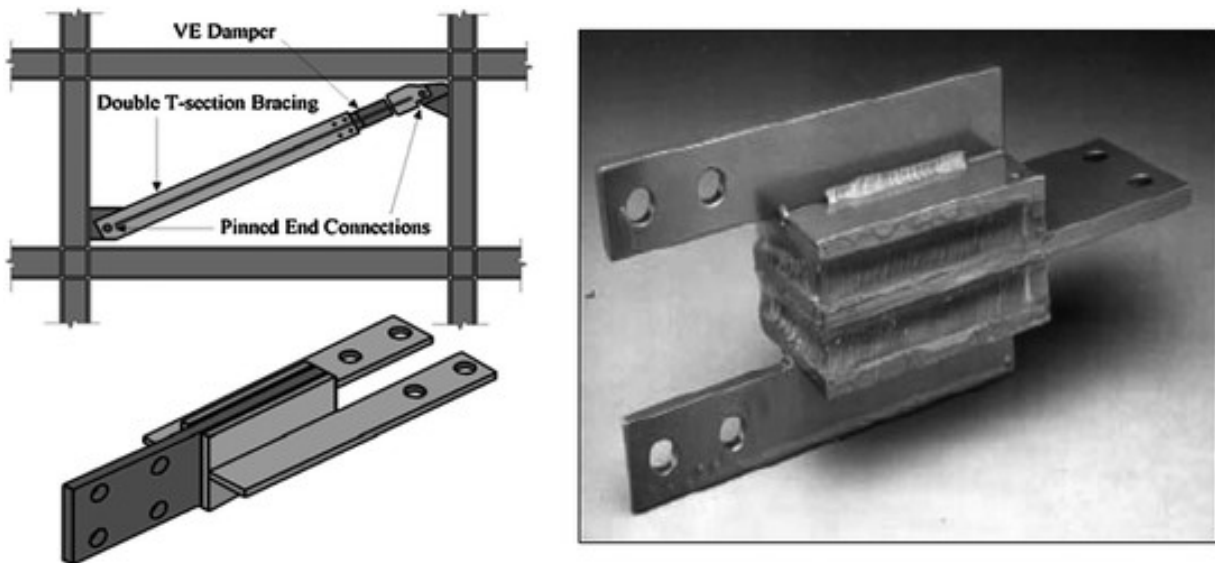


Figure 2-6 Typical Viscoelastic Damper (left), and configuration (right). Source: (Castaldo, P. 2014)

The modeling of the VE dampers is simple due to their linear behavior. Viscos-elastic devices basically have both damper and spring behavior simultaneously thus, the spring behavior controls the response of viscoelastic damper under a high level of seismic vibration. One of the advantages of these dampers would be not affiliated to any power external sources for providing energy.

2.3.7. Viscous Fluid Damper

Fluid Viscous dampers are hydraulic devices which are used to dissipate the kinetic energy of the seismic events. These devices are designed to control damping of structures in order to protect them against lateral loads, thermal motions, and seismic events. FV dampers consist of an oil cylinder and a piston which this piston can move reciprocating in the cylinder. The cylinder is full of fluid damping medium subsequently, when piston moves it pushes fluid through the piston's head. The velocity of the medium fluid is very high in this region. Hence, the pressure of the upstream converts to kinetic energy. By expanding the fluid in one side of piston, the movement of the piston become slow and loses its kinetic energy into turbulence. The pressure exist in the downstream side is very less in comparison with the upstream side of piston head pressure. The difference occurred between two side pressure leads to produce a large force which helps to resist the motion of the damper. The installed VF dampers **Figure 2-7** and their configuration is shown in figure below (**Figure 2-8**).



Figure 2-7 Viscous Fluid damper Installation. Source: <https://www.engineering-society.com/2018/03/fluid-viscous-dampers-and-structural.html>

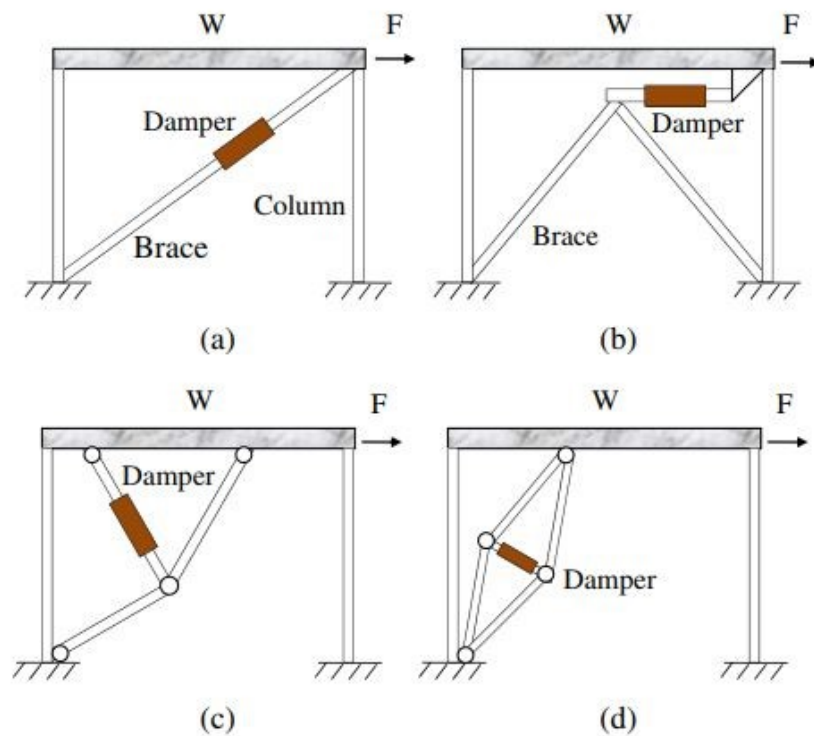


Figure 2-8 Installation of Fluid Viscous Dampers: (a) diagonal; (b) chevron; (c) toggle; (d) scissor.

Source: (Guo, Tong, et al. 2014)

This type of dampers have some advantages. For instance, they are easy to model, easy installation, no need to maintenance, and very high capacity. Although, the biggest advantage of them would be their reliability.

2.4. Building with Semi Active Energy Dissipating Systems

In semi active energy dissipation systems the mechanical properties of the damper change by using a type of energy (S. Casciati & Chen, 2012). This system mostly requires a small external power source such as battery for operation (Symans & Constantinou, 1999). In this system, the control forces are developed by utilizing the motion of the structure and then the magnitude of forces can be adjust by external power source. In the semi active energy dissipation systems, the sensors measure the excitation and/or the response of the structure. Hence, control forces are developed based on the feedback which comes from sensors. Then, the controller monitors the feedback measurements and generate suitable command signal in order to resist lateral loads. One of the advantages of the semi active systems would be guarantying the stability of the structure due to not adding any mechanical energy to the structure systems. The typical semi active devices are discussed in the following:

2.4.1. Semi Active Viscous Fluid Damper

This damper consists of a cylinder with a piston, and a valve. The force of the damper is induced with the change of the valve opening. When the valve is largely open, the fluid could flow easily inside the cylinder, thus the damping force would be low. However, when the valve opening is smaller the flow would pressurize and apply a force in the piston, hence the damping force would be more. The functionality of the opening of the valve is controlled with a control system command in order to better the response of the system (Cheng et al., 2008; Symans & Constantinou, 1997).

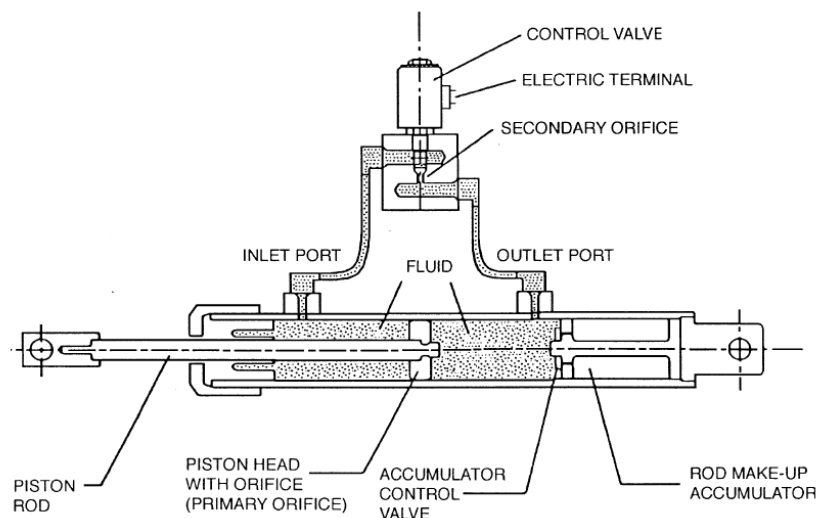


Figure 2-9 Semi Active Viscous Fluid Damper (Cheng et al., 2008)

2.4.2. Semi Active Stiffness Control Device

This system controls the stiffness of the building in order to change the frequency of the structure according to the ground motion applied to the system. The damper primarily controls the stiffness of the building to prevent resonant happen in the structure. The device consists of a hydraulic cylinder and a solenoid control valve inside it. The valve is either open or close in order to control the flow of the fluid in the tube for application of the damper force. When the valve is closed the device is out of the structure system and the beams of the structure would carry the forces applied to the building. In contrast, while the valve is open the beams are out of the system of the structure and the device would change the stiffness of the structure (Symans & Constantinou, 1999).

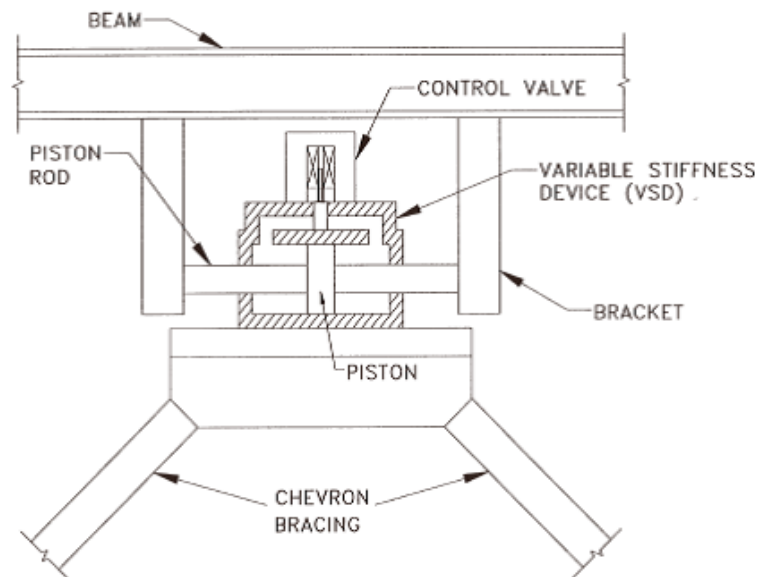


Figure 2-10 Semi-Active Stiffness Damper (Cheng et al., 2008)

2.4.3. Semi Active Tuned Mass Damper

A tuned mass damper essentially consists of a mass, stiffness, and a dashpot. The study of a semi-active tuned mass damper has been done in which the dynamic characteristics of the structure is controlled. This systems consists of a TMD with an actuator to control the stiffness of the tuned mass damper (Hrovat et al., 1983).

2.4.4. MR Damper

Magnetorheological damper (MR) are devices that are made of a cylinder containing the MR fluid. In case of application of a magnetic field this fluid would change its viscosity hence producing a force for applying to the system. By controlling the current and magnetic field applied to the device the damping force induced from the MR damper would be controlled.

2.5. Building with Active Energy Dissipating Systems

In active control system, an external forces are applied to the structure by means of controllable actuators. This systems are used in order to control the structure's response against any internal and external forces such as wind, earthquake and machinery. In these systems, sensors measure the structure responses then, the required counteracting forces for damping is evaluated by pre-defined control strategy. In other words, such systems consist of sensors which are located

in the structure in order to measure external excitations, structural vibrations, or both. The purpose of some devices are to process the measured information to compute the control forces and then control the actuators to produce the required forces to be applied to the system. Since such systems adapt themselves to different environment changes they need large external sources of power and also expensive and complex hardware. Furthermore, the forces generated from these systems is completely active hence, this energy may sometime lead to destabilize the structure. The most common active energy dissipation systems are discussed below.

2.5.1. Active Tendon System

Active Tendon System, consist of pre-stressed cables, activators, and a control device (Nigdeli & Boduroglu, 2010). The active tendon system is installed between two stores of the building. The schematic diagram of active tendon system is shown in figure below (**Figure 2-11**).

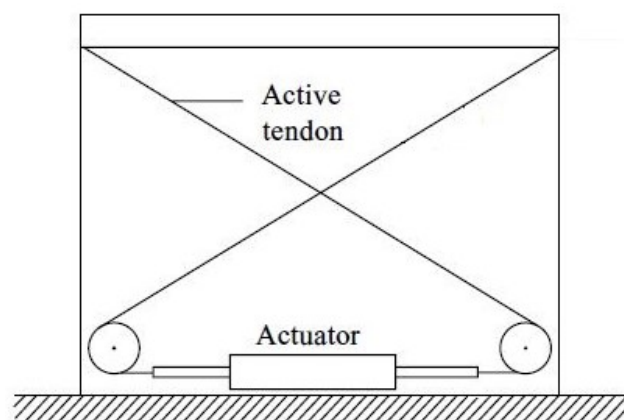


Figure 2-11 The schematic diagram of active tendon (Cheng et al., 2008)

One of the tendon's end connects to the actuator and the other end is connected to the upper floor. As it is clear in the figure that the actuator device is connected to the lower floor. In disturbance situation, the inter-story drift is produced by structural vibration which affect the tension in prestressed tendons. Here, the actuators adjust the stressed in the tendons by pulling or releasing tendons.

2.5.2. Active Brace System

Active bracing system is one of the active control devices which is used in structures in order to protect structures against seismic loads. The system consists of an actuator which is installed in the bracing between two floors, a sensor, hydraulic power supply, and control computer (Lu, 2001) (**Figure 2-12**). Basically, this system uses the existing bracing of the structure to develop an active control system by adding the actuators (Reinhorn et al., 1992). As shown in figure below (Fig.2.12), the actuator is attached to the floor consequently, the piston of the active actuator is attached to the brace. The control system here determines the direction and magnitude of the actuator's force to minimize the vibration.

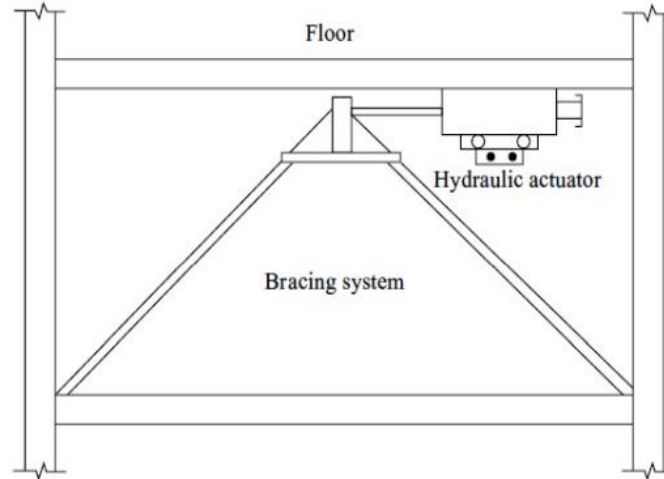


Figure 2-12 Active Bracing System with hydraulic actuator (Cheng et al., 2008)

In the system, sensor measure the motion of the structure due to excitation events. The control force is generated to resist the seismic loads finally.

2.5.3. Active Mass Damper

The typical active mass damper consist of different parts such as, sensor, controller, and actuator. Sensor is responsible to measure the response of the controlled structure and release the data associated with the response. Then, this data processed by the controller in order to determine the control output signal. Furthermore, the actuators receives these signals and consequently generate the force to be applied to protect the structure against seismic events (S. Casciati & Chen, 2012). The schematic of the AMD is shown in figure below (Fig. 2.13). The actuator is attached between the structure and the auxiliary mass, so the actuator can control the movement of the mass to increase the effectiveness of the control system.

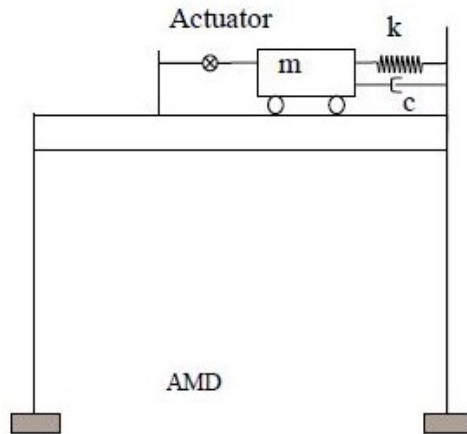


Figure 2-13 The schematic of active mass damper (Yamamoto & Sone, 2014)

Basically, the added active force from active mass damper system can improve the tuned mass damper's performance (Fu & Johnson, 2009). As it was mentioned earlier the passive TMD would be effective for the structural vibration when the first mode is dominant. But AMD has the functionality to adapt itself to different frequencies. Hence, it could be concluded that AMD is very effective in order to damp seismic loads with wide range of frequency such as earthquake.

2.5.4. Pulse Generation System

In the pulse generation systems, a pulse generator is used instead of any actuators. In this system, pulse generators use pneumatic mechanism to generate active forces (Miller et al., 1988). One of the differences of this type of systems in comparison to the hydraulic actuators would be the procedure of the generating active force. For instance, this system utilizes compressed air to generate a pulse actuation force but, as it was mentioned earlier the difference in fluid pressure is

used in hydraulic actuators. In general, the structure equipped with several pulse generators become more adaptive. Hence, each of these pulse generators can provide pneumatic force in the opposite direction of entered velocity which is detected in each of this equated pulse pneumatic locations actuators. One of the advantage of pulse generation would be cheaper cost in comparison to the hydraulic systems. In this systems, sensor measure the motion of the structure due to the excitations events. In the same procedure, the controller processes the measurements and the released data from sensors also generate the required control signal. The servo valve used this signals to regulate the flow direction and intensity, which yields a pressure difference between two actuators chambers. Thus, the control force is generated because of the pressure difference in order to resist seismic loads.

2.6. Summery

In this chapter the different systems that have been used for the mitigation of the lateral energy applied to the structures have been explained. Based on the informations provided the new systems such as semi-active dissipation systems are still under the investigations of the researches. Hence, the purpose of this thesis is to provide a new hybrid system and to evaluate the performance of the Multiple Semi-Active Tuned Mass Dampers.

Chapter 3: Modeling of Tuned Mass Dampers

3.1. Introduction

This chapter discusses the design and modeling of Tuned Mass Dampers in a structure. Furthermore, the method for tuning the dampers in a structure would be explained. Many types of dampers have been used for the dissipation of energy in mechanical systems. Tuned Mass damper is one the widely used systems that have been utilized in tall buildings for reduction of vibration of the system due to lateral forces. Basically, a tuned mass damper consists of a mass attached to the structure or building, that vibrates with the same frequency of the structure but with a time lag or phase shift. This mass is usually connected to the structure with a spring and a dashpot. The energy of the vibrations would be dissipated when the force is applied to mass through the spring-dashpot. In order to design a tuned mass damper in a structure it is needed to determine the location of the damper in the structure and the properties of the damper.

3.2. Properties of Tuned Mass Damper

As it was mentioned earlier the TMD consist of a mass that is connected to the structure with a spring-dashpot (Figure 3-1). Consequently, for the design of a TMD, the following properties are needed to be include: mass of the damper, stiffness of the structure, and damping ratio. These properties are supposed to be selected such that the TMD vibrates with the same frequency of the structure with only a phase shift. Based on different studies, the best mass chosen for the TMD in a structure is between 1 to 5 percent of the mass of the whole structure (Matta & De Stefano, 2009).

Additionally, the stiffness and damping ratio of the dampers are supposed to be calculated in a way that the frequency of the dampers should be the same as the principal frequencies of the structure.

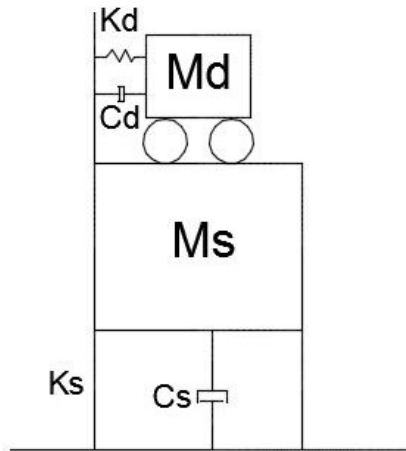


Figure 3-1 Schematic of a structure with TMD (Matta & De Stefano, 2009)

The equation of motion for a single TMD subjected to dynamic excitation is as follows (Pisal & Jangid, 2016):

$$m\ddot{x} + c\dot{x} + kx + k_d(x - x_d) = -m\ddot{x}_g(t) \quad (3-1)$$

$$m_d\ddot{x}_d + c_d(\dot{x} - \dot{x}_d) + k_d(x - x_d) = -m_d\ddot{x}_g(t) \quad (3-2)$$

The equation above can be rewritten in the following matrix form:

$$M\ddot{X}(t) + C\dot{X}(t) + KX(t) = E\ddot{x}_g(t) \quad (3-3)$$

$$X(t) = \begin{cases} x(t) \\ x_d(t) \end{cases} \quad (3-4)$$

$$M = \begin{bmatrix} M & 0 \\ 0 & m_d \end{bmatrix} \quad (3-5)$$

$$C = \begin{bmatrix} c + c_d & -c_d \\ -c_d & c_d \end{bmatrix} \quad (3-6)$$

$$K = \begin{bmatrix} k + k_d & -k_d \\ -k_d & k_d \end{bmatrix} \quad (3-7)$$

The following formulations could be used for the calculations of the stiffness and damping coefficient of the tuned mass damper (Berberian et al., 1992; McNamara, 1977):

$$\mu = \frac{m_d}{M_s}, \quad \omega_s^2 = \frac{K_s}{M_s}, \quad \omega_d^2 = \frac{k_d}{m_d} \quad (3-8)$$

$$\frac{\omega_d^2}{\omega_s^2} = \frac{2 + \mu}{2(1 + \mu)^2} \quad (3-9)$$

Where m_d, k_d are the mass and stiffness of the damper respectively, and M_s, K_s are the mass and stiffness of the structure, μ is the ratio of the mass of the damper to the mass of the structure. Based on equation above and the frequency of the structure, the frequency of the damper could be acquired. Since the ratio of the mass damper to the structure is 2 percent, the frequency of the damper is almost similar to the frequency of the structure. From equation above the stiffness of the damper could be calculated.

In order to calculate the damping coefficient of the damper the following equations would be used. The equation below is used for determination of the optimal non-dimensional damping coefficient for random excitation (Wang et al., 2019; Warburton, 1982):

$$\gamma = \sqrt{\frac{\mu(4 + 3\mu)}{8(1 + \mu)(2 + \mu)}} \quad (3-10)$$

With the calculation of γ the damping coefficient of the Tuned Mass Damper could be acquired using the equation below:

$$c_d = 2\gamma\omega_d m_d \quad (3-11)$$

In order to determine the location of TMD distributed in the structure, in this research modal analysis has been conducted. The dampers have been placed on levels of structure where the principal modes have the most effect on that level. Thus, the properties of the damper placed on the specific story has been tuned to the respected mode of the structure.

3.3. Equation of Motion

The equation of motion for an n-degree of freedom structure that has elastic materials with linear behavior with an applied ground motion is as follows:

$$\tilde{M}\ddot{X}(t) + \tilde{C}\dot{X}(t) + \tilde{K}X(t) = \tilde{F}(t) \quad (3-12)$$

Where \tilde{M} , \tilde{C} , and \tilde{K} are respectively the matrix of mass, damping coefficient, and stiffness of the system. And \ddot{X} , \dot{X} , and X are the matrix of acceleration, velocity, and displacement of the system. Finally, \tilde{F} is the matrix of applied excitation force applied to the system.

In the following the construction of the matrices above would be explained:

3.3.1. Assembling of Mass, Stiffness, and Damping Coefficient Matrix

As it was mentioned, the mass of the dampers is supposed to be about 1 to 5 percent of the mass of the whole structure. The matrix of the mass should include the assembly of both the mass of the structure of different levels and the mass of the dampers of different floors. The matrix of the mass could be described as follows:

$$\tilde{M} = \begin{bmatrix} M_{n \times n} & 0 \\ 0 & m_{n \times n} \end{bmatrix} \quad (3-13)$$

Where M is the matrix of the mass of the structure and m is the matrix of the dampers, and n is the number of stories in the structure. The mass matrices of the structure and dampers is as follow:

$$M = \text{diag}(M_1, M_2, M_3, \dots, M_n) \quad (3-14)$$

$$m = \text{diag}(m_1, m_2, m_3, \dots, m_n) \quad (3-15)$$

In the above equations the M_i describes the mass of the i^{th} floor and m_i describes the mass of the damper located on the i^{th} level.

The matrix of the stiffness of the whole system could be described as bellow:

$$\tilde{K} = \begin{bmatrix} K + k & k \\ k^T & k \end{bmatrix} \quad (3-16)$$

In the above equation K , and k are respectively the matrix of the stiffness of the structure and the stiffness of the TMDs. In the following the construction of the stiffness matrix is displayed (Lewandowski & Grzymisławska, 2009).

$$K = \begin{bmatrix} K_1 + K_2 & -K_2 & 0 & 0 \\ -K_2 & K_2 + K_3 & -K_3 & 0 \\ 0 & -K_3 & \dots & -K_n \\ 0 & 0 & -K_n & K_n \end{bmatrix} \quad (3-17)$$

$$k = \text{diag}(k_1, k_2, k_3, \dots, k_n) \quad (3-18)$$

The form of the damping coefficient matrix is displayed in similar way:

$$\tilde{C} = \begin{bmatrix} C + c & c \\ c^T & c \end{bmatrix} \quad (3-19)$$

Where, C is the matrix of the damping coefficient of the structure and c is the matrix of damping coefficient of dampers.

$$C = \begin{bmatrix} C_1 + C_2 & -C_2 & 0 & 0 \\ -C_2 & C_2 + C_3 & -C_3 & 0 \\ 0 & -C_3 & \dots & -C_n \\ 0 & 0 & -C_n & C_n \end{bmatrix} \quad (3-20)$$

$$c = \text{diag}(c_1, c_2, c_3, \dots, c_n) \quad (3-21)$$

The Rayleigh method is used to determine the damping coefficient of the main structure.

$$C = \alpha M + \beta K \quad (3-22)$$

Where, α and β are the mass proportional damping and stiffness proportional damping respectively. Assuming that the key frequencies of the structure are ω_i and ω_j , and the critical damping ratio of the structure is ξ , the α and β coefficient could be determined as follows:

$$\alpha = \frac{2\xi}{\omega_i + \omega_j} \quad (3-23)$$

$$\beta = \frac{2\omega_i\omega_j\xi}{\omega_i + \omega_j} \quad (3-24)$$

In order to obtain these coefficients, the eigenvalue and eigenvector of an undamped free vibration systems is required to be calculated. The equation of motion for an undamped free vibration system is as below:

$$M\ddot{x} + Kx = 0 \quad (3-25)$$

By solving the equation above the eigenvalue problem could be acquired:

$$K\Phi = M\Phi\Omega^2 \quad (3-26)$$

The matrices Φ and Ω are called modal matrix and spectral matrix respectively, which are displayed as follow:

$$\Phi = \begin{bmatrix} \phi_{11} & \cdots & \phi_{1n} \\ \vdots & \ddots & \vdots \\ \phi_{n1} & \cdots & \phi_{nn} \end{bmatrix} \quad (3-27)$$

$$\Omega^2 = \begin{bmatrix} \omega_1^2 & \cdots & 0 \\ \vdots & \ddots & \vdots \\ 0 & \cdots & \omega_n^2 \end{bmatrix} \quad (3-28)$$

It is known that:

$$\Phi^T M \Phi = I \quad (3-29)$$

$$\Phi^T K \Phi = \Omega^2 \quad (3-30)$$

Where, I is the unit diagonal matrix. By assuming the equation of motion in a damped system:

$$M\ddot{X} + C\dot{X} + KX = F \quad (3-31)$$

Using $X = \Phi q$ where q the modal coordinate matrix, the equation above is could be rewritten as:

$$I\ddot{q} + \Phi^T C \Phi \dot{q} + \Omega^2 q = \Phi^T F \quad (3-32)$$

Since the square matrices associated with the first and third term of the above equation are diagonal, the second term square matrix is expressed as:

$$\Phi^T C \Phi = 2\Omega\xi \quad (3-33)$$

Where the modal damping ratio matrix is explained as:

$$\xi = \begin{bmatrix} \xi_1 & \cdots & 0 \\ \vdots & \ddots & \vdots \\ 0 & \cdots & \xi_n \end{bmatrix} \quad (3-34)$$

By knowing the modal damping ratios and undamped natural frequency the matrix of damping coefficients is calculated using the following equation:

$$C = 2\Phi^{-T}\Omega\xi\Phi^{-1} \quad (3-35)$$

3.3.2. Formulation of the equation of motion

During an earthquake a lateral force would be applied to the structure that would induce vibration in the building. These vibration would result in the displacement of the structure. Assuming a single degree of freedom system and that the displacement of the ground is u_g , and the relative displacement of the lumped mass is u , the total displacement of the lumped mass would be:

$$u'(t) = u(t) + u_g(t) \quad (3-36)$$

In order to calculate the equation of motion of a structure subjected to an earthquake the concept of dynamic equilibrium could be used.

$$f_I + f_d + f_s = 0 \quad (3-37)$$

Where f_I is the force induced from inertia that could be expressed as:

$$f_I = m\ddot{u}'(t) = m(\ddot{u}_g(t) + \ddot{u}(t))$$

f_d is damping resisting force and f_s is the elastic resisting force as follows:

$$f_d = c\dot{u}(t)$$

$$f_s = ku(t)$$

Where c , and k are respectively the damping coefficient and lateral stiffness of the structure. By substituting the forces into the equation of motion could be represented as:

$$m\ddot{u}(t) + c\dot{u}(t) + ku(t) = -m\ddot{u}_g(t) \quad (3-38)$$

The equation above could be assembled into matrices for multi-degree of freedom system as follows:

$$M\ddot{U} + C\dot{U} + KU = -M\ddot{U}_g \quad (3-39)$$

Where M , C , and K are the matrices of mass, damping coefficient and stiffness of the system, and U , \dot{U} , and \ddot{U} are the matrices of the displacement, velocity and acceleration of the system respectively (Iqbal, 2009).

3.4. Summary

In this chapter the method of design, tuning and placement of the tuned mass dampers was explained. Furthermore, the formulation and calculation of multiple degree of freedom system was represented. It has been demonstrated the method for derivation of the equation of motion and the

matrices of the system. Finally, the assembling of the combined matrices of mass, stiffness, and damping coefficient of the system with multiple tuned mass damper has been demonstrated.

Chapter 4: Modeling of MR Damper

4.1.Introduction

MR dampers are type of a semi-active dampers that works with magneto-rheological fluids. The combination of MR dampers and tuned mass dampers would create a robust semi-active system that could control the vibration of the structure due to lateral force. The mechanism of the MR damper is dependent on the viscosity of the MR fluid and the current that is applied to it. While the damper is subjected to a force a current would create a magnetic field that would adjust the viscosity of the fluid to resist the applied force. The main assembly components of MR dampers consist of a cylinder and a control valve. The cylinder is filled with MR fluid and the piston is moved to apply the force on the fluid.

There are three main types of MR Fluid dampers: Mono tube, Twin tube, and double-ended MR dampers. Figure 4-1 displays the properties of a Mono Tube damper (Zhu et al., 2012). The mono tube MR damper is mainly a single-rod structure, which has only one reservoir chamber for the MR fluids. The mono tube has an accumulator with a compressed gas, which usually contains Nitrogen, which has the responsibility of accommodating the changes in the volume of the MR fluid. Furthermore, the gas in the accumulator would act as a spring when the force is generated by the damper and would maintain the first position of the piston when no force is applied.

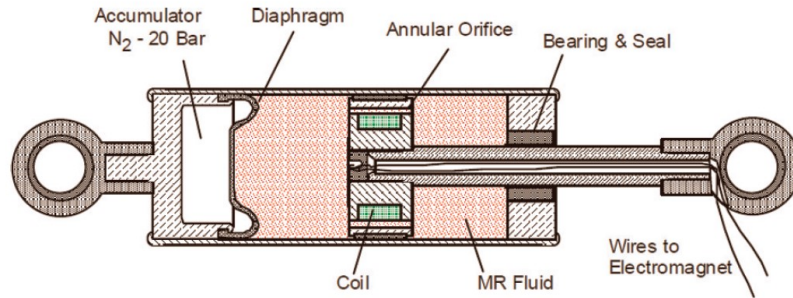


Figure 4-1 Mono Tube MR Damper

Figure 4-2 shows the properties of a Twin Tube MR Damper (Poynor, 2001). The twin tube consists of an inner housing and an outer housing. The functionality of the inner housing is similar to the reservoir of a mono tube. It is filled with MR fluid that has the responsibility to guide the piston inside the cylinder. Meanwhile, the outer housing has the same mechanism of the accumulator in a mono tube. The purpose of the outer housing is to accommodate the volume changes due to the piston movements. The other purposes of outer housing would be the protection of the internal parts of damper, and to transfer the heat induced by the movement of the piston and the volume change of the fluid to the surrounding. Additionally, a valve assembly that is called foot valve is attached to the bottom of the inner reservoir in order to regulate the flow between the inner and outer housings.

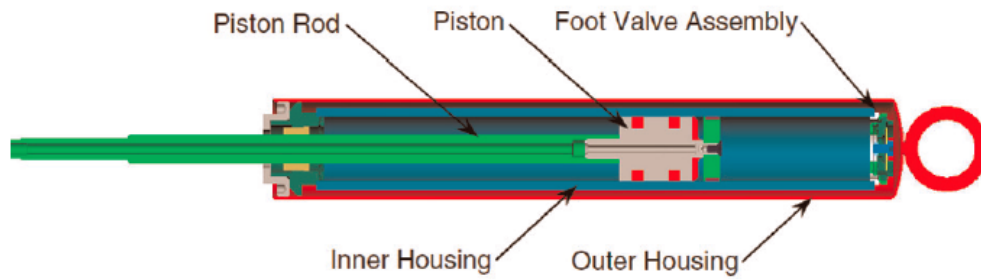


Figure 4-2 Twin Tube MR Damper

Figure 4-3 displays the properties of a double ended MR damper (Poynor, 2001). The double ended MR dampers consists of two rods with the same properties and same diameter at both ends of the piston. Since there is no volume change in the fluid there is no reason for the accumulator to compensate the change in volume. The double ended MR dampers have been used in impact and shock loading, gun recoil applications, and seismic protection in structures.

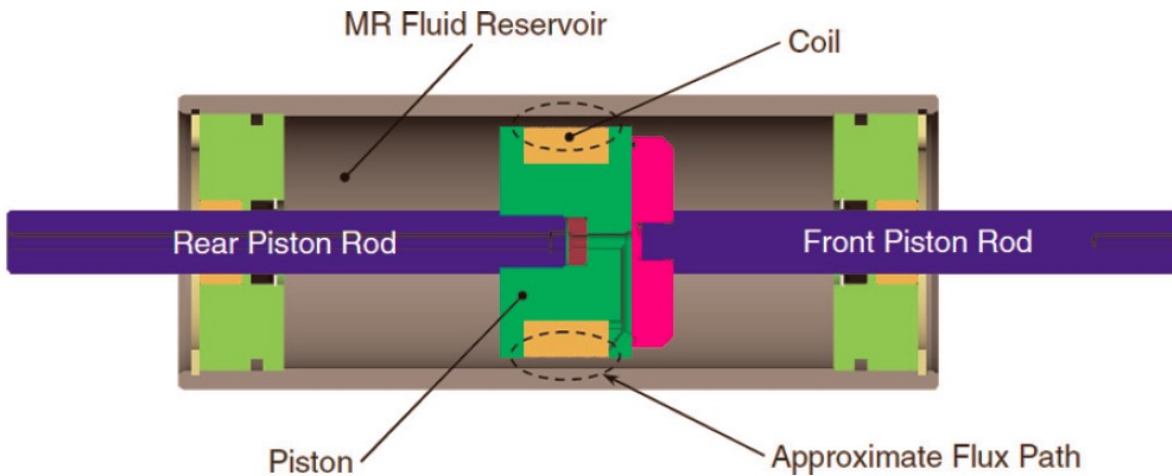


Figure 4-3 Double Ended MR Damper (Poynor, 2001)

4.2. Modeling of MR Damper

There are multiple methods that have been developed during recent years based on some experimental results. The prediction of the behavior of the MR damper is an important aspect that needs to be heeded for the design of damper. Here four method of modeling the MR damper would be discussed.

4.2.1. Bingham Model

In order to develop a model for the description of the behavior of the MR fluids, the stress-strain behavior of Bingham viscoelastic model could be utilized (Shames, 1997). The ratio of the measured shear stress versus shear strain rate is used for the definition of the plastic viscosity. Thus, for the positive values of the shear rate, $\dot{\gamma}$, the total stress is expressed as (F. Casciati et al., 2006; Spencer Jr et al., 1997):

$$\tau = \tau_{y(field)} \text{sgn}(\dot{\gamma}) + \eta \dot{\gamma} \quad (4-1)$$

Where $\tau_{y(field)}$ the shear stress is induced by the magnetic field, and η is the viscosity of fluid. Based on this model for prediction of the behavior of MR fluids, a new method has been developed for the prediction of the behavior of MR/ER dampers (R Stanway et al., 1985; RSJL Stanway et al., 1987). The parameters for the Bingham model includes a Coulomb friction element that is placed in parallel to the viscous damper. The force generated by the MR damper for the non-zero values of velocity \dot{x} is expressed as:

$$F = f_c \operatorname{sgn}(\dot{x}) + c_0 \dot{x} + f_0 \quad (4-2)$$

Where c_0 , and f_c respectively are the damping coefficient, and frictional force that are related to the yield stress of the MR fluid. f_0 is the observed force of the accumulator that would apply for the accommodation of the change in the volume of the fluid damper (F. Casciati et al., 2006; Sapiński & Filuś, 2003).

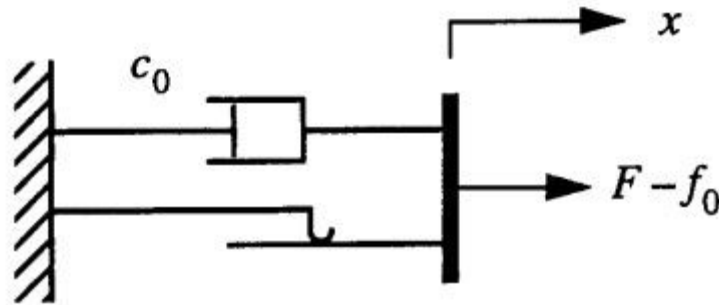


Figure 4-4 The Schematic of Bingham Model (R Stanway et al., 1985; RSJL Stanway et al., 1987)

4.2.2. Extended Bingham Model

It has been demonstrated that the Bingham model has reliable results for the force-displacement behavior of the damper (Spencer Jr et al., 1997). However, the results of the force-velocity especially when the velocity has non-linear values, contradict with the results of the experimental data. Thus, an extension has been developed for the Bingham model to predict the behavior of MR/ER dampers (Gamota & Filisko, 1991). This model in addition to converting the Bingham model in series, it has introduced a term for the standard model of linear solid (Shames,

1997). The following equation is used for the description of the extended Bingham model (Spencer Jr et al., 1997):

$$\left. \begin{aligned} F &= k_1(x_2 - x_1) + c_1(\dot{x}_2 - \dot{x}_1) + f_0 \\ &= c_0\dot{x}_1 + f_c \operatorname{sgn}(\dot{x}_1) + f_0 \\ &= k_2(x_3 - x_2) + f_0 \end{aligned} \right\} |F| > f_c \quad (4-3)$$

$$\left. \begin{aligned} F &= k_1(x_2 - x_1) + c_1\dot{x}_2 + f_0 \\ &= k_2(x_3 - x_2) + f_0 \end{aligned} \right\} |F| \leq f_c \quad (4-4)$$

(4-5)

Where c_0 is the damping coefficient of the Bingham model and $k_1, k_2,$ and c_1 are related to the standard linear model (F. Casciati et al., 2006).

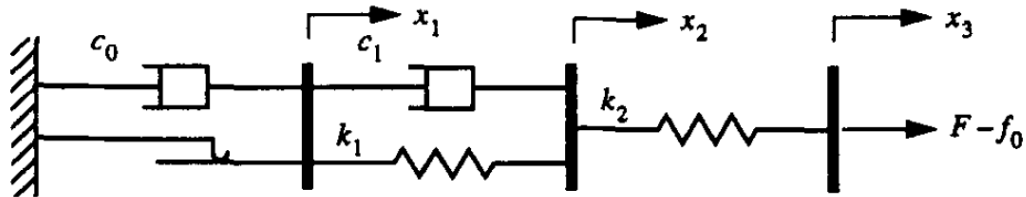


Figure 4-5 The Extended Bingham Model (Gamota & Filisko, 1991)

4.2.3. Bouc-Wen Model

The extension of the Bingham model has solved the shortcoming of unreliable results for the force-velocity behavior of the damper. However, the calculations of the equation of the extended Bingham model are time consuming and costly. Hence, another model called Bouc-Wen

model has been developed in order to have efficiency in the numerical calculations (Wen, 1976).

The equation for the calculation in this model is expressed as (Spencer Jr et al., 1997):

$$F = c_0 \dot{x} + k_0(x - x_0) + \alpha z \quad (4-6)$$

In the equation above z is the evolutionary variable that could be derived from the following equation:

$$\dot{z} = -\gamma |\dot{x}| z |z|^{n-1} - \beta \dot{x} |z|^n + A \dot{x} \quad (4-7)$$

The parameter γ, β, A should be adjusted to maintain the linearity of the pre and post yield region.

Furthermore, the force induced from the accumulator could be taken into account from the x_0 and k_0 that are available in the equations.

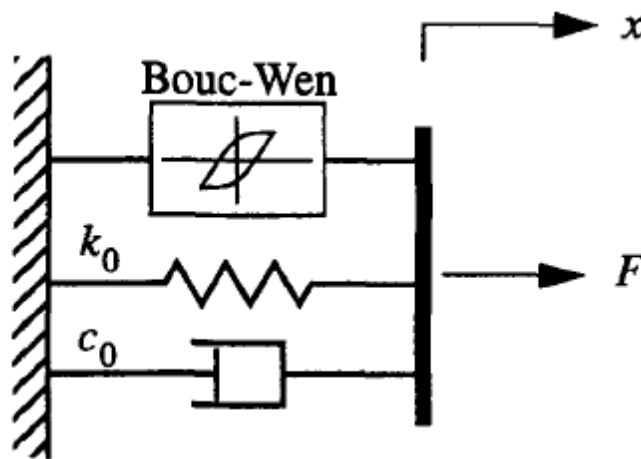


Figure 4-6 The Schematic of Bouc-Wen Model (Spencer Jr et al., 1997)

4.2.4. Modified Bouc-Wen Model

Similar to the Bingham model, the Bouc-Wen model has the shortcoming of unreliability in the prediction of the non-linearity in force-velocity of the MR damper. Another model that is called the modified Bouc-Wen was developed by Spencer (Spencer Jr et al., 1997). Figure 4-7 demonstrates the schematic of this model. Based on the Newton's third law the forces on both sides of the solid in the upper section of the model should be equal, therefore:

$$c_1\dot{y} = \alpha z + k_0(x - y) + c_0(\dot{x} - \dot{y}) \quad (4-8)$$

Where the evolutionary variable z could be expressed as:

$$\dot{z} = -\gamma|\dot{x} - \dot{y}|z|z|^{(n-1)} - \beta(\dot{x} - \dot{y})|z|^n + A(\dot{x} - \dot{y}) \quad (4-9)$$

By solving the equations above it would result into:

$$\dot{y} = \frac{1}{(c_0 + c_1)} [\alpha z + c_0\dot{x} + k_0(x - y)] \quad (4-10)$$

Furthermore, in order to calculate the force of the MR damper, all of the available forces in the system should be summed up.

$$F = \alpha z + c_0(\dot{x} - \dot{y}) + k_0(x - y) + k_1(x - x_0) \quad (4-11)$$

By considering 4-7 in the equation above results in:

$$F = c_1\dot{y} + k_1(x - x_0) \quad (4-12)$$

In these equation k_1 displays the stiffness of the accumulator, c_0 defines the viscos damping at large velocities, c_1 is a dashpot that represents the roll-off at low velocities, k_0 is a parameter to control the stiffness at large velocities, and x_0 is the initial displacement of the spring associated with k_1 the accumulator.

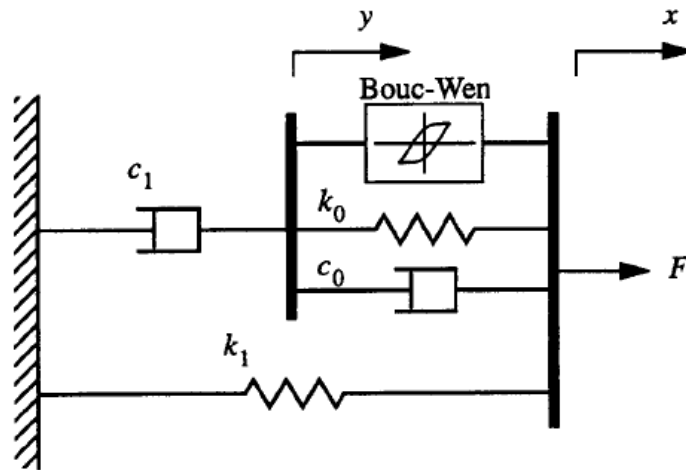


Figure 4-7 Modified Bouc-Wen Model (Spencer Jr et al., 1997)

4.3. Large-Scale MR Damper

The value of the damping force is related to the area of the activation region. Activation region is the area of MR fluid that the viscosity would change due to the created magnetic field. By utilizing larger area for the activation region, the value of the MR damper for could be increased. However, in the single-stage MR dampers the increasing of the activation region would not have significant effect on the damper's force, since the force of the damper is sensitive to the fluid gap in the activation region. Hence, the multi-stage MR dampers have been developed in order to

increase the area of the activation points that are established by the additional coils with similar cross-sectional geometry (Poynor, 2001). Since in the civil engineering a huge value of damping force is required, a 20 ton multi-stage piston MR damper has been developed. There is about 1.5 km of copper wire that is wired in three different sections of the piston, producing four valve region for the fluid to flow (Yang et al., 2002).

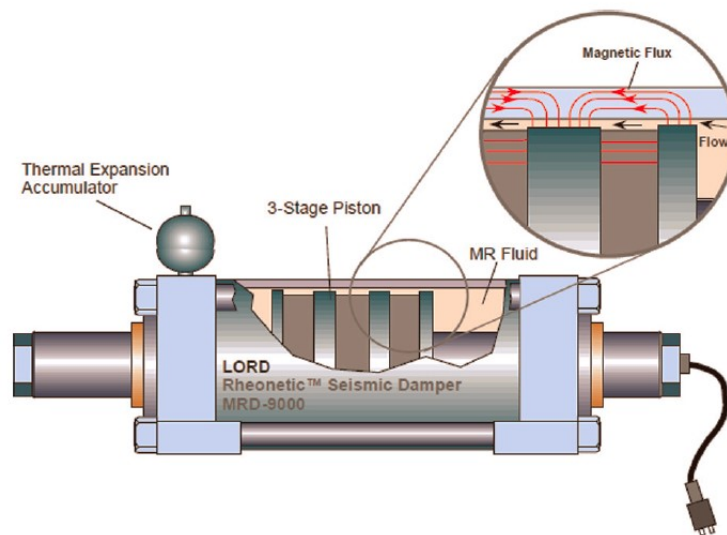


Figure 4-8 Schematic of the 20 ton MR Fluid Damper made by LORD company (Yang et al., 2002)

The outer housing of the damper is the region for producing the magnetic field that is required for the application of MR damper force. As it was mentioned earlier the fluid is in the four chambers between the pistons that would be pressurized by the pistons at both ends. This damper is in the category of the double-ended MR damper, hence it is not required to provide accumulator for the change in the volume of the fluid. However, a thermal expansion accumulator has been utilized in order to transfer the heat from the fluid volume change to the surroundings. The inner diameter of

the damper is 20.3 cm and it has the stroke of ± 8 cm. the length of the damper is 1 m and it has a mass of 250 kg and could contain about 6 liters of MR fluid.

Table 4-1 The Details of the properties of MDR-9000 MR damper (Yang et al., 2002)

stroke	± 8 cm
F_{ma}/F_{min}	10.1@10cm/s
Cylinder bore	20.32 cm
Max. input power	<50 W
Max. force (nominal)	200,000 n
Effective axial pole length	8.4 cm
Coils	3×1050 turns
Fluid $\eta/\tau_0^2(field)$	2×10^{-10} s/Pa
Apparent fluid η	1.3 Pa-s
Fluid $\tau_0(field)$ max	62 kPa
Gap	2 mm
Active fluid volume	90 cm^3
Wire	16 gauge
Inductance (L)	6.6 henries
Coil resistance (R)	3×7.3 ohms

The damping force could be calculated using the modified Bouc-Wen model as follows:

$$F = c_0 \dot{y} + k_1(x - x_0) \quad (4-13)$$

$$\dot{y} = \frac{1}{c_0 + c_1} [\alpha z + c_0 \dot{x} + k_0(x - y)] \quad (4-14)$$

$$\dot{z} = -\gamma |x - y| |z|^{n-1} - \beta (\dot{x} - \dot{y}) |z|^n + A(\dot{x} - \dot{y}) \quad (4-15)$$

Where for the large-scale 20 ton MR damper the coefficients of α , c_0 , and c_1 are as follows:

$$\alpha(i) = 16566i^3 - 87071i^2 + 168326i + 15114 \quad (4-16)$$

$$c_0(i) = 437097i^3 - 1545407i^2 + 1641376i + 457741 \quad (4-17)$$

$$c_1(i) = -9363108i^3 + 5334183i^2 + 48788640i - 2791630 \quad (4-18)$$

4.4. Summary

In this chapter, different types of MR dampers such as Mono tube, twin tube, and double ended MR damper with their properties have been discussed. Furthermore, the methods for the numerical analysis of these dampers have been explained and the modified Bouc-Wen method has been chosen for the analysis of MR dampers in this thesis. Also the MDR-9000 MR damper with the capacity of 200 kN is considered as the MR dampers used in the modeled building frames.

Chapter 5: Modeling of Semi-Active Multiple Tuned Mass Damper

5.1.Introduction

In this chapter the methods of formulation and calculation of a system with the semi-active tuned mass dampers which is state-space statement would be explained. Furthermore, a method of control algorithm called Linear Quadratic Regression (LQR) would be described. Moreover, in order to study the behavior of the structure installed with SAMTMD, a 15 story structure located at Vancouver, British Columbia, Canada, has been designed. The response of the structure with and without the energy dissipating instrument would be studied and compared.

5.2.State Space Equations

The general equation of motion was explained in precious chapter. The equation of motion for the system with semi-active TMD could be rewritten as follows:

$$M\ddot{x} + C_s\dot{x} + Kx = \Gamma f - M\Lambda\ddot{x}_g \quad (5-1)$$

Where, M , C , and K are the mass, damping coefficient, and stiffness matrices of the system. x is the vector of displacement, f is the vector of magnitude of the control force of MR damper, \ddot{x}_g is the ground motion, Γ is the vector of the placement of the MR Damper defined as -1 for the indices

related to the story of the MR damper and 0 for the rest, and the elements of the vector Λ is defined as 1 for indices related to the story of the structure and 0 for the rest.

The state space equation could be given by:

$$\dot{x} = Ax + Bf + E\ddot{x}_g \quad (5-2)$$

And

$$y = Cx + Df \quad (5-3)$$

Where

$$A = \begin{bmatrix} 0_{2n \times 2n} & I_{2n \times 2n} \\ -M^{-1}K & -MC \end{bmatrix} \quad (5-4)$$

$$B = \begin{bmatrix} 0_{2n \times 2n} \\ M^{-1}K \end{bmatrix} \quad (5-5)$$

$$C = \begin{bmatrix} I_{2n \times 2n} & 0_{2n \times 2n} \\ 0_{2n \times 2n} & I_{2n \times 2n} \\ -M^{-1}K & -M^{-1}C_s \end{bmatrix} \quad (5-6)$$

$$C = \begin{bmatrix} I_{2n \times 2n} & 0_{2n \times 2n} \\ 0_{2n \times 2n} & I_{2n \times 2n} \\ -M^{-1}K & -M^{-1}C_s \end{bmatrix} \quad (5-7)$$

$$D = \begin{bmatrix} 0_{2n \times 1} \\ M^{-1}\Gamma \end{bmatrix} \quad (5-8)$$

$$E = - \begin{bmatrix} 0_{2n \times 1} \\ \Lambda \end{bmatrix} \quad (5-9)$$

5.3.LQR Control Algorithm

The Linear Quadratic Regression (LQR) algorithm was first introduced by Kalman (Kalman, 1960) in order to calculate the gain's control matrix by a feedback strategy. It should be noted that LQR has no steady state error and can respond faster compared to some other controllers such as PIDs (Nasir et al., 2008). The goal of this algorithm is to minimize the quadratic criterion $J(u)$ and bring back the state x to its dynamic equilibrium (Barnett & Storey, 1967, 1968). The criterion $J(u)$ is defined as follows:

$$J(u) = \int_{t_0}^t [x(t)^T Q(t)x(t) + u(t)^T R(t)u(t)] dt \quad (5-10)$$

The parameters R and Q are the importance factor of x and u which are the displacement of the structure and damping force respectively.

$$f_c = -K \quad (5-11)$$

$$K = R^{-1}(N^T + B^T P) \quad (5-12)$$

K is the optimal gain of the control which is found by optimizing the quadratic criterion, and P is the solution of the Riccati differential equation:

$$-PBB^T + PA + A^T P + Q = 0 \quad (5-13)$$

Based on equations above the desired force of the MR damper could be acquired. However, since the MR damper's input is the current's voltage, the calculated desired force should be converted to the voltage in order to be able to control the damper. A clipping algorithm could be used for the conversion of the damping force to current (Pohoryles & Duffour, 2015).

$$v_c = v_{max} H\{(f_c - f_{MR}) \cdot f_{MR}\} \quad (5-14)$$

Where v_{max} is the maximum current of the MR damper, and H is the Heaviside function.

5.4. Case Study of a Structure with Multiple Tuned Mass Dampers Integrated with MR Dampers

In order to study the behavior of the structure with Semi-Active Tuned Mass Damper (SAMTMD), a 15 story steel moment resisting frame building located in Vancouver based on NBCC 2015 and CSA S16-14 has been designed. The building has five bays of 5 m in each direction. The dead and live load are considered to be 6 kPa and 2.4 kPa, respectively. It is assumed that the structure is located on a soil class C. the structural damping is considered to be 2 percent in order to better comprehend the effects of the dampers on the structure. In order to simplify the calculations of the structure, after the building was designed, it was converted to a 2D model (shear storey building). The 2D model has been decided in a way that the seismic behavior of the structure was not compromised. The mass and the damping of the structure was remained the same while the stiffness was modified in order to achieve the same seismic response with the 3D model.

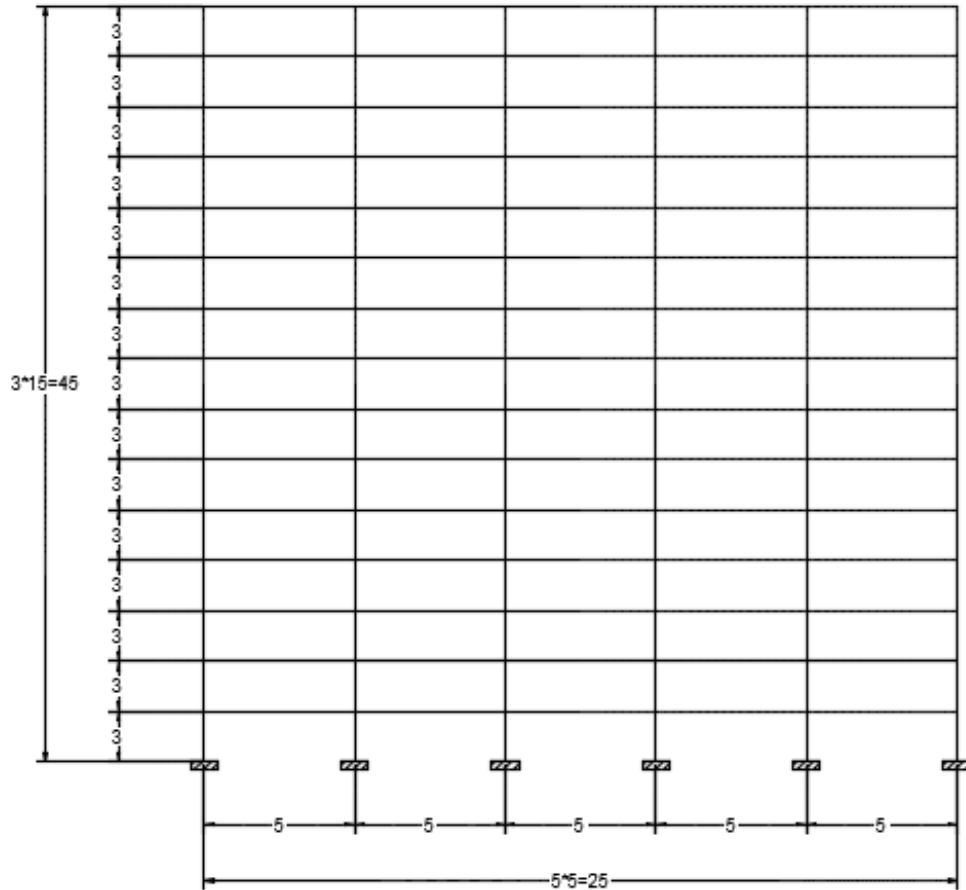


Figure 5-1 The 2D Model of The Modelled Structure

As it was mentioned in Chapter 3, in order to decide the placement of the TMDs a modal analysis was conducted and based on that the location of the TMDs were chosen. Figure 5-2 displays the mode shapes of the structure. Based on this figure it was decided to 3 dampers on the levels 5, 10, and 15 of the building. The dampers were tuned based on the mode that was chosen. For the damper located on 5th floor the period of the second mode, the damper on 10th floor the period of the third mode, and the damper on the top floor the period of the first mode was chosen. The maximum stroke length of 200 Cm have been chosen for the TMDs.

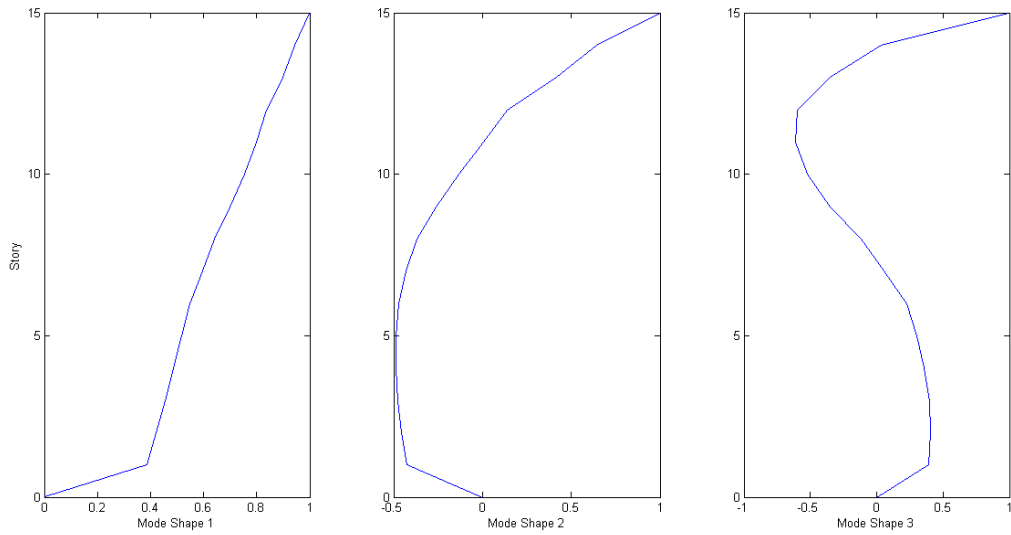


Figure 5-2 First 3 Mode Shapes of the Modelled Structure

Based on **Figure 5-3** the optimized location of the tuned mass damper could be determined using the mode shapes of the structure as it was mentioned above.

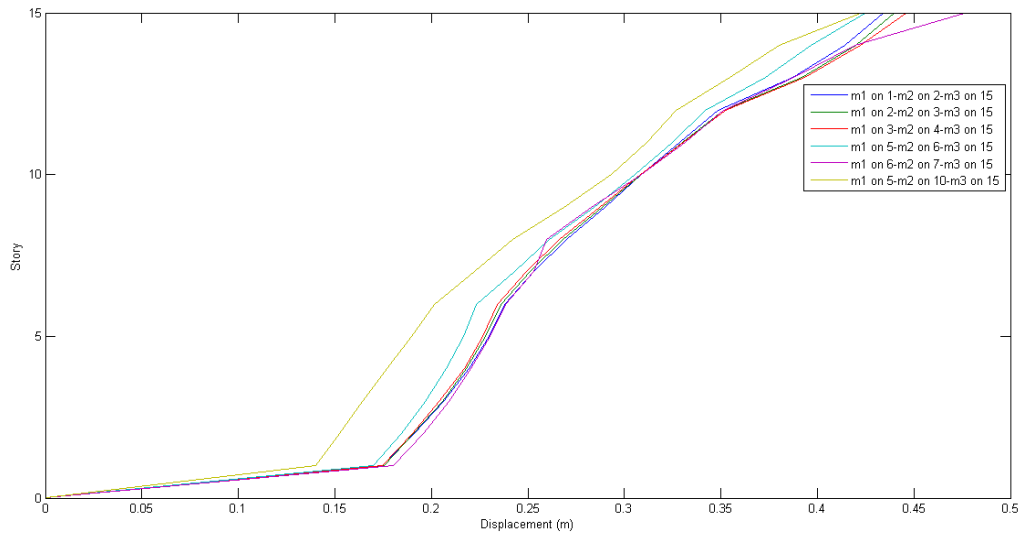


Figure 5-3 The Comparison of the Location of the TMDs

Table 5-1 displays the period of the structure for different modes. The first three modes have been chosen for the placement and tuning of the tuned mass dampers.

Table 5-1 Frequencies and Periods of the Structure

Mode #	The Angular Frequency	Period
Mode 1	2.35	2.67
Mode 2	5.81	1.08
Mode 3	9.56	0.66
Mode 4	13.87	0.45
Mode 5	17.88	0.35
Mode 6	23.10	0.27
Mode 7	26.60	0.24
Mode 8	30.49	0.21
Mode 9	36.66	0.17
Mode 10	41.37	0.15
Mode 11	44.48	0.14
Mode 12	49.52	0.13
Mode 13	57.22	0.11
Mode 14	67.62	0.09
Mode 15	74.57	0.08

The displacement of the floors of the structure under the earthquake of Northridge with and without multiple tuned mass dampers, obtained from time history analysis, is shown in the following comparative graphs (Figure 5-4):

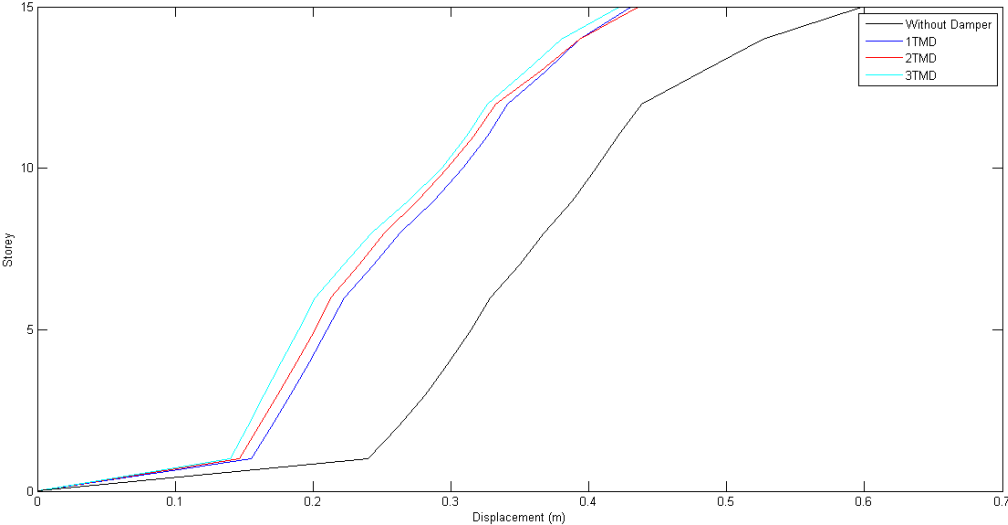


Figure 5-4 Response of the Structure with and without TMDs

Based on the figure above it could be observed that the maximum displacement of the structure with TMDs is improved by 33 percent. Meanwhile, it should be noted that the structure with distributed TMD with a similar cumulative mass have a very similar behavior.

5.5.Sensitivity Analysis

In order to understand the relative behavior of the structure to the distribution of the mass, a sensitivity analysis has been conducted. In this method the displacement of the floors with different

distributions of the mass of dampers have been compared and the maximum and minimum displacement has been displayed and compared with sensitivity graphs (Figure 5-5). In this graph the sensitivity of the displacement of the structure to the distribution of the mass on different levels is demonstrated.

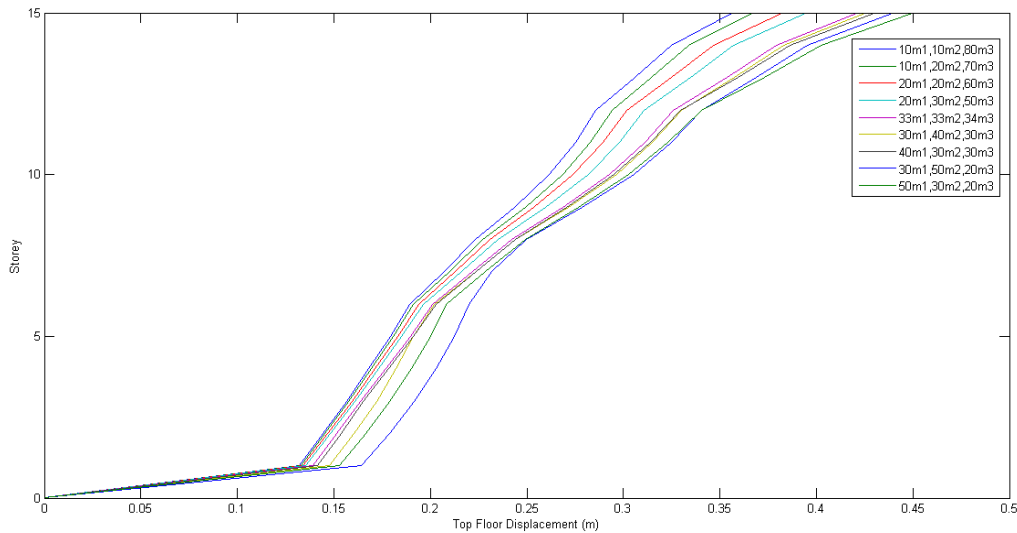


Figure 5-5 Sensitivity of the Mass Distribution

In the figure above m_1 , m_2 , and m_3 are the masses on 5th, 10th, and 15th floor, respectively. Based on this figure the best mass distribution is for the 10 percent for the masses on the 5th and 10th floor and 80 percent of mass for the 15th floor damper.

In this research for verification of the efficient behavior of the SAMTMD a series of 10 earthquake records that are scaled in accordance to the response spectrum of Vancouver have been applied to the designed 15 story building frame (Al Atik & Abrahamson, 2010). These records have been extracted from the Pacific Earthquake Engineering Research Center (PEER) ground motion

database ("PEER Ground Motion Database," 2018) representing strong earthquakes suggested by FEMA P-695 (FEMA, 2009). Specifications of the selected earthquakes are in the table below:

Table 5-2 Earthquake Records

Event	Year	Magnitude	Duration	Name of The Station	
Northridge	1994	6.70	45.31	Beverly Hills - 14145 Mulhol	Far-Field
Duzce, Turkey	1999	7.10	55.90	Strike-slip	Far-Field
Cape Mendocino	1992	7.00	36.00	Rio Dell Overpass - FF	Far-Field
Hector Mine	1999	7.10	29.98	Strike-slip	Far-Field
Imperial Valley	1979	6.50	99.92	Strike-slip	Near-Field
Kobe, Japan	1995	6.90	40.96	Nishi-Akashi	Near-Field
Chi-Chi, Taiwan	1999	7.6	149.96	CHY002	Near-Field
Kocaeli	1999	7.5	27.18	Duzce	Far-Field
Loma Prieta	1989	6.9	39.99	Capitola	Near-Field
Manjil	1990	7.4	45.98	Abbar	Far-Field

Below are the time series acceleration of the ground motions that are used in this research:

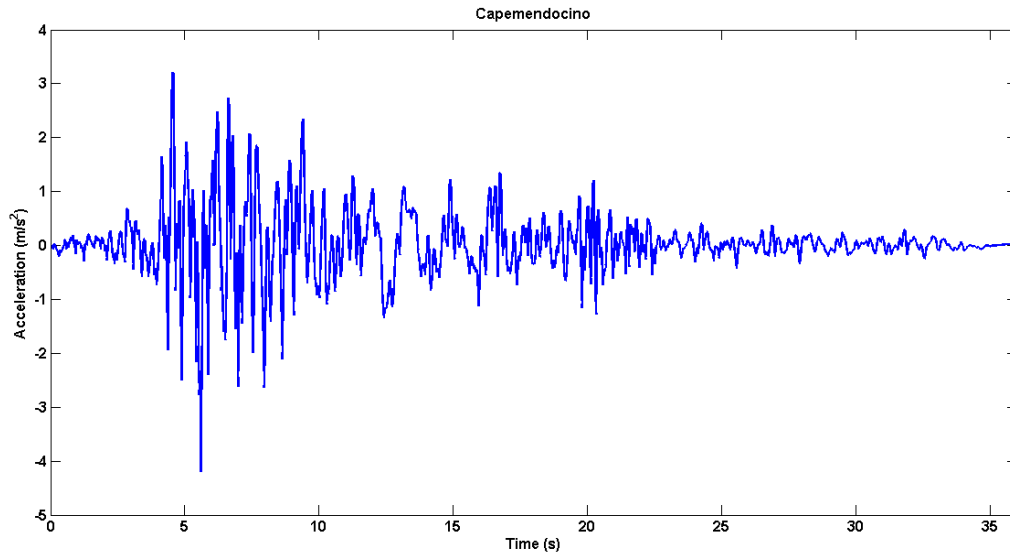


Figure 5-6 Ground Motion Acceleration of Capemendocino Earthquake

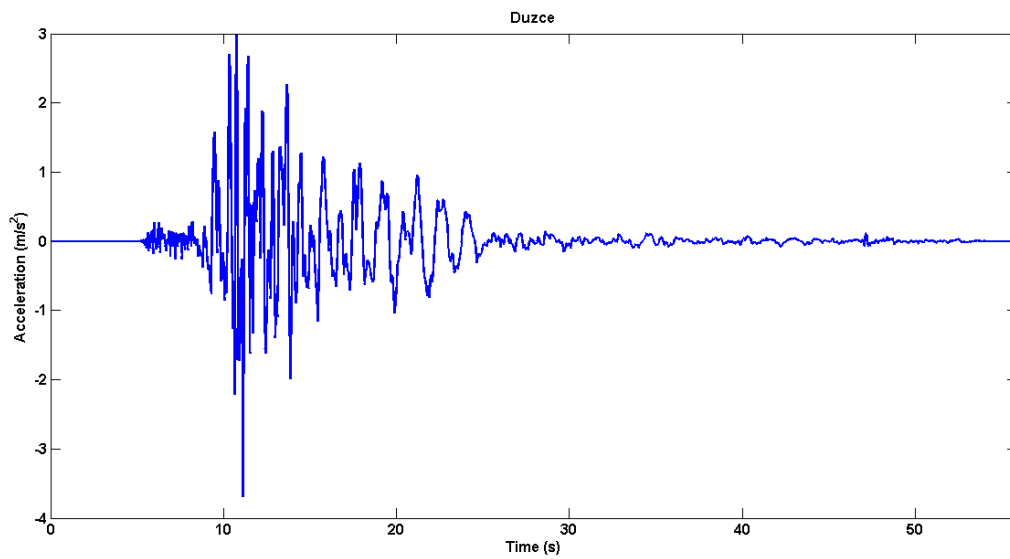


Figure 5-7 Ground Motion Acceleration of Duzce Earthquake

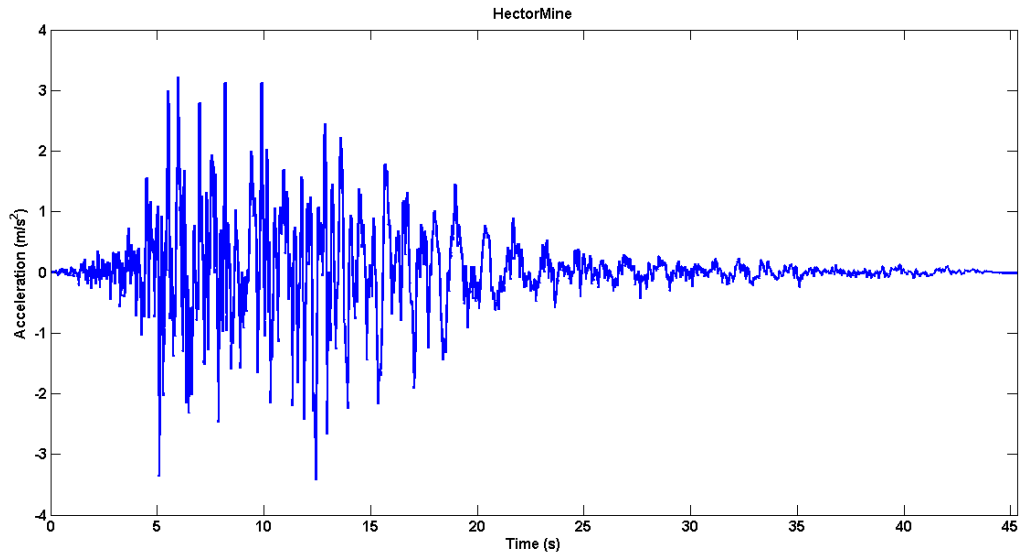


Figure 5-8 Ground Motion Acceleration of Hector Mine Earthquake

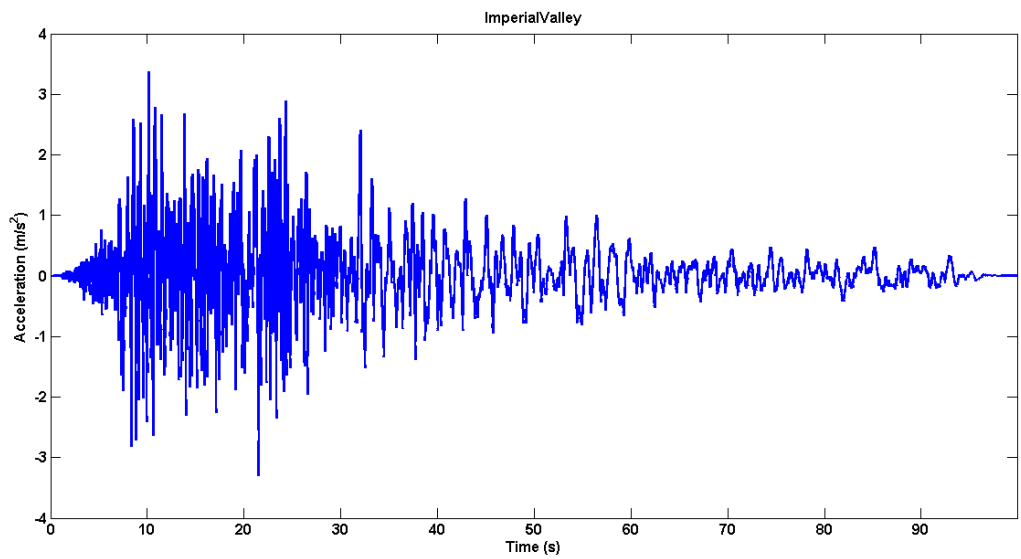


Figure 5-9 Ground Motion Acceleration of Imperial Valley Earthquake

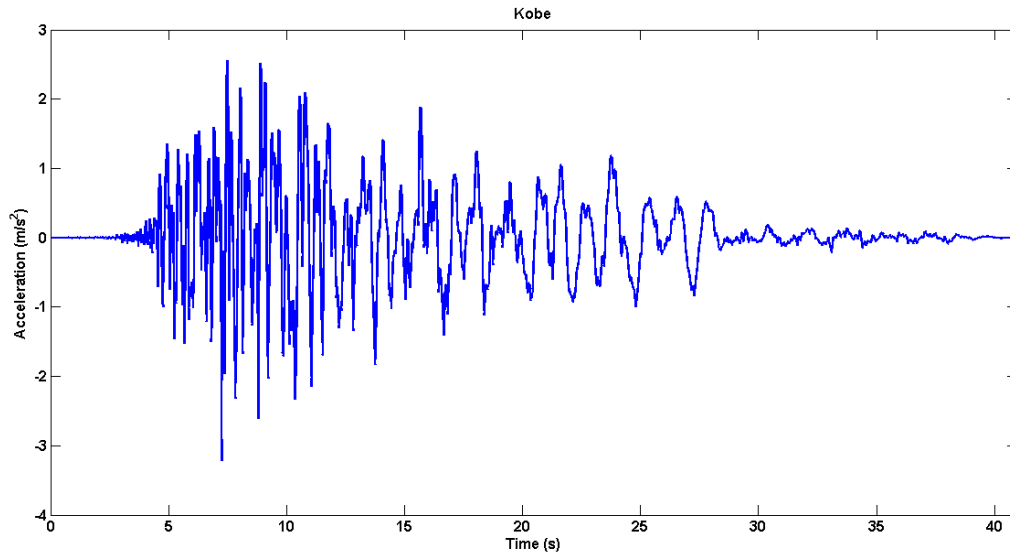


Figure 5-10 Ground Motion Acceleration of Kobe Earthquake

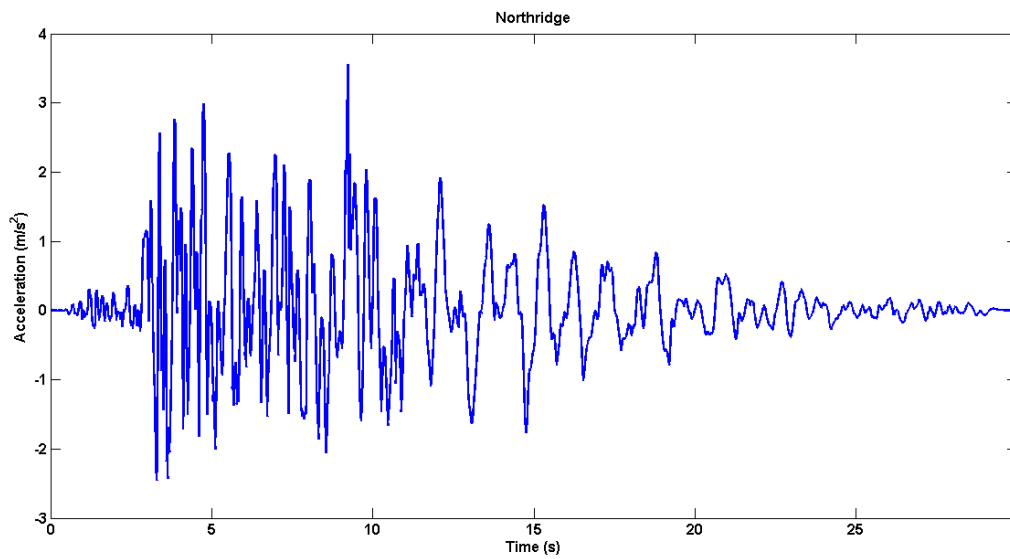


Figure 5-11 Ground Motion Acceleration of Northridge Earthquake

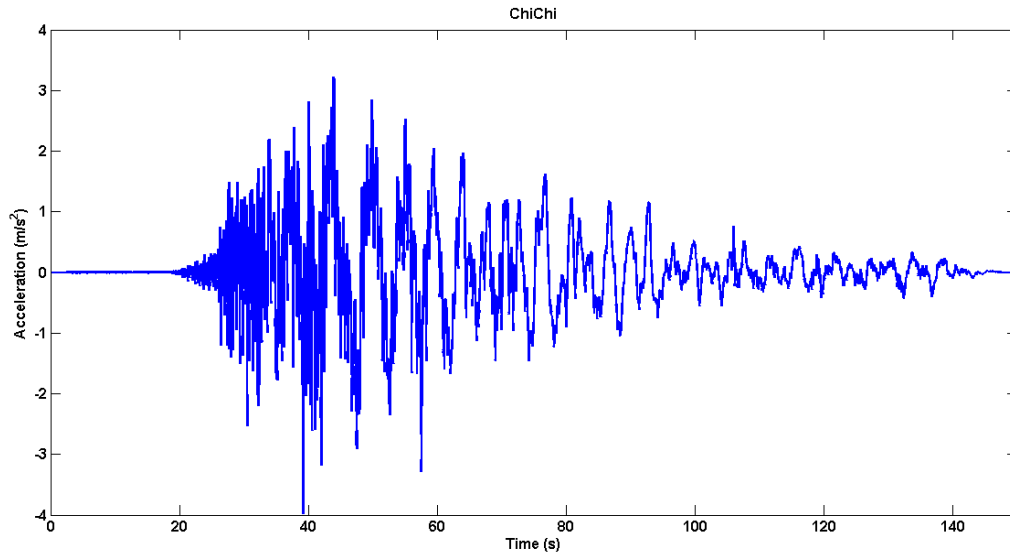


Figure 5-12 Ground Motion Acceleration of Chi-Chi Earthquake

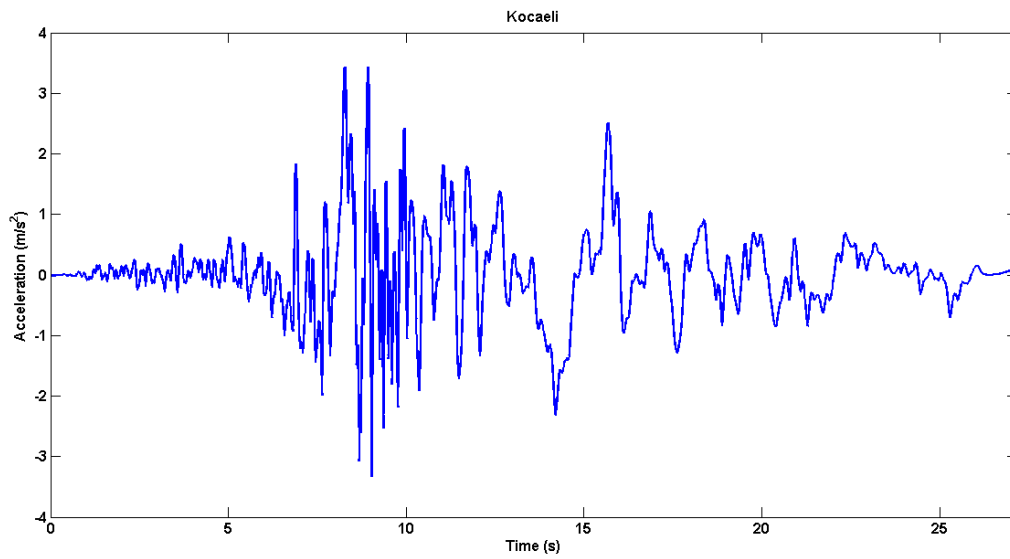


Figure 5-13 Ground Motion Acceleration of Kocaeli Earthquake

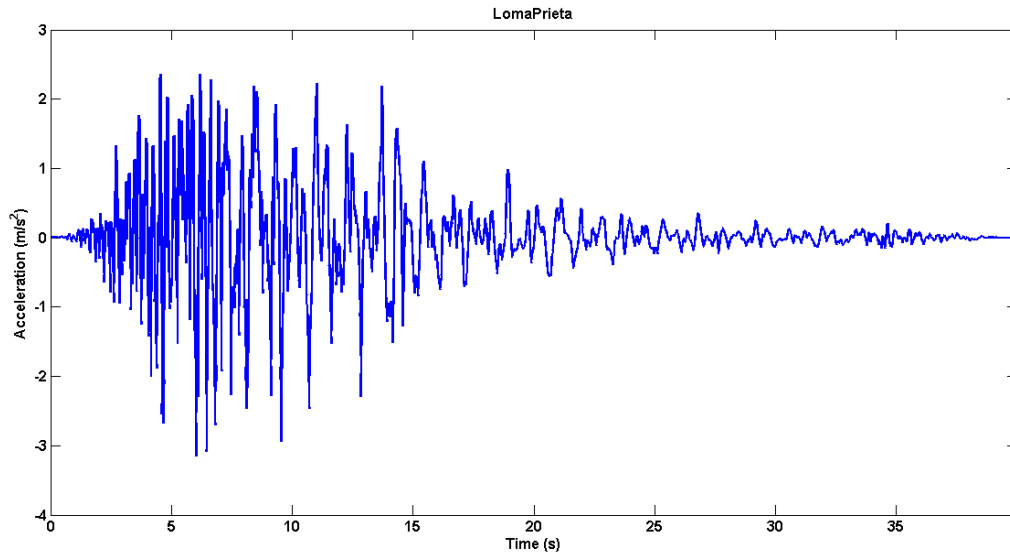


Figure 5-14 Ground Motion Acceleration of Loma Prieta Earthquake

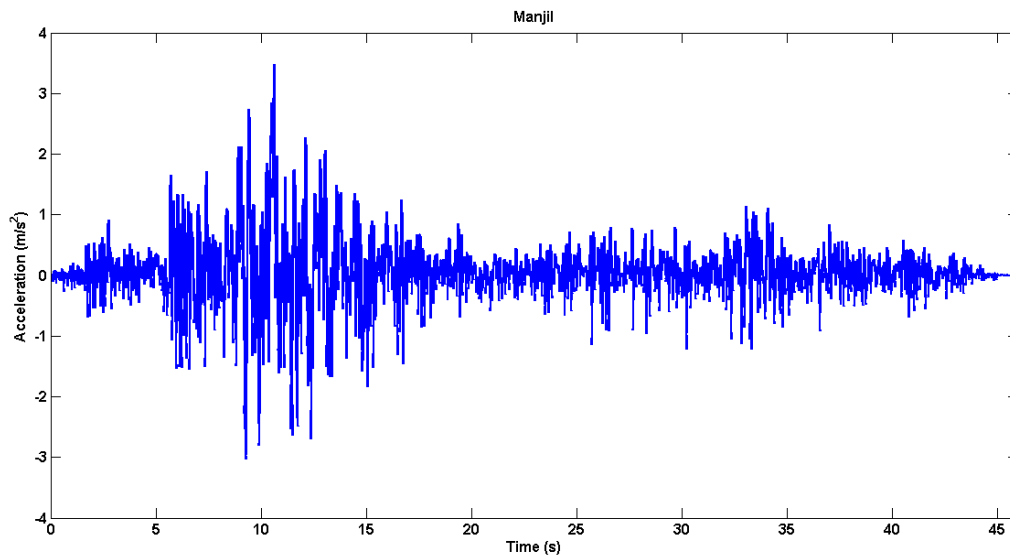


Figure 5-15 Ground Motion Acceleration of Manjil Earthquake

The following figures display the response spectrum of the scaled and unscaled earthquake records:

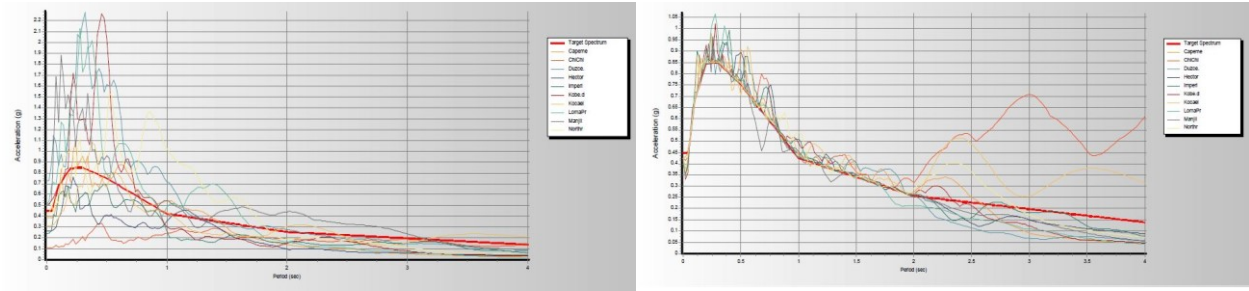


Figure 5-16 Unscaled and Scaled Spectrum

The figure below displays the placement of the installed dampers in the case study (Figure 5-17):

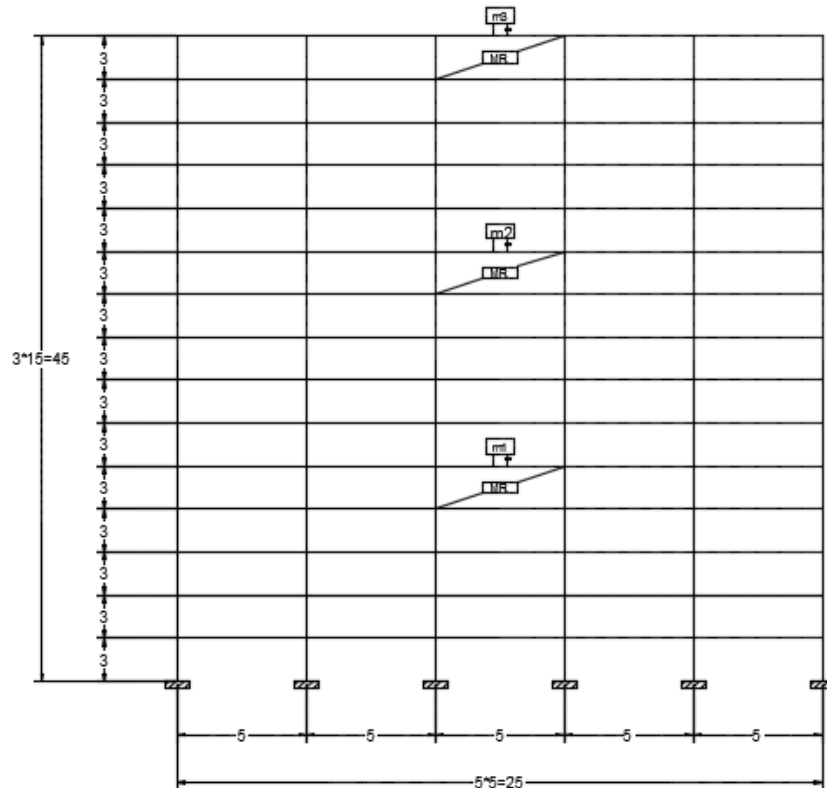


Figure 5-17 The Placement of the Dampers in the Modelled Structure

In this research for the time history analysis of the structure with SAMTMD subjected to earthquake the Simulink software and MATLAB software have been used.

Figure below displays a schematic of the model in the SIMULINK:

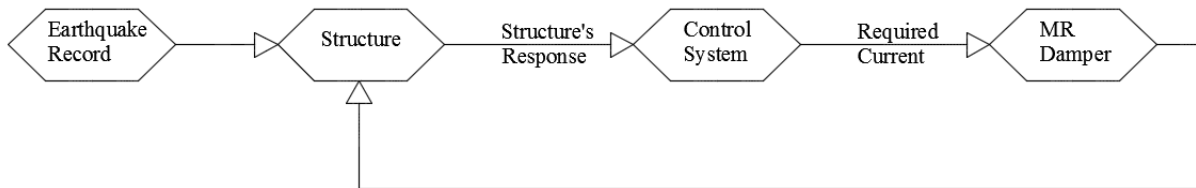


Figure 5-18 The Schematic Block Diagram of the Modelled System Including the Structure and Dampers

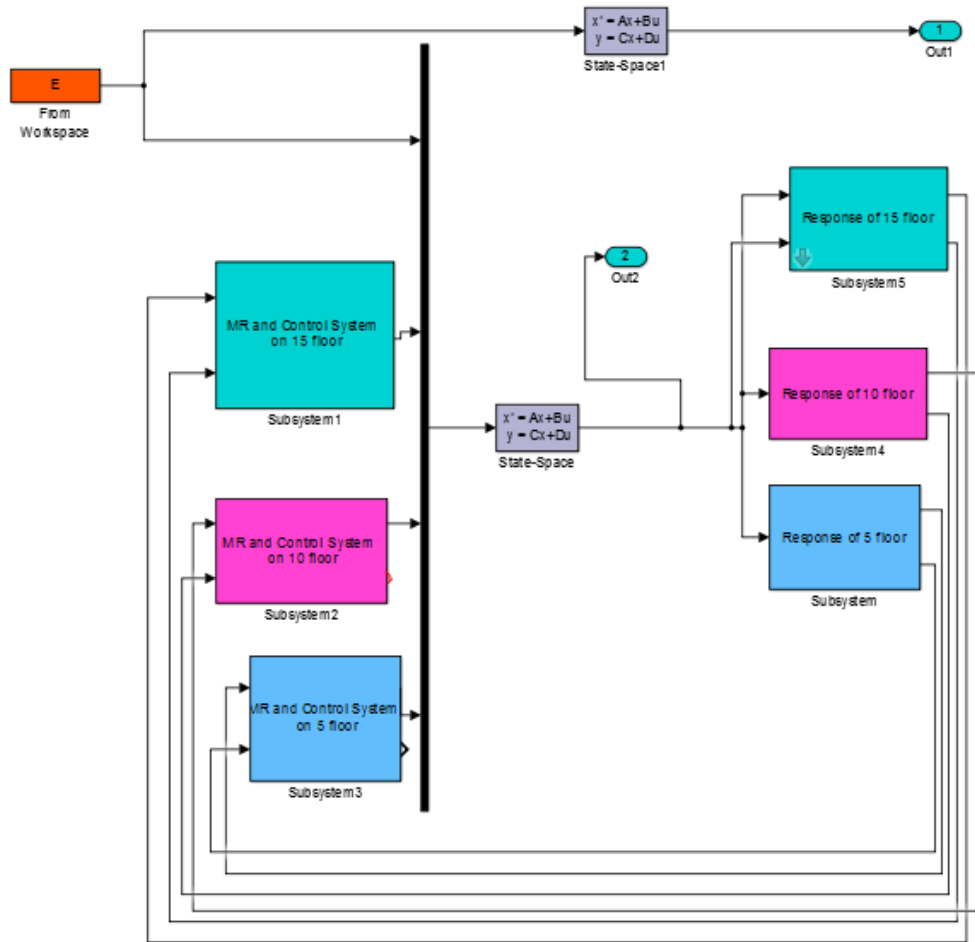


Figure 5-19 The details of the Block Diagram of the Modelled System in Simulink Software

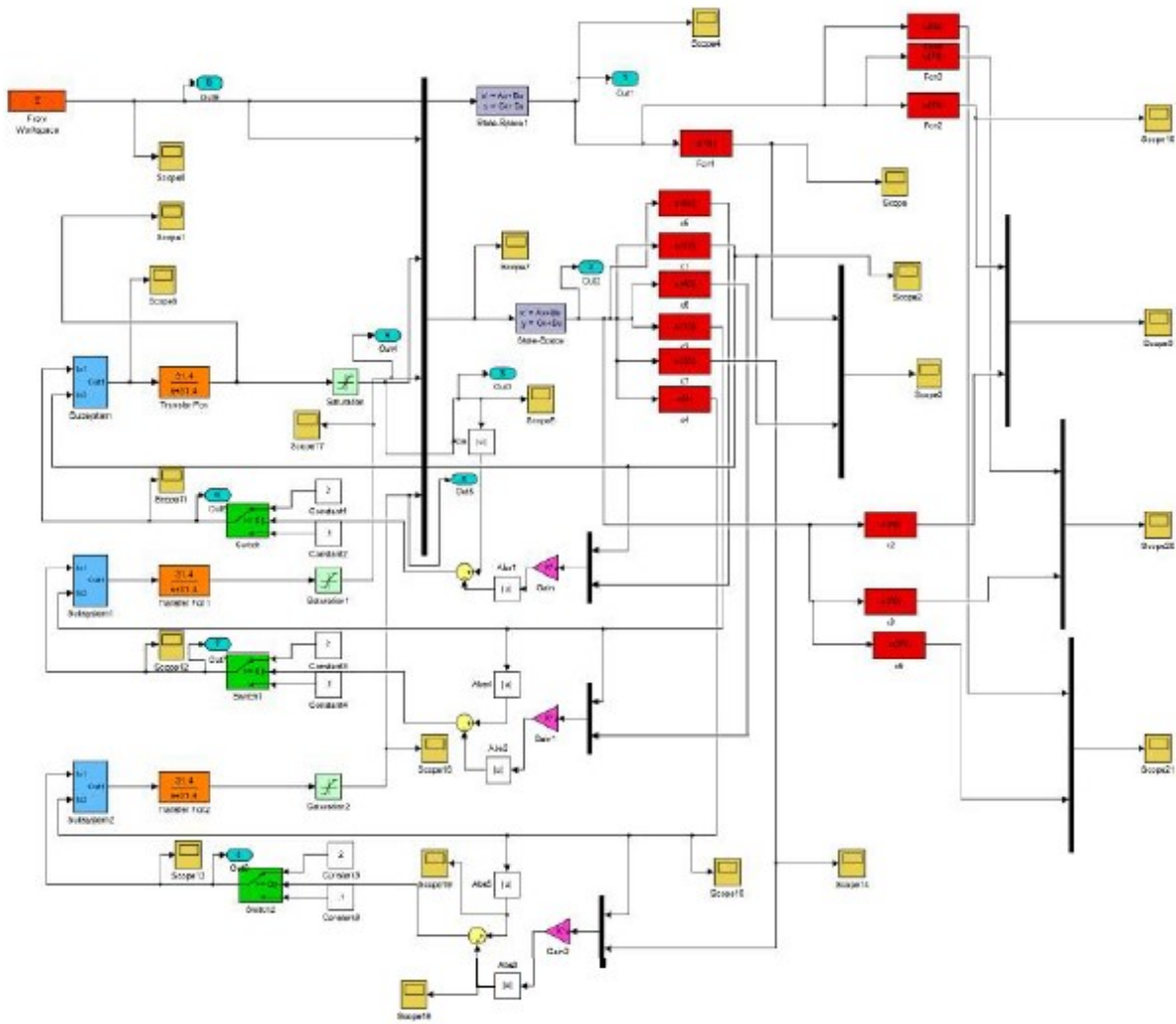


Figure 5-20 The Schematic Block Diagram of the Modelled System Including the Structure and Dampers in Simulink Software

The structure block in the figure above contains the stiffness, mass, and damping coefficient of the structure. In this step, the analysis of the structure would be processed and the response of the structure such as acceleration, velocity, and displacement of the structure would be calculated. According to the response of the structure in each time step the control system block which contains the LQR control algorithm would estimate the required force for the optimized behavior

of the structure. As it was explained in Chapter 5.3 the MR damper's input is current; hence, when the required force is less than the damper's force the maximum current capacity of the damper is applied, otherwise the minimum current is applied. Furthermore, the force of the damper is calculated and then applied to the structure. This process will continue for the duration of the earthquake.

5.6. Analytical Results

In the following seismic analytical results for the simulated structure equipped with SAMTMD energy dissipating system exposed for the selected earthquake records are discussed. The figures below illustrate the graphs of the applied current and produced resistance damping force of the MR damper located on the top floor for the selected earthquake records. Additionally, the demand-time graphs, in which the demands are the acceleration, velocity and displacement of the system, for the 15th floor of the structure is displayed. These graphs display the effect of multiple semi active dampers in a structure. It is observed that by installation of MSATMD energy dissipating system, the average of the maximum seismic demands of the structure including acceleration, velocity, and displacement are reduced significantly. The performance of the introduced MSATMD energy dissipating system in decreasing the seismic response of the structure for the selected earthquake records are discussed in the following.

5.6.1. Analytical results for the modelled structure exposed to Capemendocino Earthquake:

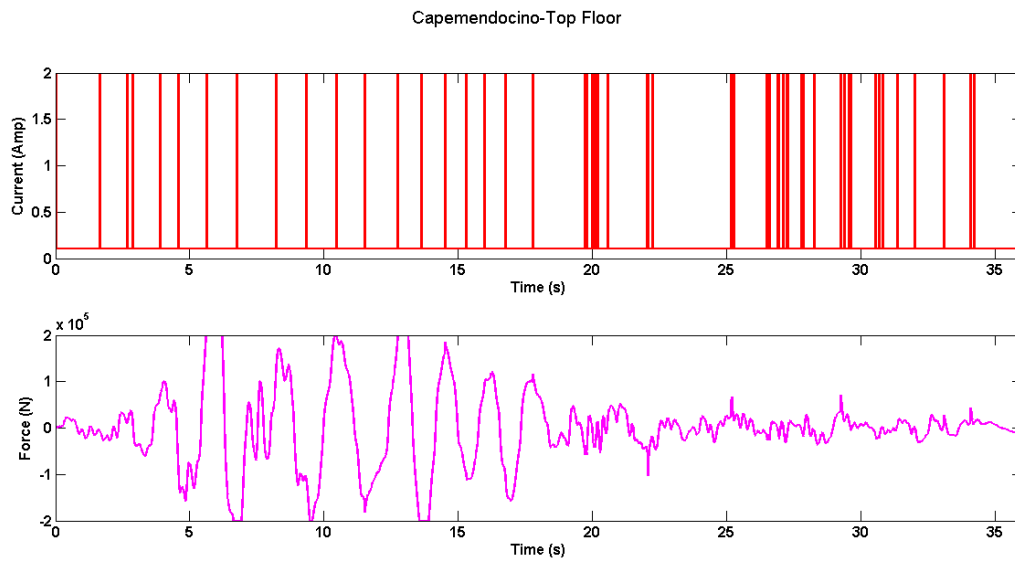


Figure 5-21 The Applied Electricity Current and Adaptive Resistance Force of the MR Damper for Capemendocino Earthquake

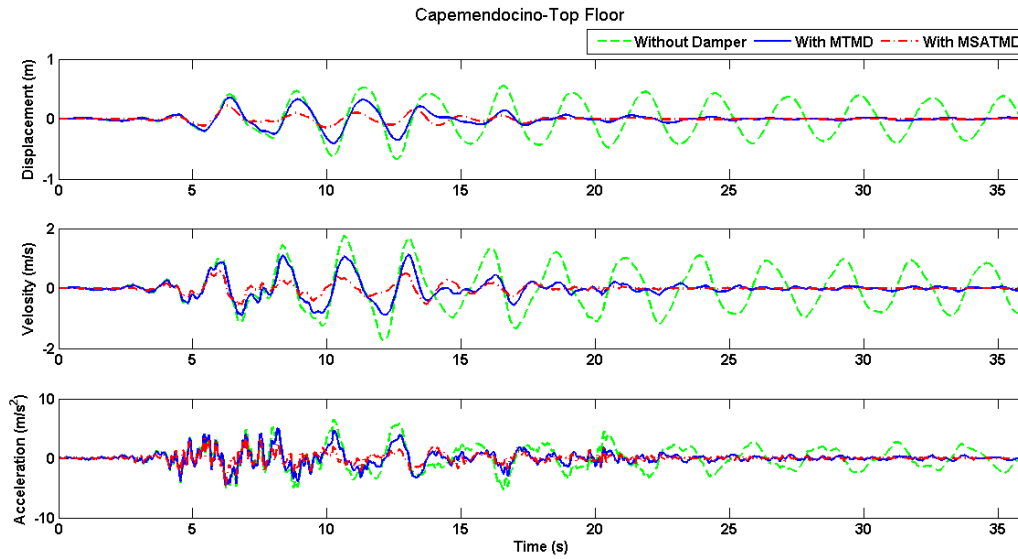


Figure 5-22 Response of the 15th floor under the Capmendocino Excitation

The graph above and the resulted analytical data indicate that the maximum displacement, Velocity, and acceleration on the top floor of the modelled structure are reduced by about 54, 52, and 42 percent respectively. The stroke length of the TMDs is displayed in the following table:

Table 5-3- The Stroke Length of TMDs

	MTMD (m)	SAMTMD (m)
<i>TMD on 5th floor</i>	0.392	0.273
<i>TMD on 10th floor</i>	0.503	0.294
<i>TMD on 15th floor</i>	1.798	1.031

5.6.2. Analytical results for the modelled structure exposed to Duzce Earthquake:

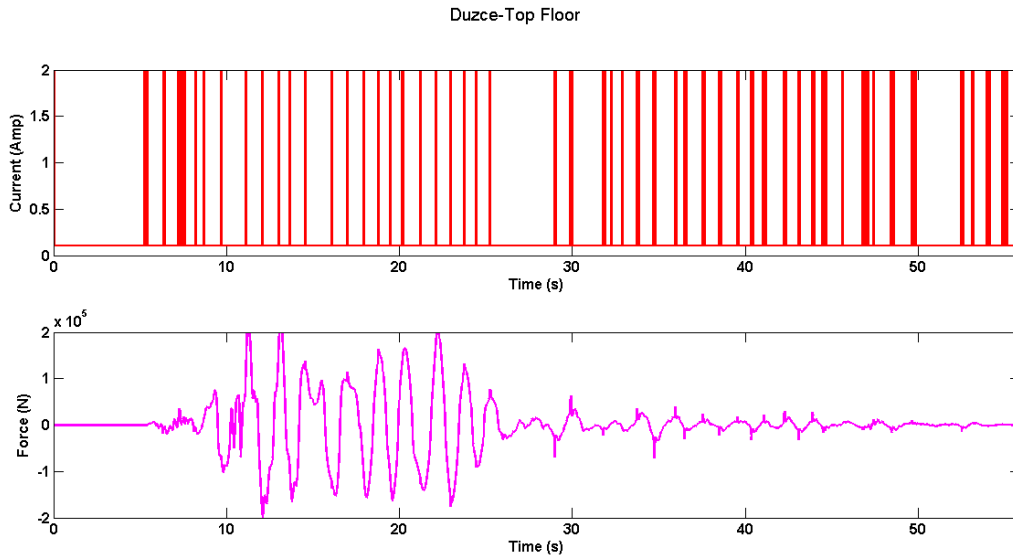


Figure 5-23 The Applied Electricity Current and Adaptive Resistance Force of the MR Damper for Duzce Earthquake

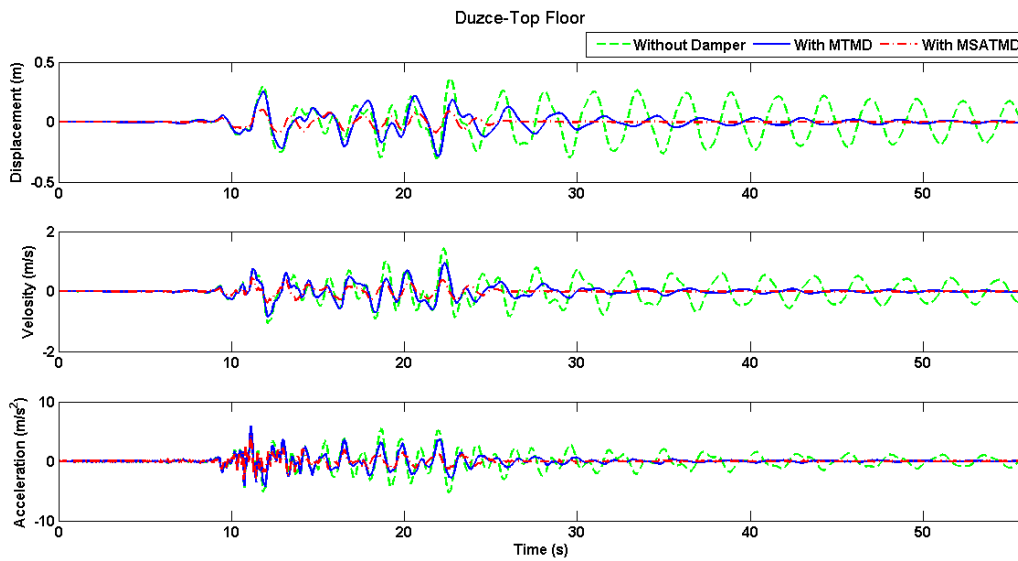


Figure 5-24 Response of the 15th floor under the Duzce Excitation

The graph above and the resulted analytical data indicate that the maximum displacement, Velocity, and acceleration on the top floor of the modelled structure are reduced by about 69, 52, and 30 percent respectively. The stroke length of the TMDs is displayed in the following table:

Table 5-4- The Stroke Length of TMDs

	MTMD (m)	SAMTMD (m)
<i>TMD on 5th floor</i>	0.223	0.200
<i>TMD on 10th floor</i>	0.236	0.208
<i>TMD on 15th floor</i>	0.864	0.569

5.6.3. Analytical results for the modelled structure exposed to Hector Mine Earthquake:

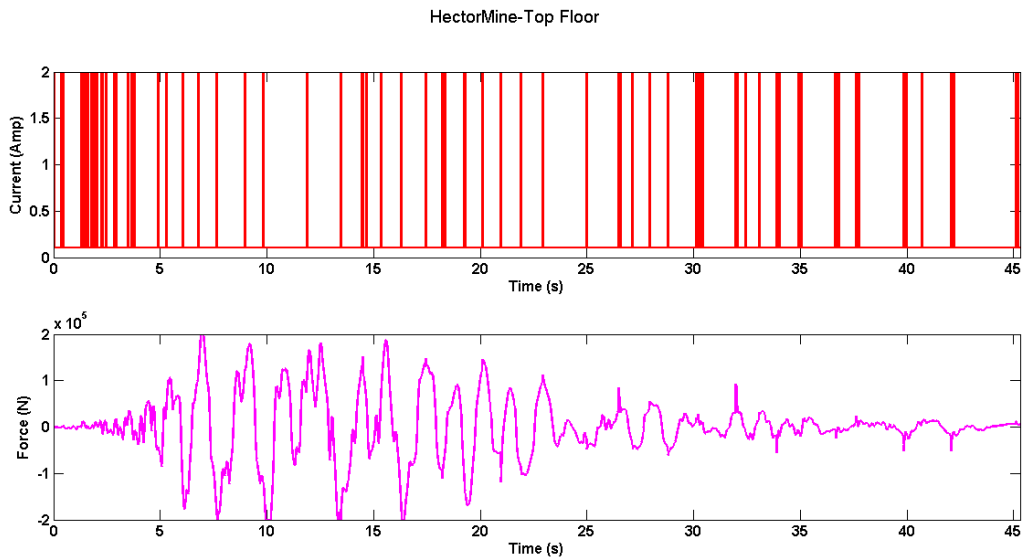


Figure 5-25 The Applied Electricity Current and Adaptive Resistance Force of the MR Damper for Hector Mine Earthquake

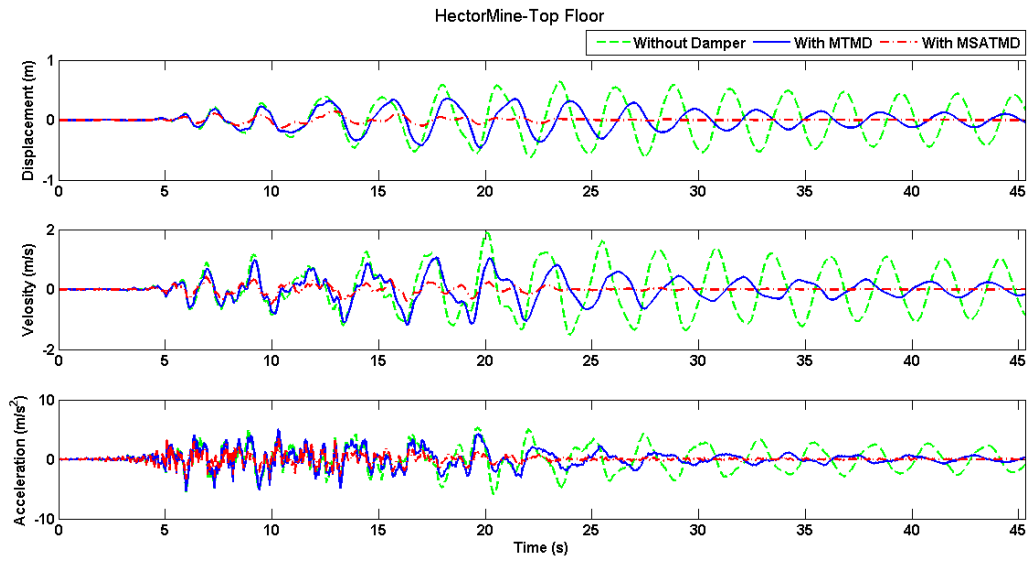


Figure 5-26 Response of the 15th floor under the Hector Mine Excitation

The graph above and the resulted analytical data indicate that the maximum displacement, Velocity, and acceleration on the top floor of the modelled structure are reduced by about 73, 62, and 47 percent, respectively. The stroke length of the TMDs is displayed in the following table:

Table 5-5- The Stroke Length of TMDs

	MTMD (m)	SAMTMD (m)
<i>TMD on 5th floor</i>	0.414	0.264
<i>TMD on 10th floor</i>	0.461	0.364
<i>TMD on 15th floor</i>	1.945	1.183

5.6.4. Analytical results for the modelled structure exposed to Imperial Valley Earthquake:

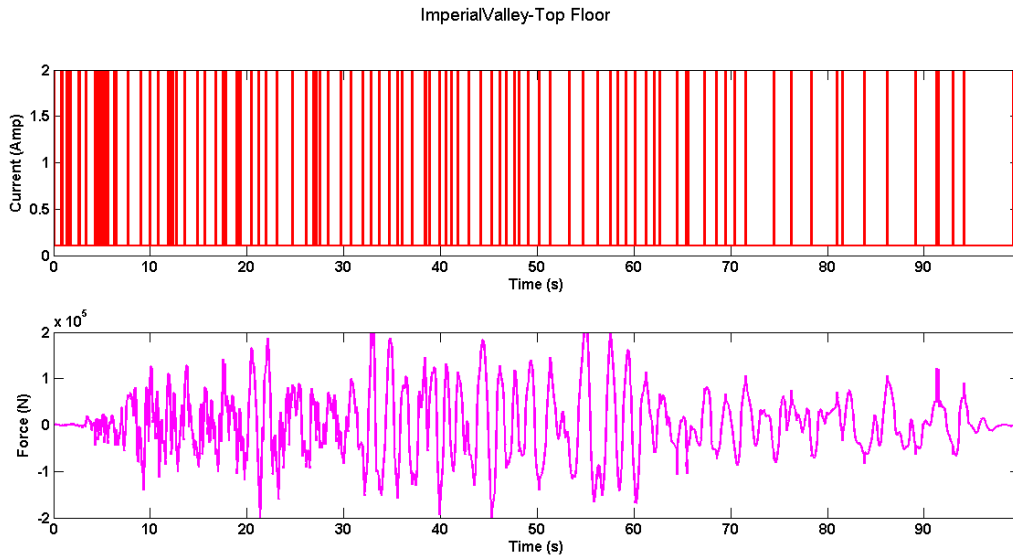


Figure 5-27 The Applied Electricity Current and Adaptive Resistance Force of the MR Damper for Imperial Valley Earthquake

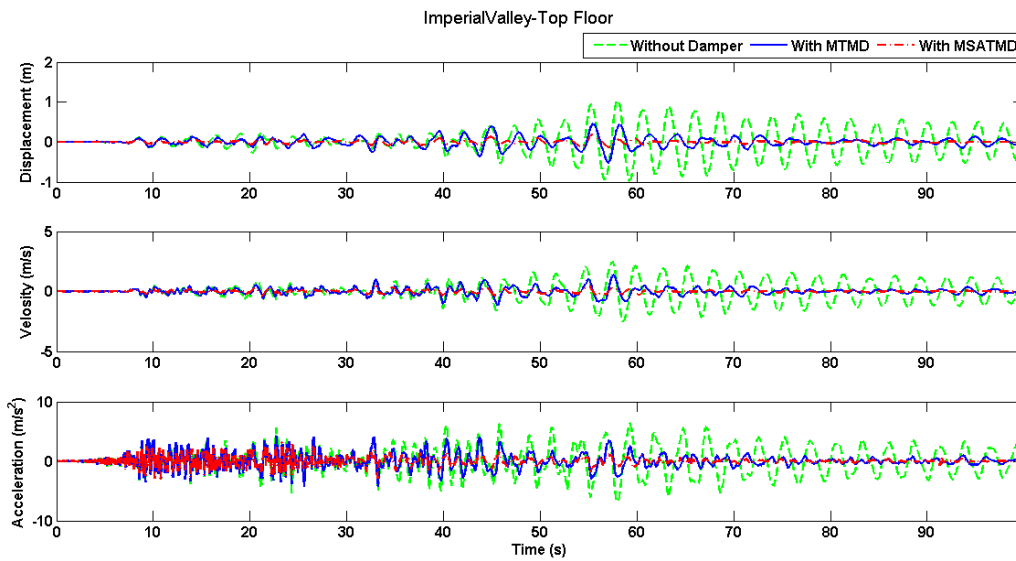


Figure 5-28 Response of the 15th floor under the Imperial Valley Excitation

The graph above and the resulted analytical data indicate that the maximum displacement, Velocity, and acceleration on the top floor of the modelled structure are reduced by about 74, 72, and 41 percent respectively. The stroke length of the TMDs is displayed in the following table:

Table 5-6- The Stroke Length of TMDs

	MTMD (m)	SAMTMD (m)
<i>TMD on 5th floor</i>	0.587	0.315
<i>TMD on 10th floor</i>	0.760	0.392
<i>TMD on 15th floor</i>	1.441	1.241

5.6.5. Analytical results for the modelled structure exposed to Kobe Earthquake:

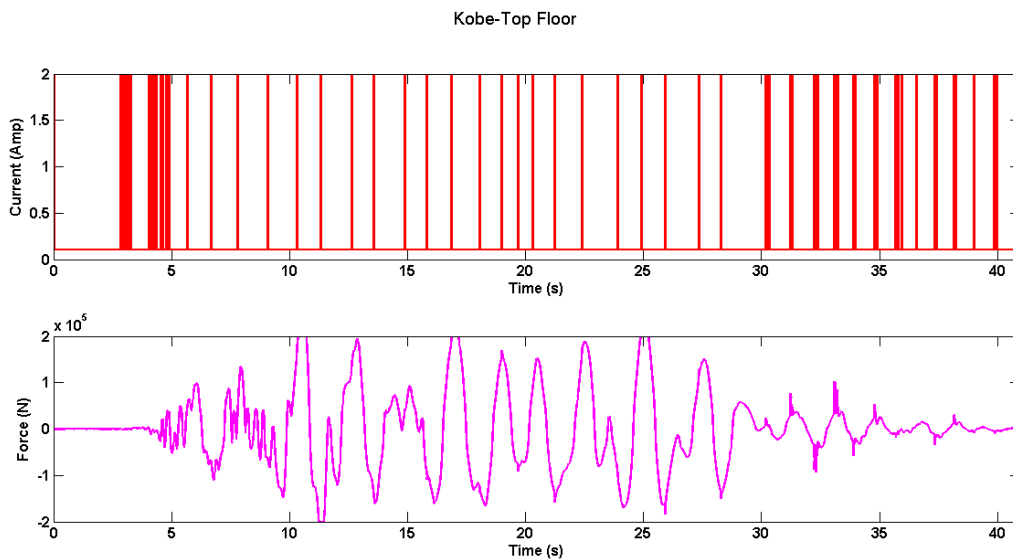


Figure 5-29 The Applied Electricity Current and Adaptive Resistance Force of the MR Damper for Kobe Earthquake

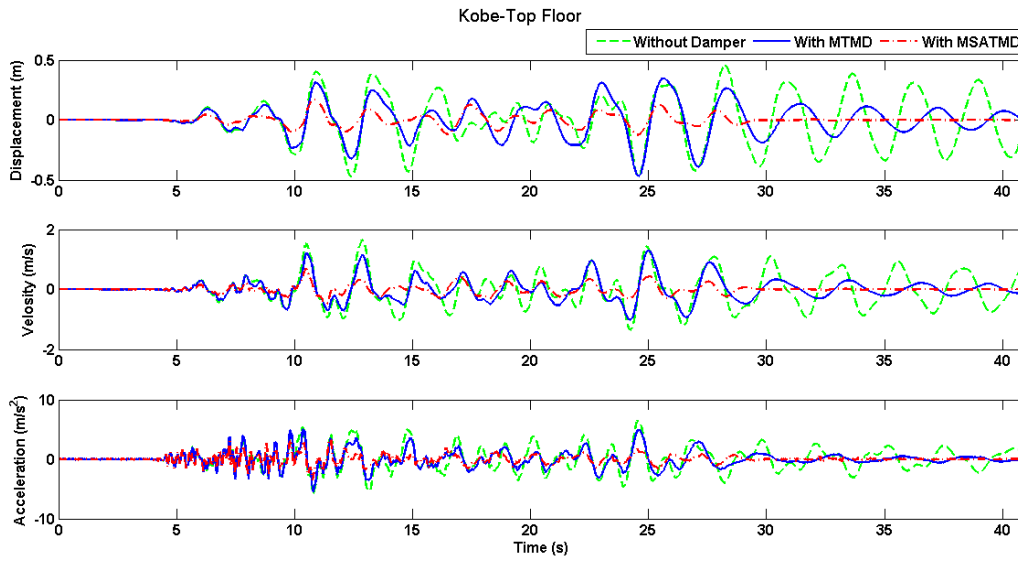


Figure 5-30 Response of the 15th floor under the Kobe Excitation

The graph above and the resulted analytical data indicate that the maximum displacement, Velocity, and acceleration on the top floor of the modelled structure are reduced by about 72, 69, and 12 percent, respectively. The stroke length of the TMDs is displayed in the following table:

Table 5-7- The Stroke Length of TMDs

	MTMD (m)	SAMTMD (m)
<i>TMD on 5th floor</i>	0.336	0.273
<i>TMD on 10th floor</i>	0.354	0.301
<i>TMD on 15th floor</i>	1.273	1.162

5.6.6. Analytical results for the modelled structure exposed to Northridge Earthquake:

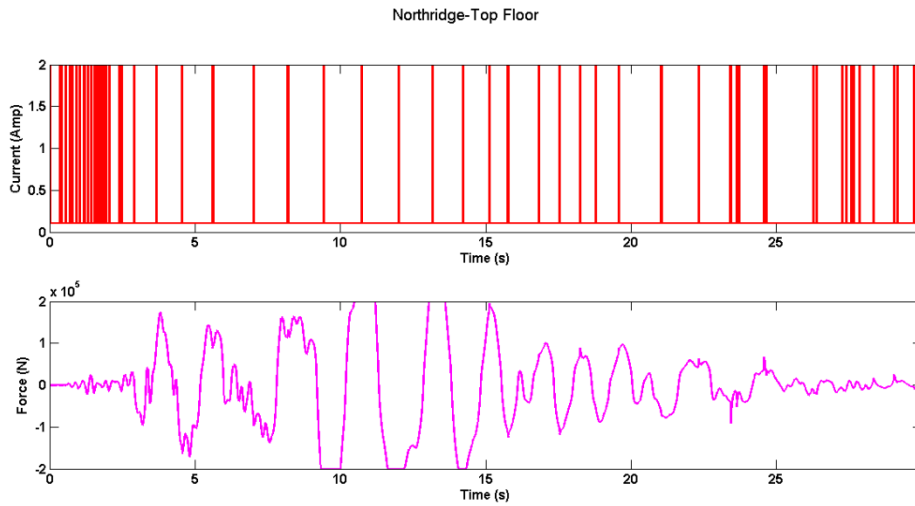


Figure 5-31 The Applied Electricity Current and Adaptive Resistance Force of the MR Damper for Northridge Earthquake

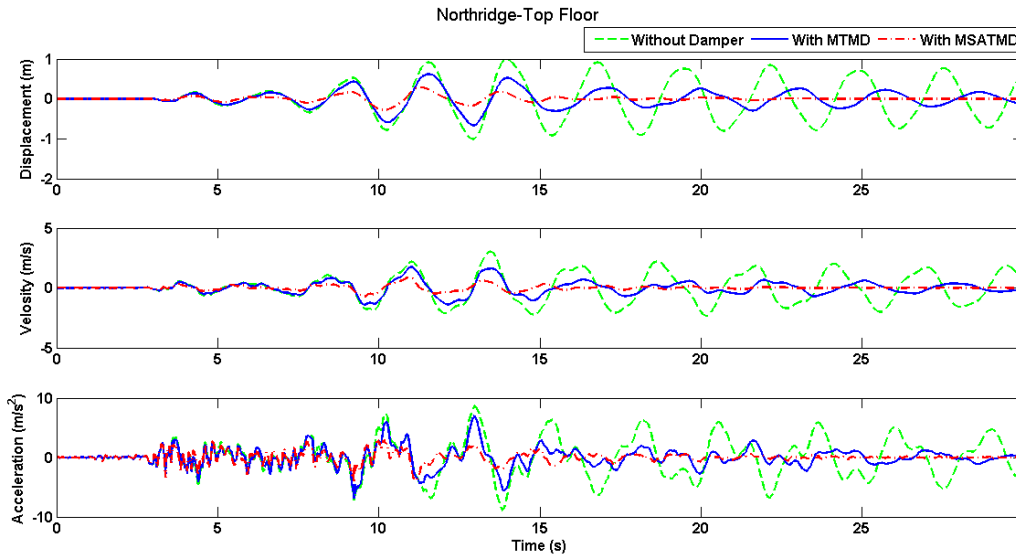


Figure 5-32-Response of the 15th floor under the Northridge Excitation

The graph above and the resulted analytical data indicate that the maximum displacement, Velocity, and acceleration on the top floor of the modelled structure are reduced by about 56, 58, and 40 percent, respectively. The stroke length of the TMDs is displayed in the following table:

Table 5-8- The Stroke Length of TMDs

	MTMD (m)	SAMTMD (m)
<i>TMD on 5th floor</i>	0.696	0.420
<i>TMD on 10th floor</i>	0.746	0.468
<i>TMD on 15th floor</i>	1.873	1.440

5.6.7. Analytical results for the modelled structure exposed to Chi-Chi Earthquake:

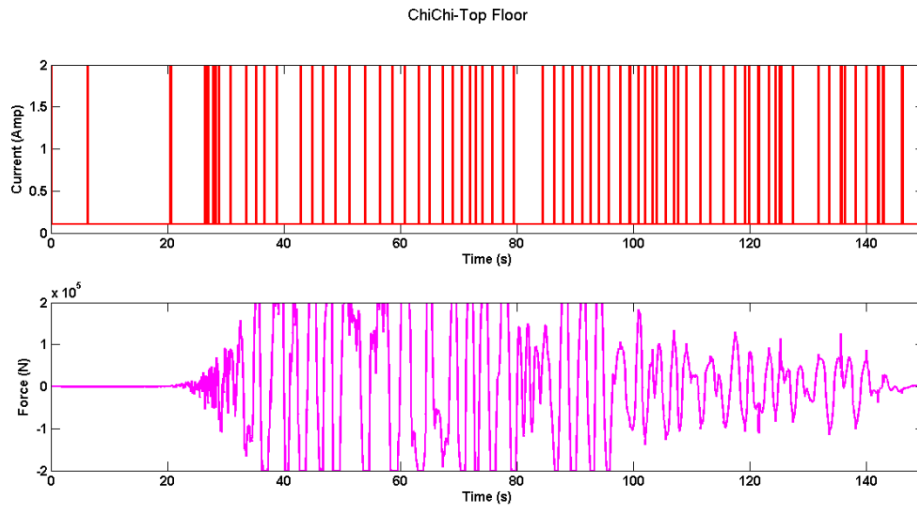


Figure 5-33 The Applied Electricity Current and Adaptive Resistance Force of the MR Damper for Chi-Chi Earthquake

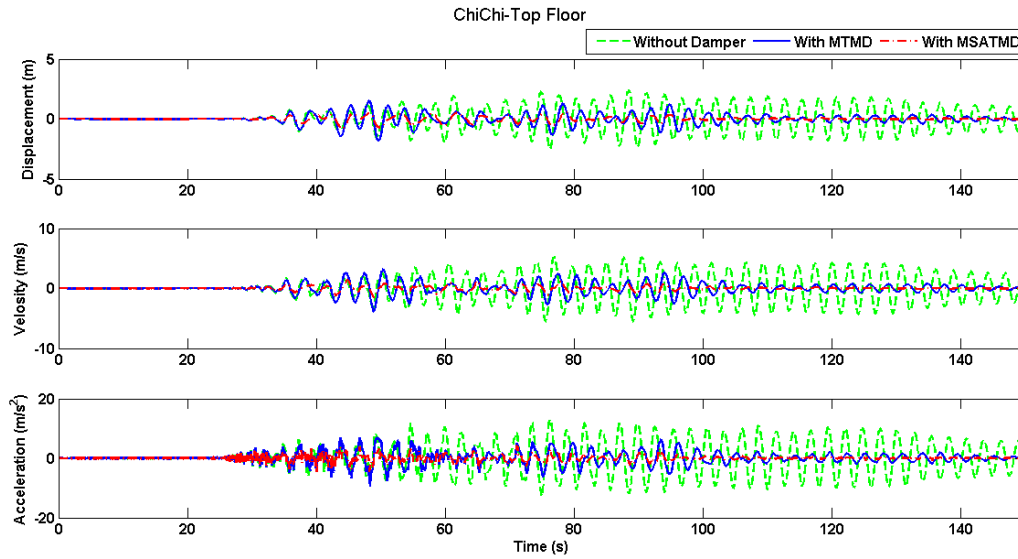


Figure 5-34 Response of the 15th floor under the Chi-Chi Excitation

The graph above and the resulted analytical data indicate that the maximum displacement, Velocity, and acceleration on the top floor of the modelled structure are reduced by about 81, 83, and 71 percent, respectively. The stroke length of the TMDs is displayed in the following table:

Table 5-9- The Stroke Length of TMDs

	MTMD (m)	SAMTMD (m)
<i>TMD on 5th floor</i>	0.885	0.540
<i>TMD on 10th floor</i>	1.044	0.854
<i>TMD on 15th floor</i>	1.885	1.462

5.6.8. Analytical results for the modelled structure exposed to Kocaeli Earthquake:

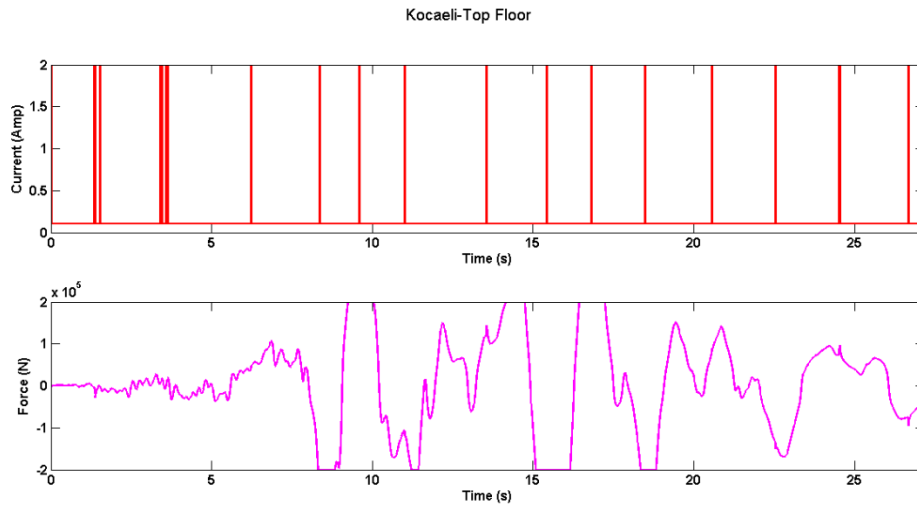


Figure 5-35 The Applied Electricity Current and Adaptive Resistance Force of the MR Damper for Kocaeli Earthquake

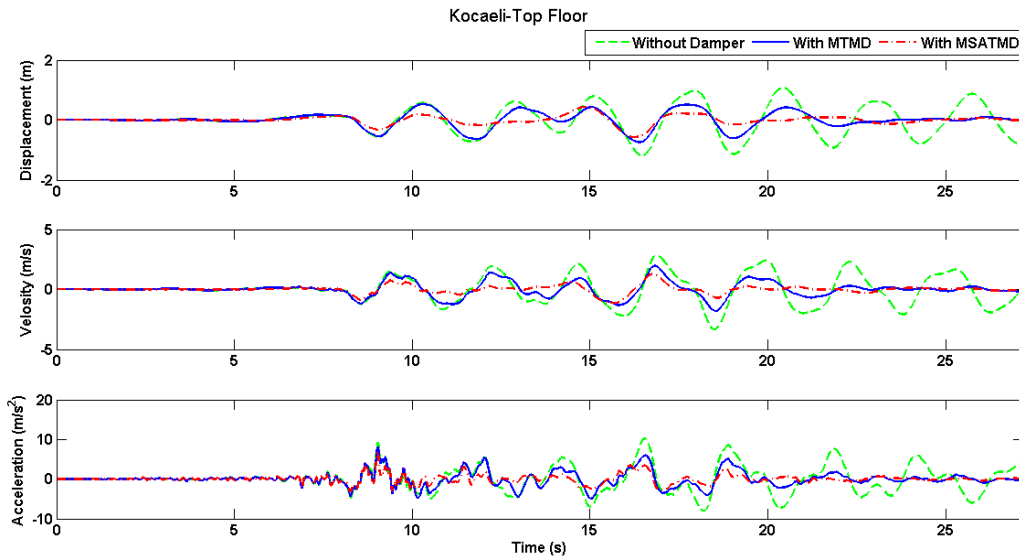


Figure 5-36- Response of the 15th floor under the Kocaeli Excitation

The graph above and the resulted analytical data indicate that the maximum displacement, Velocity, and acceleration on the top floor of the modelled structure are reduced by about 31, 58, and 21 percent, respectively. The stroke length of the TMDs is displayed in the following table:

Table 5-10- The Stroke Length of TMDs

	MTMD (m)	SAMTMD (m)
<i>TMD on 5th floor</i>	0.720	0.528
<i>TMD on 10th floor</i>	0.876	0.629
<i>TMD on 15th floor</i>	1.812	1.412

5.6.9. Analytical results for the modelled structure exposed to LomaPrieta Earthquake:

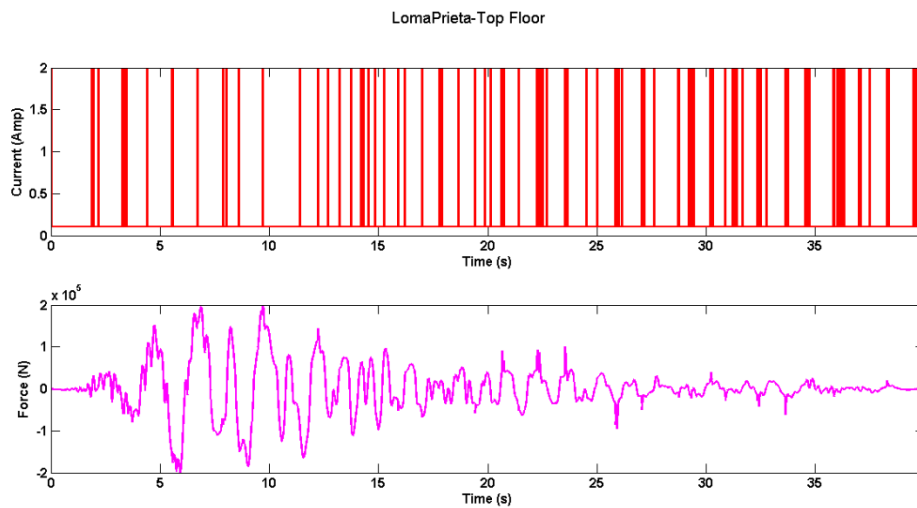


Figure 5-37 The Applied Electricity Current and Adaptive Resistance Force of the MR Damper for Loma Prieta Earthquake

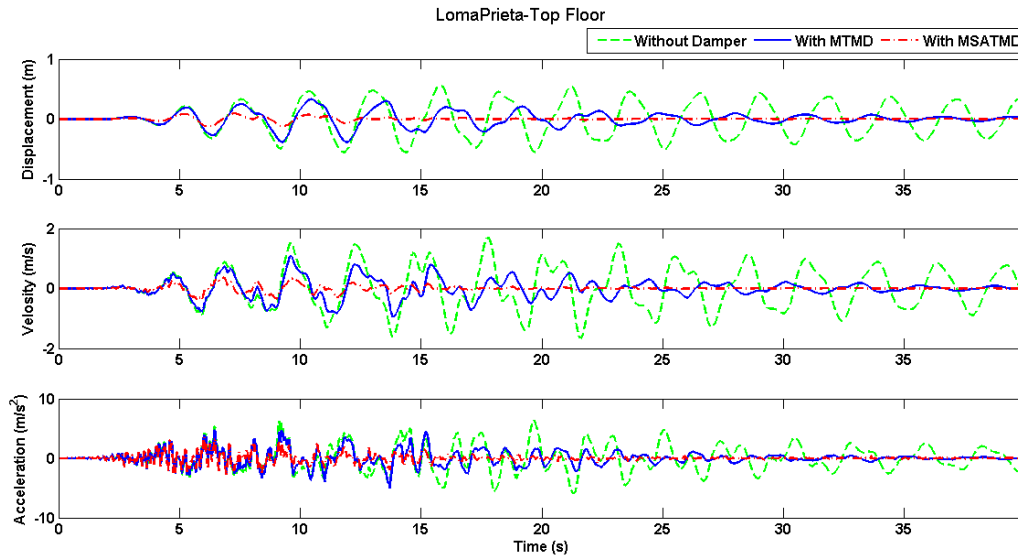


Figure 5-38 Response of the 15th floor under the Loma Prieta Excitation

The graph above and the resulted analytical data indicate that the maximum displacement, Velocity, and acceleration on the top floor of the modelled structure are reduced by about 64, 51, and 26 percent, respectively. The stroke length of the TMDs is displayed in the following table:

Table 5-11- The Stroke Length of TMDs

	MTMD (m)	SAMTMD (m)
<i>TMD on 5th floor</i>	0.435	0.243
<i>TMD on 10th floor</i>	0.452	0.287
<i>TMD on 15th floor</i>	1.696	1.042

5.6.10. Analytical results for the modelled structure exposed to Manjil Earthquake:

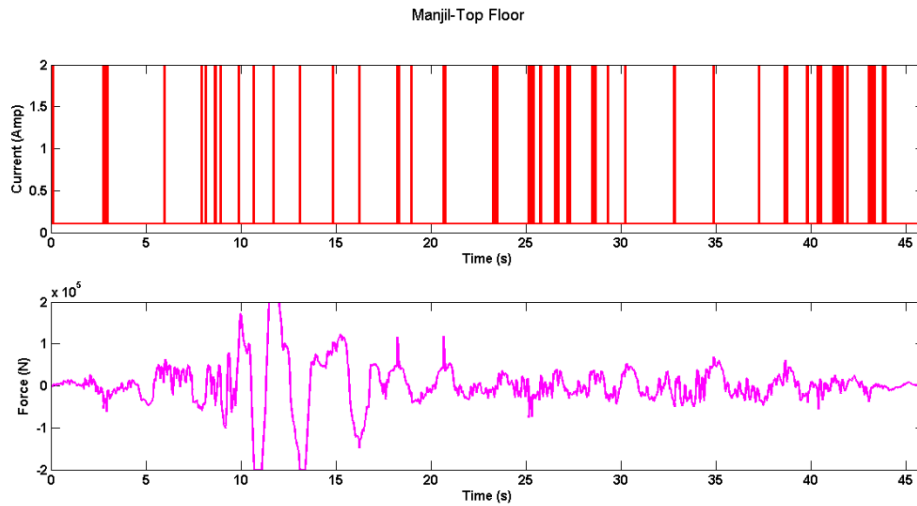


Figure 5-39 The Applied Electricity Current and Adaptive Resistance Force of the MR Damper for Manjil Earthquake

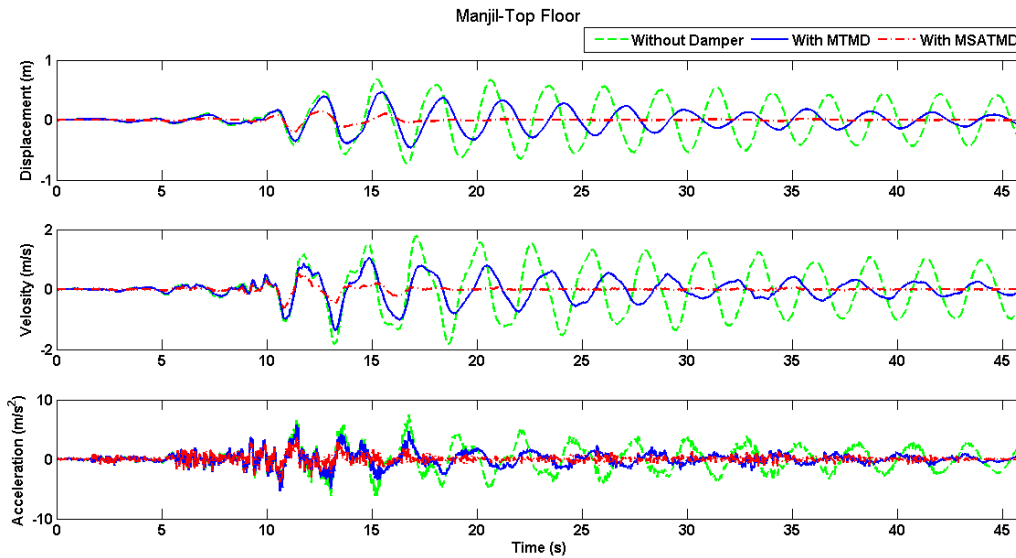


Figure 5-40- Response of the 15th floor under the Manjil Excitation

The graph above and the resulted analytical data indicate that the maximum displacement, Velocity, and acceleration on the top floor of the modelled structure are reduced by about 77, 70, and 42 percent, respectively. The stroke length of the TMDs is displayed in the following table:

Table 5-12- The Stroke Length of TMDs

	MTMD (m)	SAMTMD (m)
<i>TMD on 5th floor</i>	0.435	0.260
<i>TMD on 10th floor</i>	0.526	0.331
<i>TMD on 15th floor</i>	1.813	1.342

The following figure displays the displacement of stories of the structure under different excitation.

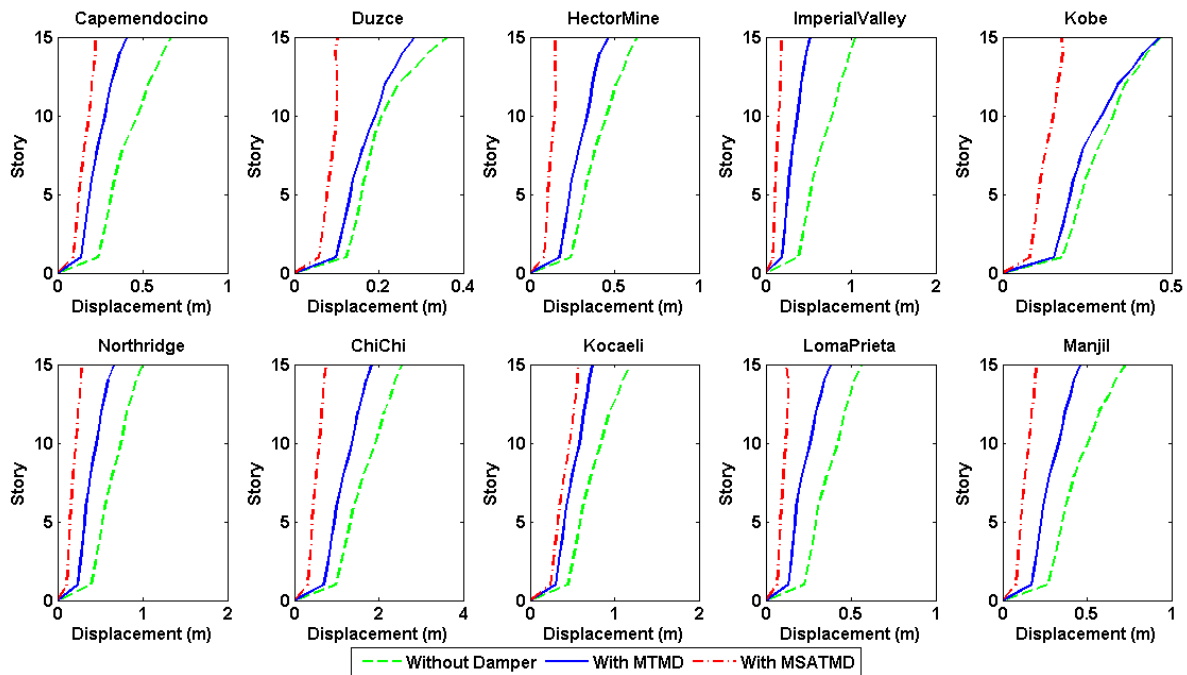


Figure 5-41 Displacement of the Structure

The following figures demonstrate that the mean and standard deviation of the displacement of the structure for 10 earthquake records have been reduced with the utilization of SAMTMDs. Furthermore, Table 5-13 displays the values of mean and standard deviation of the base shear of the structure have also decreased.

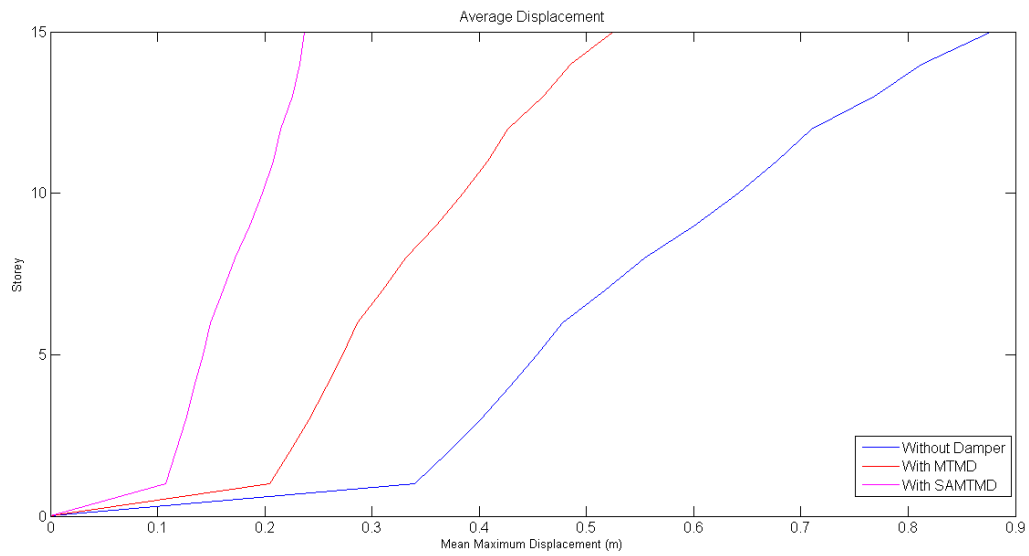


Figure 5-42 Mean Displacement of the Structure of the 10 Earthquake Records

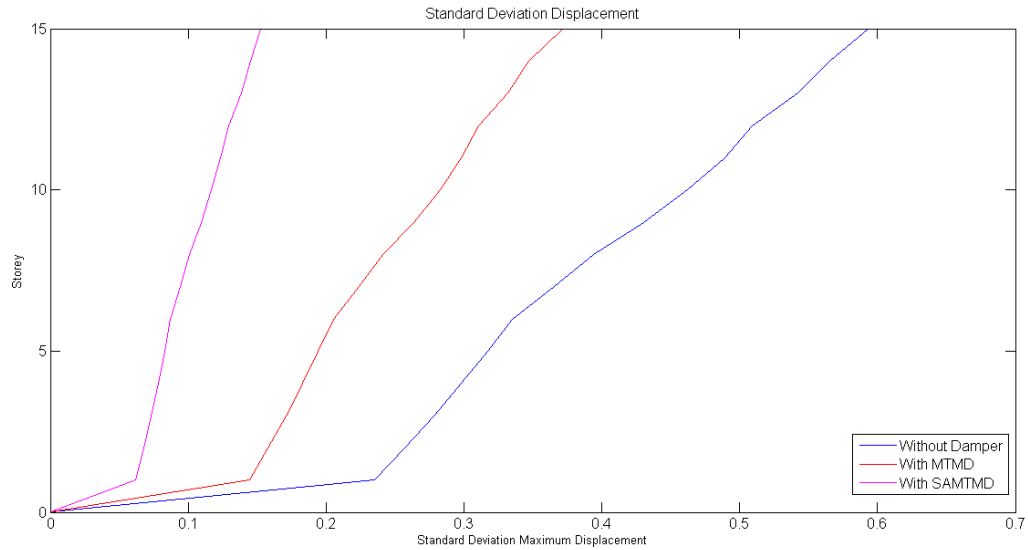


Figure 5-43 Standard Deviation of the Displacement of the Structure of the 10 Earthquake Records

Table 5-13 Mean and Standard Deviation of the Base Shear of the Structure

	Mean Value (kN)	Standard Deviation
<i>Without TMD</i>	1061852	647022.8
<i>With MTMD</i>	637824.8	357798.9
<i>With SAMTMD</i>	329514	153500.3

5.6.11. Energy Dissipation

The energy index of the signal of the system is determined using the following equation (Oppenheim et al., 1998):

$$E = \int_0^t |D(t)|^2 dt \quad (5-15)$$

Where E is the energy index of the signal, D is the displacement of the structure and t is the earthquake time. The following bar chart (Figure 5-44) displays how MTMD, and SAMTMD reduces the energy of the structure. The resulted data illustrate that the semi-active system can dissipate the energy more efficiently compared to the system equipped with MTMD.

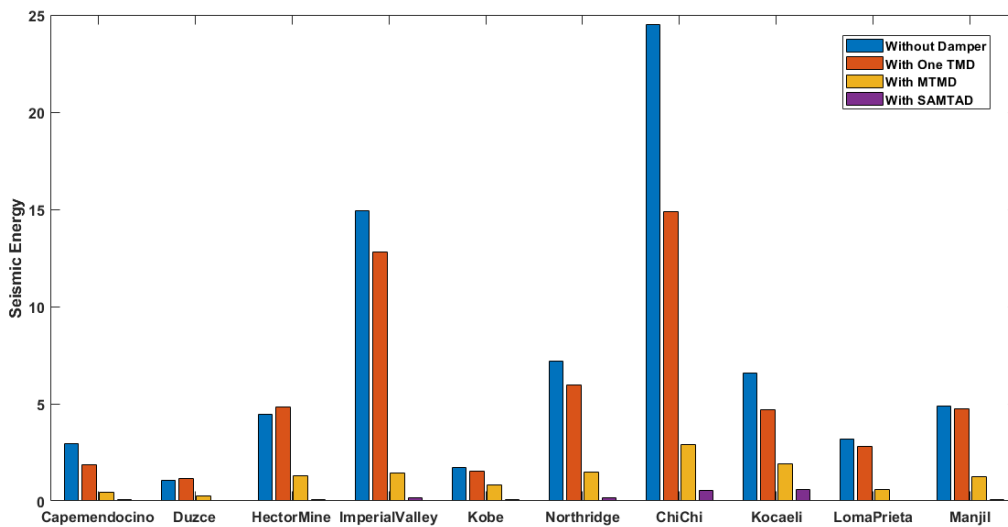


Figure 5-44 The Seismic Energy of the Structure in the Top Floor

It is observed that the system with MTMD has dissipated the induced energy index of the structure on the top floor by 77, 80, 58, 83, 77, and 79 percent for the Capemendocino, Duzce, Hector Mine, Imperial Valley, Kobe, and Northridge earthquakes, respectively. Meanwhile, in the system with

SAMTMD the energy dissipation percentages are increased by 97, 98, 96, 98, 97, and 97 for the mentioned earthquakes, respectively.

5.7.Summary

In this chapter first, the state space equation of the system with and without dampers is explained. Then, the Linear Quadratic Regression (LQR) control algorithm used in this research is discussed. Furthermore, the placement of the TMDs on different levels of the modelled structure is determined and sensitivity analysis for the distribution of the mass of the TMDs is conducted. In addition, the block diagram of the system and the model in Simulink Software, including the structure the MTMD and SAMTMD, are illustrated. Finally, the response of the structure with and without the MTMD, and SAMTMD considering the seismic demands is determined and compared.

Chapter 6: Summary and Conclusion

6.1. Summary

In this research a 15-Storey moment resisting steel structure is designed according to NBCC 2015 and CSA-S16. Then, by using MATLAB and Simulink software the structure is simulated and MTMD and SATMD systems are implemented to modelled structure.

To determine the seismic behavior of the structure equipped with the mentioned energy damping systems a set of earthquake records are applied to the modelled structure. Then, the seismic demands of the structure with and without the MTMD and SAMTMD systems are investigated. The applied earthquakes are chosen from the strongest and most destructive earthquakes which are occurred in the past.

The MTMDs that are used in this study, are a set of three tuned mass dampers which have the accumulated total mass of 2 percent of the whole structure. These TMDs are distributed on different levels of the structure in an optimized configuration based on the modal analysis of the modelled structure.

In order to improve the seismic performance of the structure a controllable adaptive MR damper, with the capacity of 200 KN, has been paired with each of the TMDs to control and enhance the seismic demands of the structure including displacement, velocity, acceleration, and energy dissipation. The MR dampers performance are commanded and controlled by a linear quadratic regression control system.

6.2. Conclusions

In this research, the analytical results have demonstrated that the MTMD has improved the seismic demands of the simulated structure. Furthermore, by adding the controlled adaptive MR dampers, paired with the MTMD, the combined energy dissipating system is concerted to a semi-active multiple tuned mass dampers (SAMTMD). This combined damping system has notably enhanced the seismic response of the system exposed to the 6 selected harsh earthquakes decreasing displacement, velocity, acceleration, and seismic energy of the structure.

The comparative analyses using the data acquired from the MATLAB and Simulink software have illustrated the following achievement.

- It is observed that by equipping the structure with the MTMD energy dissipating system, the average maximum seismic displacement, velocity demands are decreased by about 27, 29, and 14 percent, respectively. Meanwhile, the induced vibration energy of the top floor is reduced by about 76 percent.
- The analytical results illustrate that by installing MR dampers paired with each TMD, the structure would have a notable effective energy dissipating system that mitigates the seismic demands of the structure including the average of maximum displacement, maximum velocity, maximum acceleration, and vibration energy of the top floor by about 67, 61, 35, and 97 percent, respectively.

- The results display that although the earthquakes have different characteristics pattern and durations, both MTMD and SAMTMD work efficiently exposed to the applied earthquakes.
- The superior performance of the SAMTMD as compared to MTMD shows that the MR dampers controlled with the LQR control system can be properly set and matched with the Tuned Mass Dampers. This leads to an excellent performance of the combined energy damping system.
- The results indicate that the method of placement of the dampers based on the modal analysis is an efficient method for optimizing the damper location.
- Another advantage of the system is that the system works using a small amount of external energy which can be provided by batteries. Therefore, this system can be operational in harsh conditions such as electrical outage that may occur during an earthquake.

6.3.Scope for Future Work

For the future researches the followings are suggested:

- Other types of control system such as Fuzzy Logic, Neural Networks, etc. can be utilized to command and control the behavior of the SAMTMD system.
- A method of optimization could be proposed for the tuning of the parameters of the tuned mass dampers in the structure such as Genetic Algorithm, Neural Networks, Cellular Automata, etc.

- Larger number of earthquakes including near-field and far-field records could be applied to the system to investigate the performance of the energy damping system and structural response.

Reference

- Al Atik, L., & Abrahamson, N. (2010). An improved method for nonstationary spectral matching. *Earthquake Spectra*, 26(3), 601-617.
- Barnett, S., & Storey, C. (1967). Analysis and synthesis of stability matrices. *Journal of Differential Equations*, 3(3), 414-422.
- Barnett, S., & Storey, C. (1968). Some results on the sensitivity and synthesis of asymptotically stable linear and non-linear systems. *Automatica*, 4(4), 187-194.
- Bathaei, A., Zahrai, S. M., & Ramezani, M. (2018). Semi-active seismic control of an 11-DOF building model with TMD+ MR damper using type-1 and-2 fuzzy algorithms. *Journal of Vibration and Control*, 24(13), 2938-2953.
- Berberian, M., Qorashi, M., Jackson, J., Priestley, K., & Wallace, T. (1992). The Rudbar-Tarom earthquake of 20 June 1990 in NW Persia: preliminary field and seismological observations, and its tectonic significance. *Bulletin of the seismological society of America*, 82(4), 1726-1755.
- Bozer, A., & Özsarıyıldız, Ş. S. (2018). Free parameter search of multiple tuned mass dampers by using artificial bee colony algorithm. *Structural Control and Health Monitoring*, 25(2), e2066.
- Casciati, F., Magonette, G., & Marazzi, F. (2006). *Technology of semiactive devices and applications in vibration mitigation*: John Wiley & Sons.
- Casciati, S., & Chen, Z. (2012). An active mass damper system for structural control using real-time wireless sensors. *Structural Control and Health Monitoring*, 19(8), 758-767.
- Cheng, F. Y., Jiang, H., & Lou, K. (2008). *Smart structures: innovative systems for seismic response control*: CRC press.
- Constantinou, M. C., Soong, T. T., & Dargush, G. F. (1998). Passive energy dissipation systems for structural design and retrofit.

- Doocy, S., Daniels, A., Packer, C., Dick, A., & Kirsch, T. D. (2013). The human impact of earthquakes: a historical review of events 1980-2009 and systematic literature review. *PLoS currents*, 5.
- Duputel, Z., Rivera, L., Kanamori, H., & Hayes, G. (2012). W phase source inversion for moderate to large earthquakes (1990–2010). *Geophysical Journal International*, 189(2), 1125-1147.
- Esteki, K., Bagchi, A., & Sedaghati, R. (2011). Semi-active tuned mass damper for seismic applications. *Smart materials, structures & NDT in aerospace*.
- FEMA. (2009) Quantification of Building Seismic Performance Factors. Federal Emergency Management Agency.
- Fu, T. S., & Johnson, E. A. (2009). *Control strategies for a distributed mass damper system*. Paper presented at the American Control Conference, 2009. ACC'09.
- Gamota, D., & Filisko, F. (1991). Dynamic mechanical studies of electrorheological materials: moderate frequencies. *Journal of rheology*, 35(3), 399-425.
- Han, B., & Li, C. (2006). Seismic response of controlled structures with active multiple tuned mass dampers. *Earthquake Engineering and Engineering Vibration*, 5(2), 205-213.
- Hrovat, D., Barak, P., & Rabins, M. (1983). Semi-active versus passive or active tuned mass dampers for structural control. *Journal of engineering mechanics*, 109(3), 691-705.
- Iqbal, M. F. (2009). *Application of magneto-rheological dampers to control dynamic response of buildings*. Concordia University.
- Kalman, R. E. (1960). Contributions to the theory of optimal control. *Bol. Soc. Mat. Mexicana*, 5(2), 102-119.
- Kanamori, H., & Anderson, D. L. (1975). Theoretical basis of some empirical relations in seismology. *Bulletin of the seismological society of America*, 65(5), 1073-1095.
- Langenheim, V., Wright, T., Okaya, D., Yeats, R., Fuis, G., Thygesen, K., & Thybo, H. (2011). Structure of the San Fernando Valley region, California: Implications for seismic hazard and tectonic history. *Geosphere*, 7(2), 528-572.
- Lewandowski, R., & Grzymisławska, J. (2009). Dynamic analysis of structures with multiple tuned mass dampers. *Journal of Civil Engineering and Management*, 15(1), 77-86.
- Li, C., & Zhu, B. (2007). Investigation of response of systems with active multiple tuned mass dampers. *Structural Control and Health Monitoring: The Official Journal of the International Association for Structural Control and Monitoring and of the European Association for the Control of Structures*, 14(8), 1138-1154.
- Lin, C.-C., Lin, G.-L., & Chiu, K.-C. (2017). Robust design strategy for multiple tuned mass dampers with consideration of frequency bandwidth. *International Journal of Structural Stability and Dynamics*, 17(01), 1750002.
- Lin, P., Chung, L., & Loh, C. (2005). Semiactive control of building structures with semiactive tuned mass damper. *Computer-Aided Civil and Infrastructure Engineering*, 20(1), 35-51.
- Lu, L.-Y. (2001). Discrete-time modal control for seismic structures with active bracing system. *Journal of Intelligent Material Systems and Structures*, 12(6), 369-381.
- Malekghasemi, H., Ashasi-Sorkhabi, A., Ghaemmaghami, A. R., & Mercan, O. (2015). Experimental and numerical investigations of the dynamic interaction of tuned liquid damper–structure systems. *Journal of Vibration and Control*, 21(14), 2707-2720.
- Matta, E., & De Stefano, A. (2009). Seismic performance of pendulum and translational roof-garden TMDs. *Mechanical Systems and Signal Processing*, 23(3), 908-921.

- McNamara, R. J. (1977). Tuned mass dampers for buildings. *Journal of the Structural Division*, 103(9), 1785-1798.
- Miller, R., Masri, S., Deghanyar, T., & Caughey, T. (1988). Active vibration control of large civil structures. *Journal of engineering mechanics*, 114(9), 1542-1570.
- Nasir, A. N. K., Ahmad, M. A., & Rahmat, M. F. a. (2008). *Performance comparison between LQR and PID controllers for an inverted pendulum system*. Paper presented at the AIP Conference Proceedings.
- Nigdeli, S., & Boduroglu, M. (2010). *Active Tendons for Seismic Control of Buildings*. Paper presented at the International Conference on Mechanical Science and Engineering.
- Nolen-Hoeksema, S., & Morrow, J. (1991). A prospective study of depression and posttraumatic stress symptoms after a natural disaster: the 1989 Loma Prieta Earthquake. *Journal of personality and social psychology*, 61(1), 115.
- Oppenheim, A. V., Willsky, A. S., & Nawab, S. H. (1998). *Señales y sistemas*: Pearson Educación.
- PEER Ground Motion Database. (2018). Retrieved from <https://ngawest2.berkeley.edu/site>
- Pisal, A. Y., & Jangid, R. (2016). Dynamic response of structure with tuned mass friction damper. *International Journal of Advanced Structural Engineering*, 8(4), 363-377.
- Pohoryles, D. A., & Duffour, P. (2015). Adaptive control of structures under dynamic excitation using magnetorheological dampers: an improved clipped-optimal control algorithm. *Journal of Vibration and Control*, 21(13), 2569-2582.
- Poynor, J. C. (2001). *Innovative designs for magneto-rheological dampers*. Virginia Tech.
- Reinhorn, A. M., Soong, T. T., Lin, R., Riley, M. A., Wang, Y., Aizawa, S., & Higashino, M. (1992). Active bracing system: a full scale implementation of active control. *National Center for Earthquake Engineering Research*. 14 Aug. 1992. Buffalo. US.
- Sapiński, B., & Filuś, J. (2003). Analysis of parametric models of MR linear damper. *Journal of Theoretical and Applied Mechanics*, 41(2), 215-240.
- Shames, I. H. (1997). *Elastic and inelastic stress analysis*: CRC Press.
- Singh, M. P., Singh, S., & Moreschi, L. M. (2002). Tuned mass dampers for response control of torsional buildings. *Earthquake engineering & structural dynamics*, 31(4), 749-769.
- Spencer Jr, B., Dyke, S., Sain, M., & Carlson, J. (1997). Phenomenological model for magnetorheological dampers. *Journal of engineering mechanics*, 123(3), 230-238.
- Stanway, R., Sproston, J., & Stevens, N. (1985). Non-linear identification of an electro-rheological vibration damper. *IFAC Proceedings Volumes*, 18(5), 195-200.
- Stanway, R., Sproston, J., & Stevens, N. (1987). Non-linear modelling of an electro-rheological vibration damper. *Journal of Electrostatics*, 20(2), 167-184.
- Symans, M. D., & Constantinou, M. C. (1997). Seismic testing of a building structure with a semi-active fluid damper control system. *Earthquake engineering & structural dynamics*, 26(7), 759-777.
- Symans, M. D., & Constantinou, M. C. (1999). Semi-active control systems for seismic protection of structures: a state-of-the-art review. *Engineering structures*, 21(6), 469-487.
- Toda, S., Stein, R. S., Reasenber, P. A., Dieterich, J. H., & Yoshida, A. (1998). Stress transferred by the 1995 Mw= 6.9 Kobe, Japan, shock: Effect on aftershocks and future earthquake probabilities. *Journal of Geophysical Research: Solid Earth*, 103(B10), 24543-24565.

- Wang, S.-J., Lee, B.-H., Chuang, W.-C., Chiu, I.-C., & Chang, K.-C. (2019). Building mass damper design based on optimum dynamic response control approach. *Engineering structures*, 187, 85-100.
- Warburton, G. (1982). Optimum absorber parameters for various combinations of response and excitation parameters. *Earthquake engineering & structural dynamics*, 10(3), 381-401.
- Wen, Y.-K. (1976). Method for random vibration of hysteretic systems. *Journal of the engineering mechanics division*, 102(2), 249-263.
- Xu, K., & Igusa, T. (1992). Dynamic characteristics of multiple substructures with closely spaced frequencies. *Earthquake engineering & structural dynamics*, 21(12), 1059-1070.
- Xu, Z.-D., Huang, X.-H., Xu, F.-H., & Yuan, J. (2019). Parameters optimization of vibration isolation and mitigation system for precision platforms using non-dominated sorting genetic algorithm. *Mechanical Systems and Signal Processing*, 128, 191-201.
- Yamamoto, M., & Sone, T. (2014). Behavior of active mass damper (AMD) installed in high-rise building during 2011 earthquake off Pacific coast of Tohoku and verification of regenerating system of AMD based on monitoring. *Structural Control and Health Monitoring*, 21(4), 634-647.
- Yang, G., Spencer Jr, B., Carlson, J., & Sain, M. (2002). Large-scale MR fluid dampers: modeling and dynamic performance considerations. *Engineering structures*, 24(3), 309-323.
- Zhu, X., Jing, X., & Cheng, L. (2012). Magnetorheological fluid dampers: A review on structure design and analysis. *Journal of Intelligent Material Systems and Structures*, 23(8), 839-873.

Appendix I: Analytical Results of the Structure on Floors of Existing Dampers

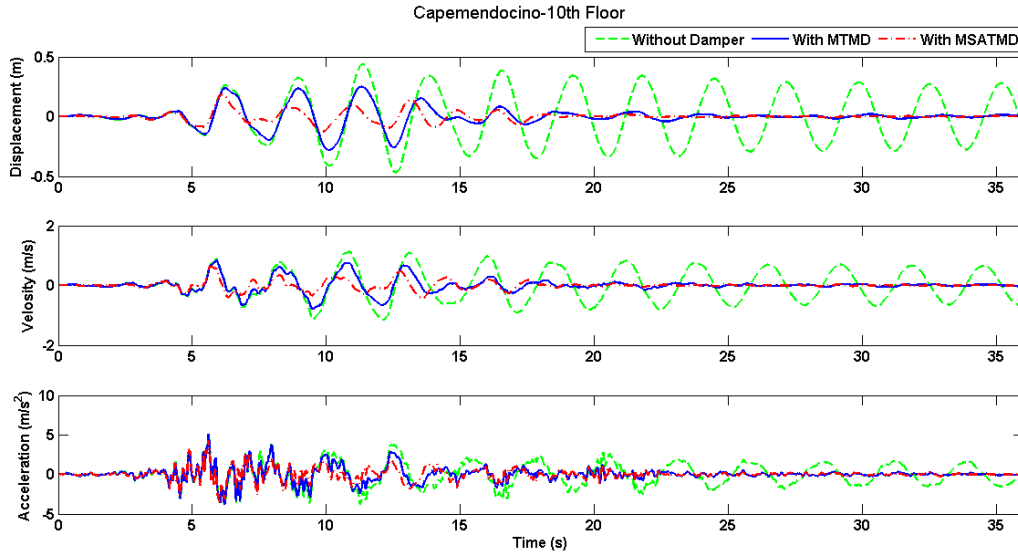


Figure 6-1 -Response of the 10th floor under the Capmendocino Excitation

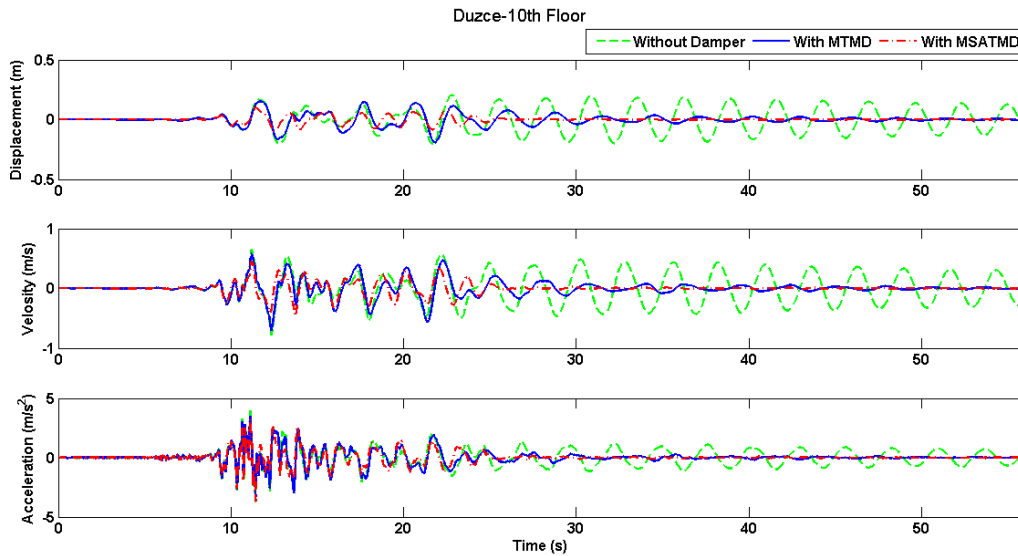


Figure 6-2- Response of the 10th floor under the Duzce Excitation

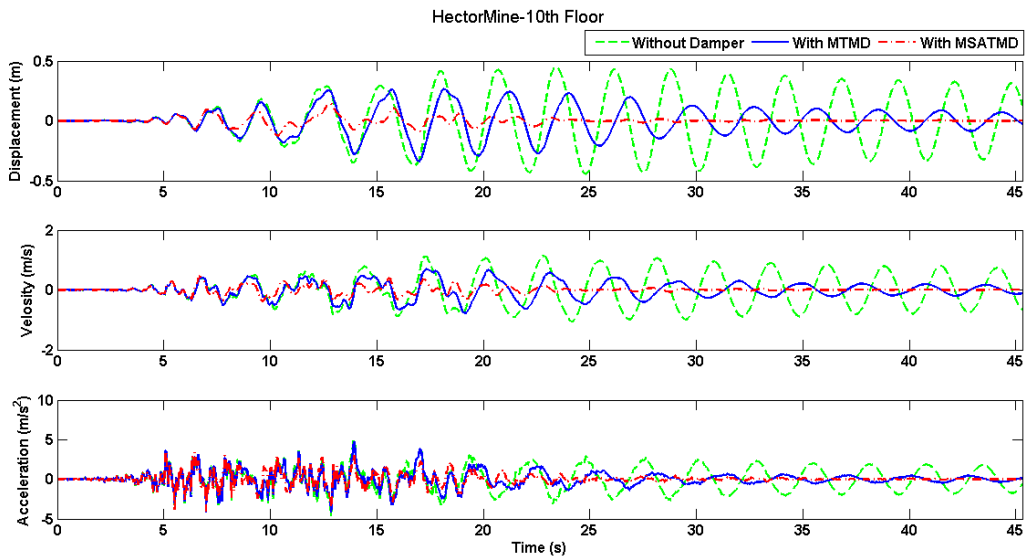


Figure 6-3- Response of the 10th floor under the Hector Mine Excitation

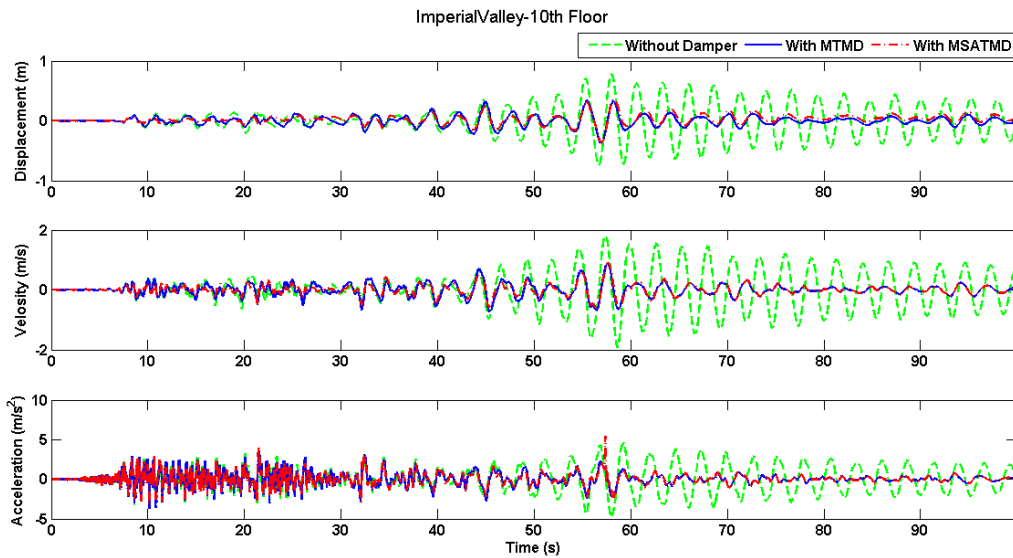


Figure 6-4- Response of the 10th floor under the Imperial Valley Excitation

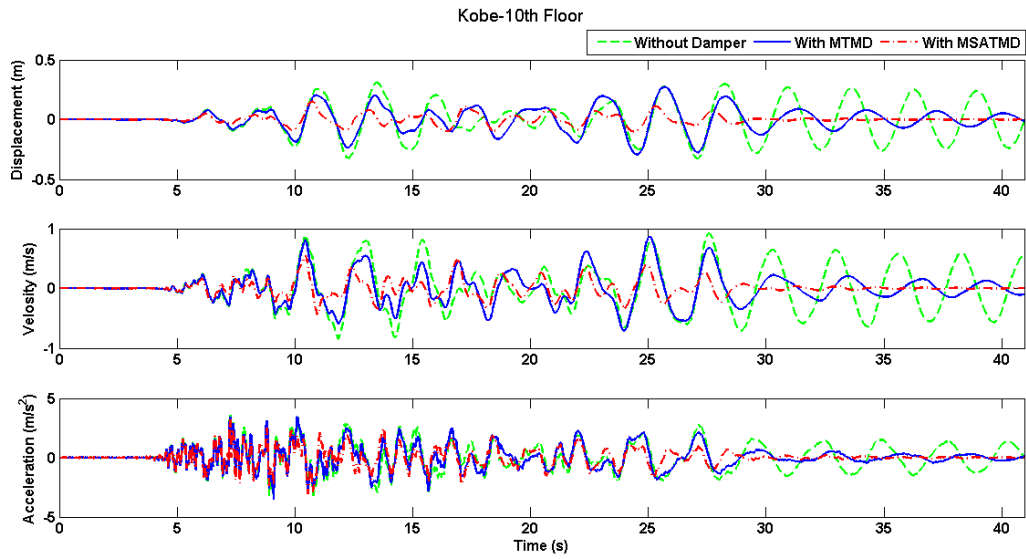


Figure 6-5- Response of the 10th floor under the Kobe Excitation

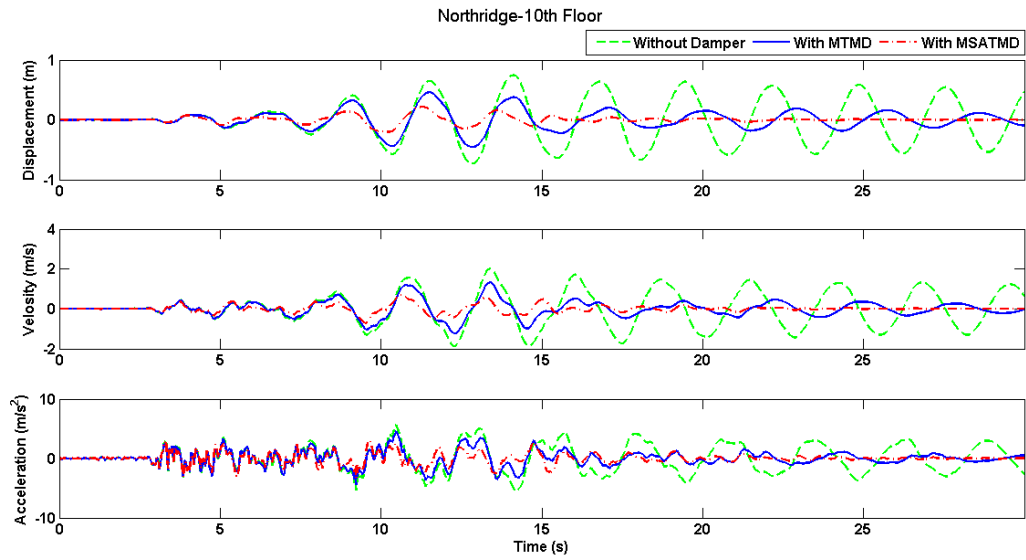


Figure 6-6- Response of the 10th floor under the Northridge Excitation

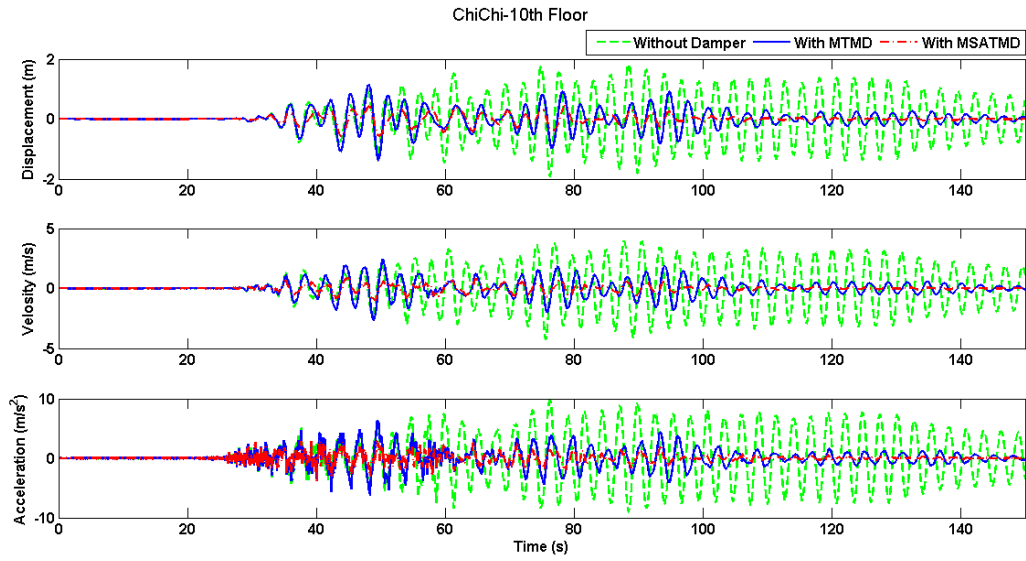


Figure 6-7- Response of the 10th floor under the Chi-Chi Excitation

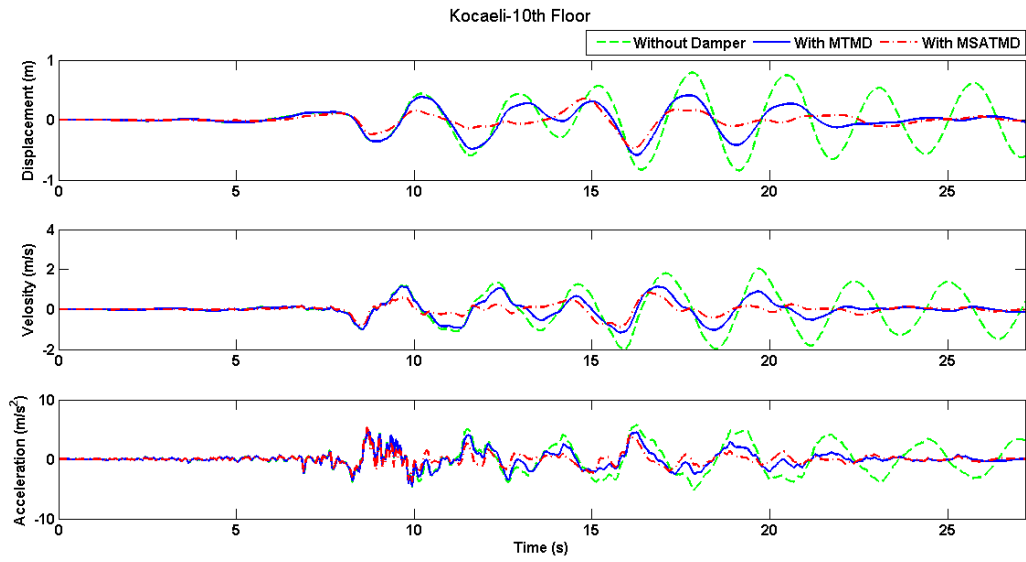


Figure 6-8- Response of the 10th floor under the Kocaeli Excitation

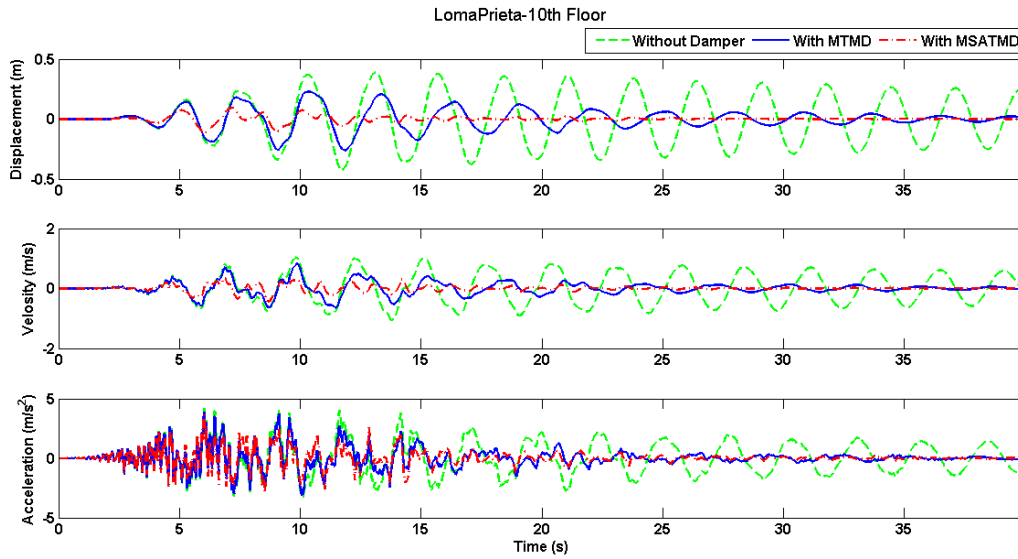


Figure 6-9- Response of the 10th floor under the Loma Prieta Excitation

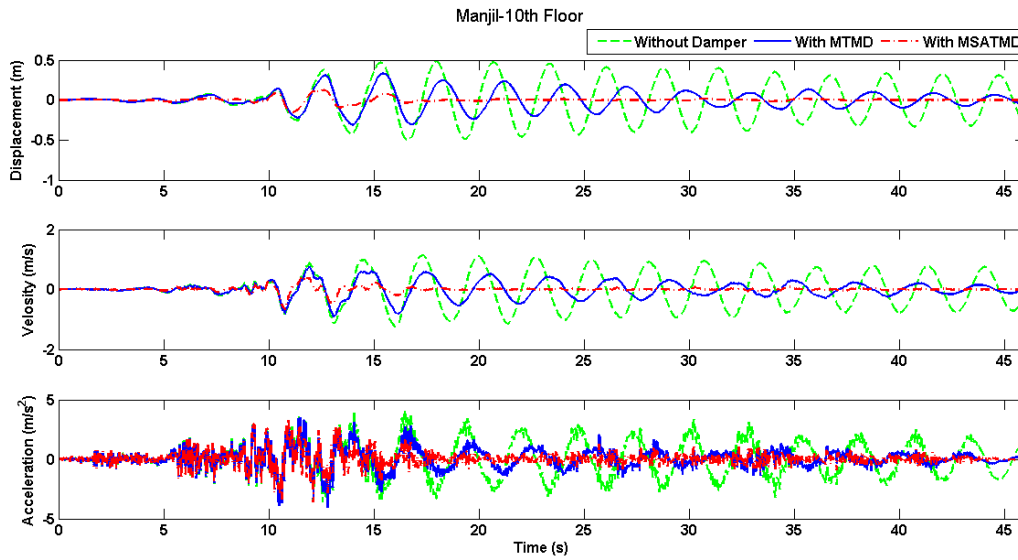


Figure 6-10- Response of the 10th floor under the Manjil Excitation

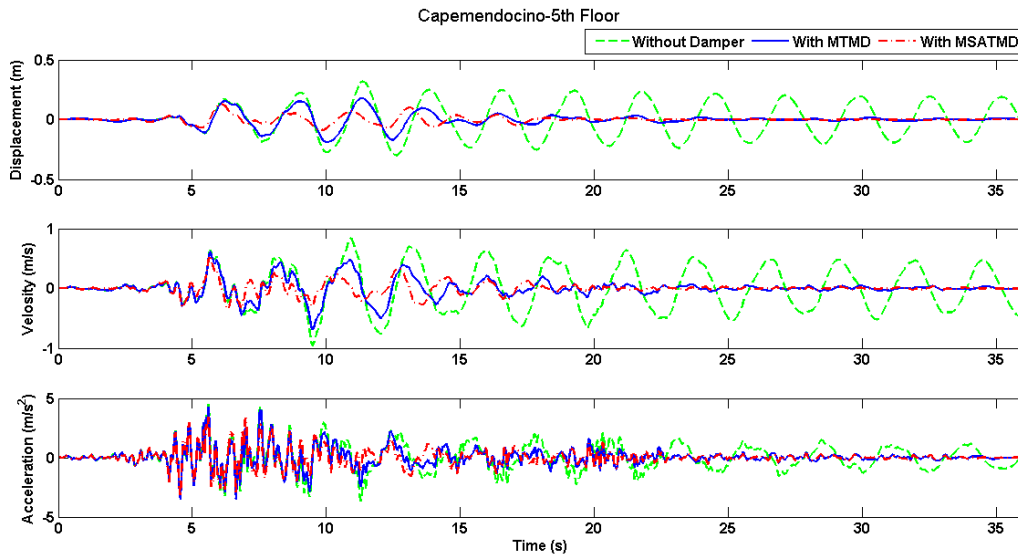


Figure 6-11- Response of the 5th floor under the Capemendocino Excitation

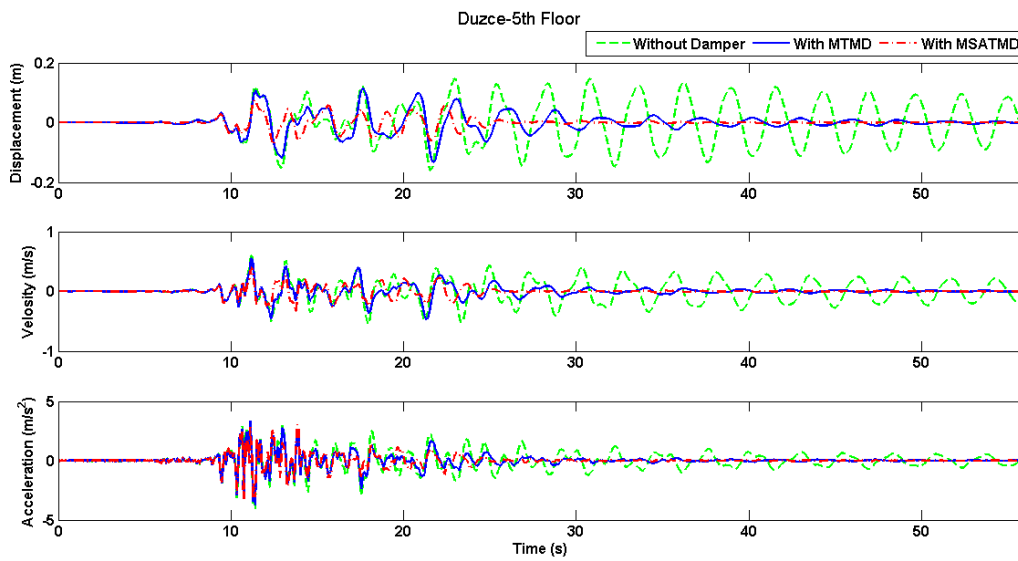


Figure 6-12- Response of the 5th floor under the Duzce Excitation

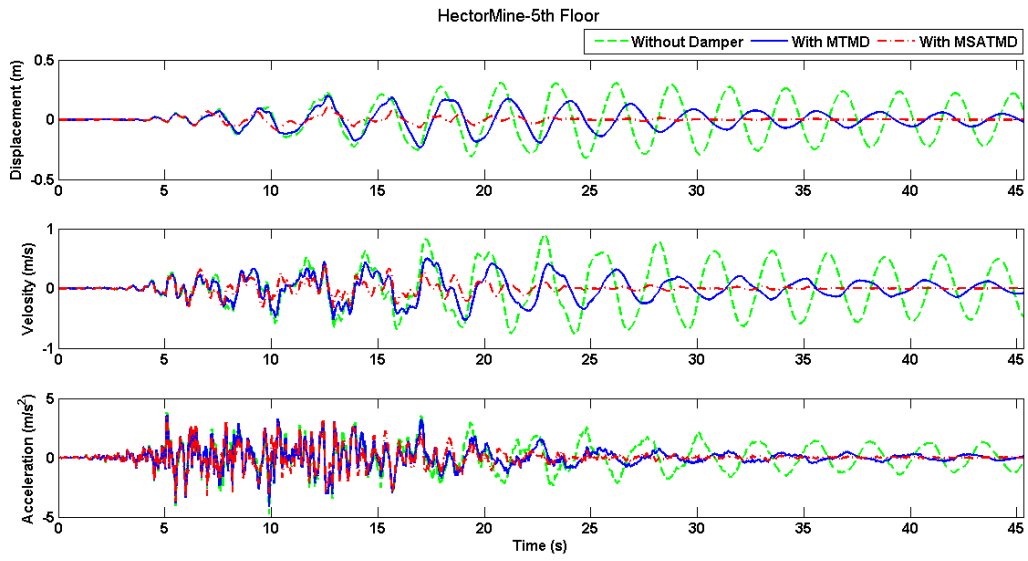


Figure 6-13- Response of the 5th floor under the Hector Mine Excitation

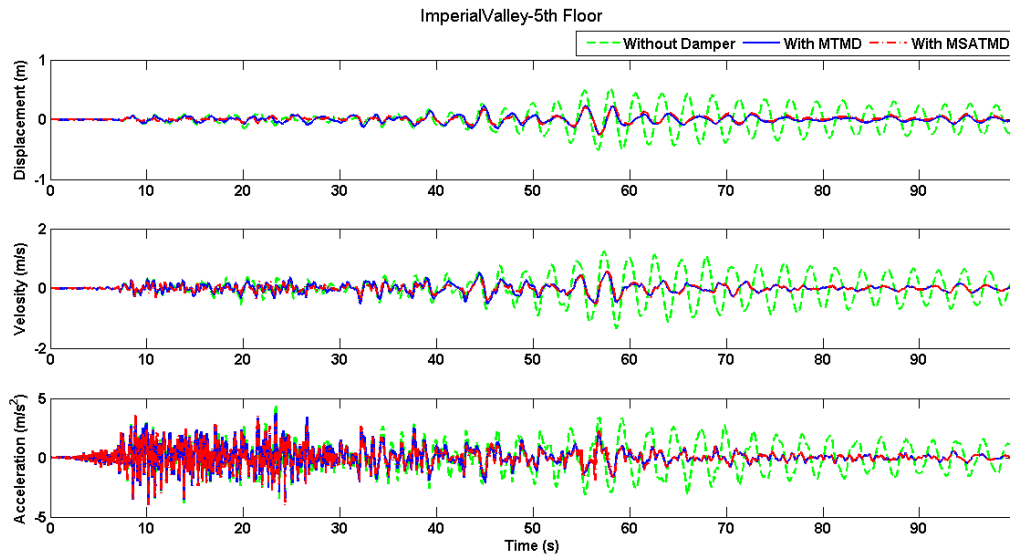


Figure 6-14- Response of the 5th floor under the Imperial Valley Excitation

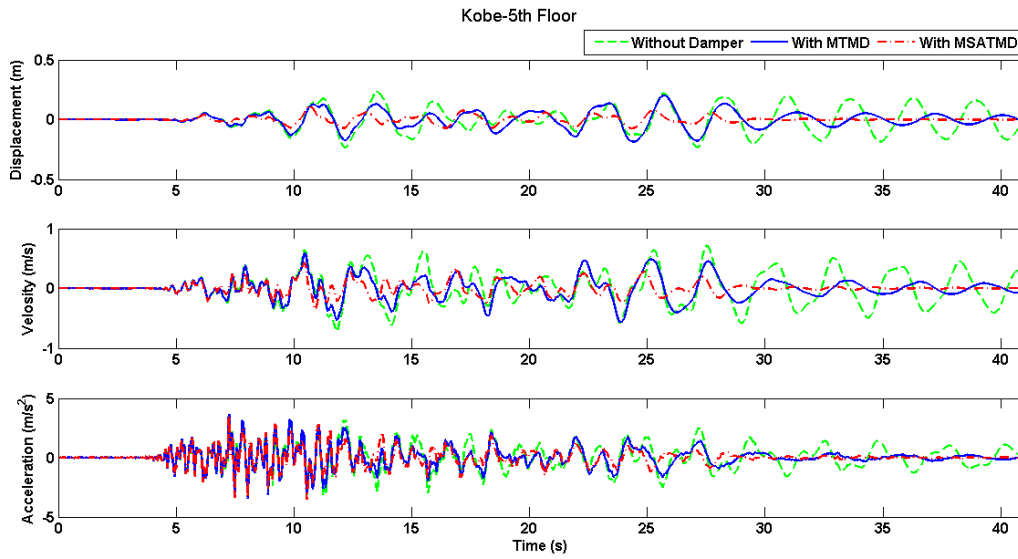


Figure 6-15- Response of the 5th floor under the Kobe Excitation

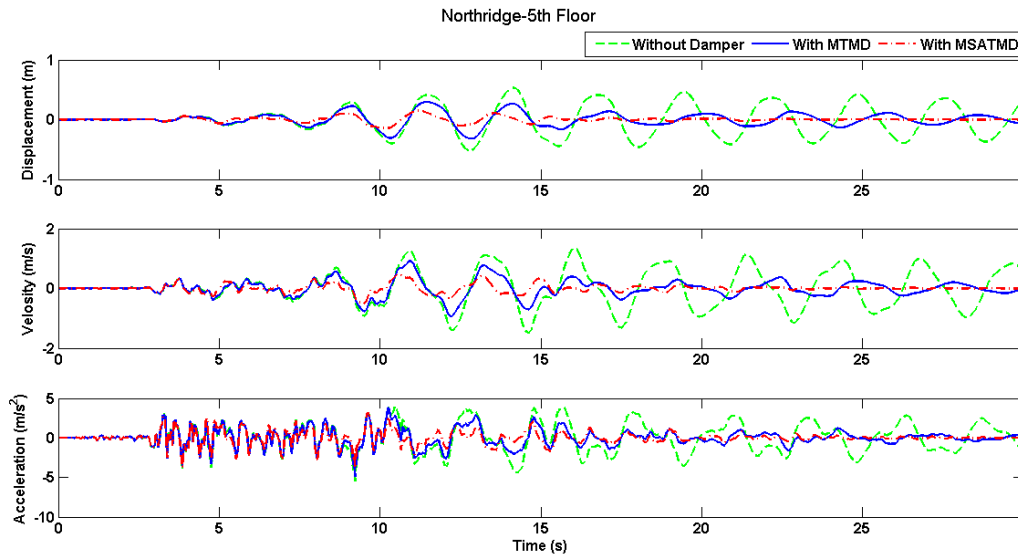


Figure 6-16- Response of the 5th floor under the Northridge Excitation

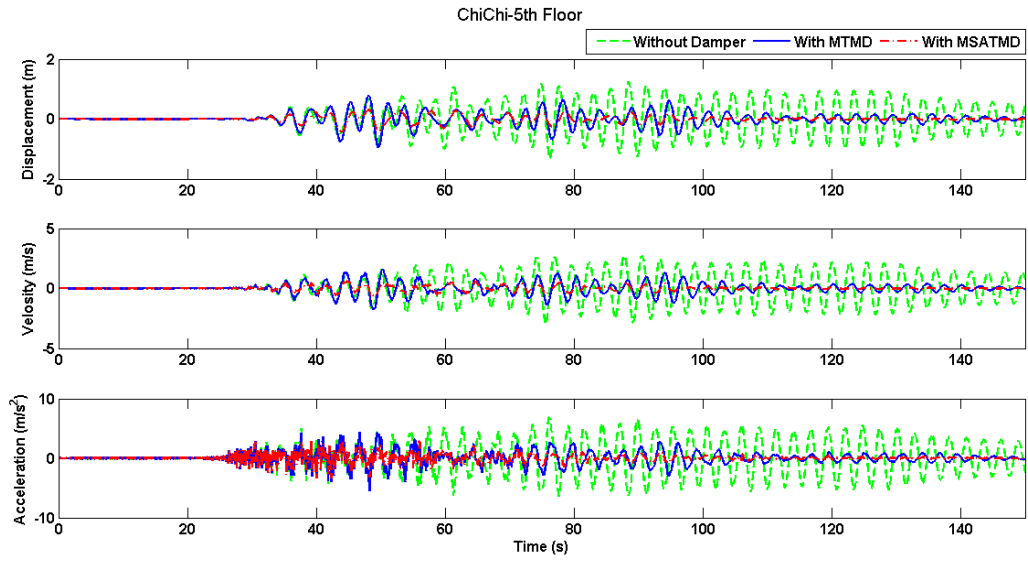


Figure 6-17- Response of the 5th floor under the Chi-Chi Excitation

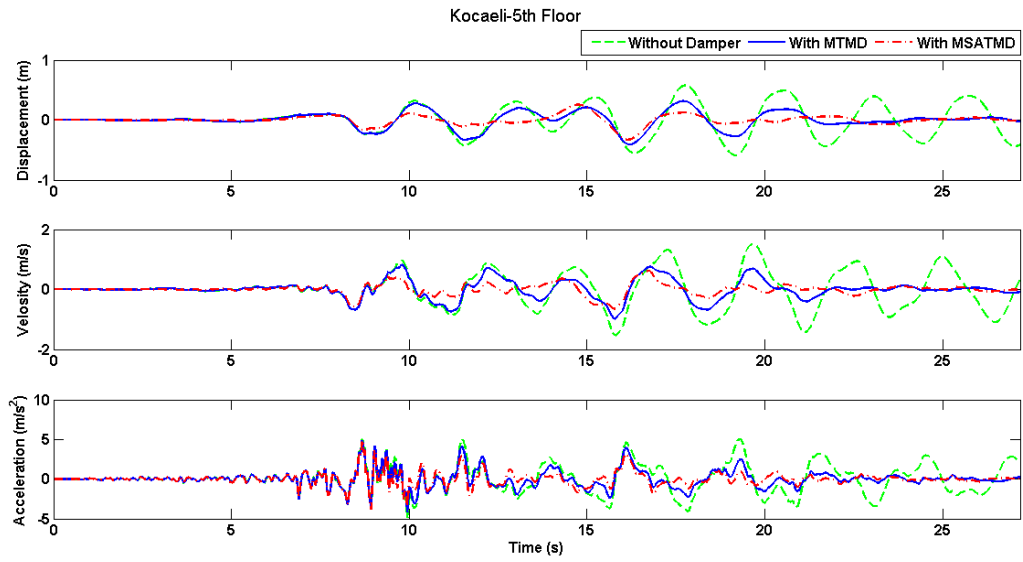


Figure 6-18- Response of the 5th floor under the Kocaeli Excitation

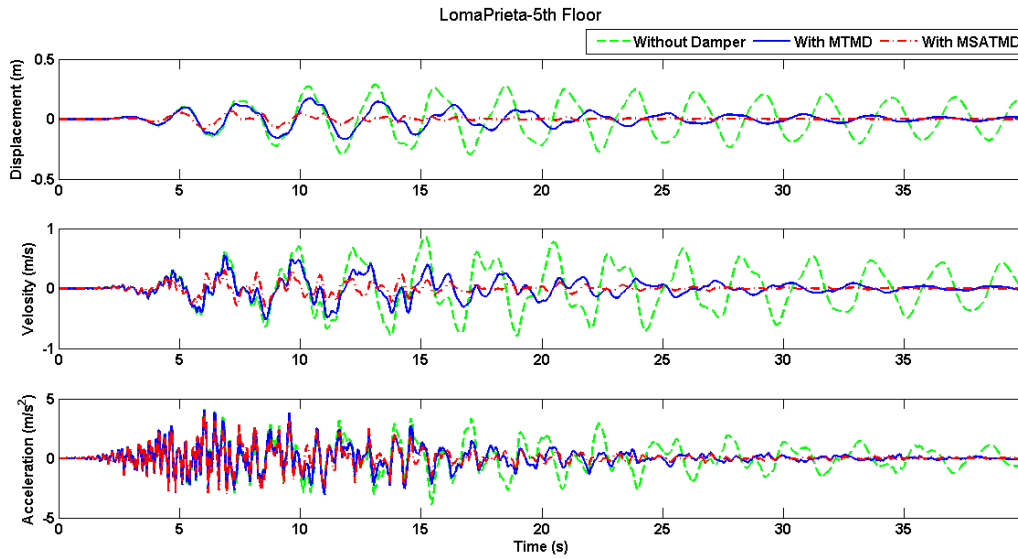


Figure 6-19- Response of the 5th floor under the Loma Prieta Excitation

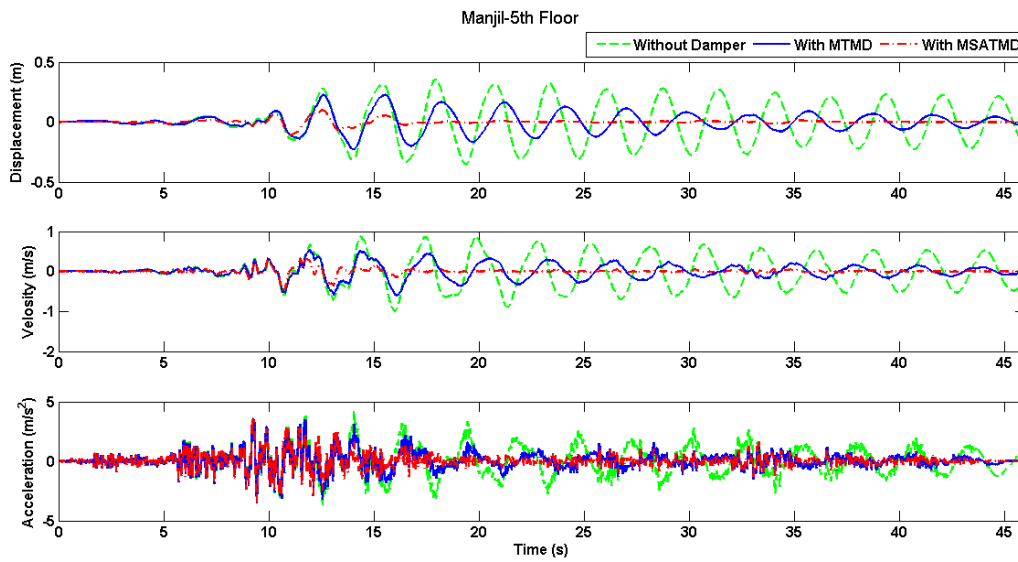


Figure 6-20- Response of the 5th floor under the Manjil Excitation

Appendix II: Analytical Results of the Structure on Different Floors

Table 6-1-Maximum Displacement of Structure under the Capmendocino Earthquake

<i>Floor</i>	Without Damper	With MTMD	With SAMTMD
<i>1</i>	0.114	0.064	0.059
<i>2</i>	0.124	0.069	0.065
<i>3</i>	0.133	0.074	0.071
<i>4</i>	0.141	0.079	0.076
<i>5</i>	0.149	0.083	0.082
<i>6</i>	0.156	0.086	0.087
<i>7</i>	0.167	0.097	0.096
<i>8</i>	0.179	0.109	0.104
<i>9</i>	0.196	0.124	0.112
<i>10</i>	0.211	0.138	0.119
<i>11</i>	0.225	0.149	0.123
<i>12</i>	0.236	0.160	0.126
<i>13</i>	0.256	0.184	0.135
<i>14</i>	0.276	0.213	0.139
<i>15</i>	0.311	0.267	0.143

Table 6-2- Maximum Displacement of Structure under the Duzce Earthquake

<i>Floor</i>	Without Damper	With MTMD	With SAMTMD
<i>1</i>	0.263	0.187	0.120
<i>2</i>	0.286	0.204	0.131
<i>3</i>	0.309	0.219	0.141
<i>4</i>	0.329	0.233	0.149
<i>5</i>	0.349	0.245	0.156
<i>6</i>	0.368	0.254	0.163
<i>7</i>	0.401	0.269	0.173
<i>8</i>	0.430	0.281	0.181
<i>9</i>	0.468	0.296	0.188
<i>10</i>	0.503	0.315	0.193
<i>11</i>	0.533	0.334	0.196
<i>12</i>	0.559	0.353	0.198
<i>13</i>	0.604	0.381	0.201
<i>14</i>	0.638	0.402	0.205
<i>15</i>	0.687	0.430	0.207

Table 6-3- Maximum Displacement of Structure under the Hector Mine Earthquake

<i>Floor</i>	Without Damper	With MTMD	With SAMTMD
<i>1</i>	0.082	0.070	0.034
<i>2</i>	0.089	0.077	0.037
<i>3</i>	0.096	0.083	0.040
<i>4</i>	0.102	0.089	0.042
<i>5</i>	0.108	0.095	0.045
<i>6</i>	0.113	0.100	0.047
<i>7</i>	0.122	0.109	0.051
<i>8</i>	0.130	0.118	0.054
<i>9</i>	0.139	0.129	0.057

10	0.147	0.139	0.059
11	0.154	0.147	0.061
12	0.159	0.153	0.061
13	0.177	0.166	0.060
14	0.194	0.177	0.059
15	0.216	0.197	0.056

Table 6-4- Maximum Displacement of Structure under the Imperial Valley Earthquake

<i>Floor</i>	Without Damper	With MTMD	With SAMTMD
1	0.228	0.138	0.064
2	0.250	0.151	0.070
3	0.270	0.163	0.075
4	0.290	0.175	0.081
5	0.309	0.187	0.085
6	0.327	0.197	0.090
7	0.359	0.215	0.098
8	0.388	0.232	0.105
9	0.426	0.254	0.115
10	0.460	0.274	0.125
11	0.490	0.290	0.133
12	0.514	0.304	0.140
13	0.555	0.328	0.151
14	0.584	0.346	0.157
15	0.621	0.374	0.160

Table 6-5- Maximum Displacement of Structure under the Kobe Earthquake

<i>Floor</i>	Without Damper	With MTMD	With SAMTMD
1	0.182	0.107	0.066
2	0.199	0.118	0.072
3	0.215	0.128	0.078
4	0.231	0.138	0.084
5	0.245	0.147	0.090
6	0.258	0.156	0.095

7	0.281	0.172	0.104
8	0.301	0.187	0.112
9	0.327	0.206	0.121
10	0.349	0.223	0.128
11	0.367	0.234	0.131
12	0.380	0.243	0.133
13	0.400	0.254	0.134
14	0.411	0.261	0.131
15	0.423	0.284	0.117

Table 6-6- Maximum Displacement of Structure under the Northridge Earthquake

<i>Floor</i>	Without Damper	With MTMD	With SAMTMD
1	0.240	0.140	0.111
2	0.262	0.153	0.121
3	0.281	0.164	0.131
4	0.299	0.177	0.141
5	0.315	0.190	0.150
6	0.328	0.201	0.159
7	0.350	0.222	0.174
8	0.368	0.242	0.187
9	0.388	0.269	0.204
10	0.405	0.293	0.217
11	0.421	0.312	0.225
12	0.438	0.327	0.230
13	0.482	0.355	0.236
14	0.526	0.380	0.245
15	0.599	0.423	0.262

Table 6-7- Maximum Displacement of Structure under the Chi-Chi Earthquake

<i>Floor</i>	Without Damper	With MTMD	With SAMTMD
1	0.337	0.191	0.076
2	0.369	0.208	0.083
3	0.399	0.225	0.090

4	0.427	0.241	0.096
5	0.454	0.257	0.101
6	0.480	0.271	0.107
7	0.524	0.295	0.115
8	0.565	0.318	0.123
9	0.616	0.347	0.132
10	0.663	0.373	0.140
11	0.704	0.395	0.147
12	0.737	0.413	0.153
13	0.792	0.445	0.160
14	0.832	0.468	0.163
15	0.884	0.504	0.161

Table 6-8- Maximum Displacement of Structure under the Kocaeli Earthquake

<i>Floor</i>	Without Damper	With MTMD	With SAMTMD
1	0.196	0.155	0.114
2	0.213	0.169	0.124
3	0.229	0.182	0.134
4	0.244	0.194	0.143
5	0.257	0.205	0.151
6	0.268	0.215	0.159
7	0.285	0.231	0.172
8	0.299	0.245	0.183
9	0.315	0.262	0.197
10	0.326	0.277	0.209
11	0.334	0.288	0.219
12	0.338	0.297	0.227
13	0.342	0.309	0.238
14	0.341	0.318	0.245
15	0.364	0.332	0.251

Table 6-9- Maximum Displacement of Structure under the Loma Prieta Earthquake

<i>Floor</i>	Without Damper	With MTMD	With SAMTMD
	0.100	0.089	0.062

1	0.110	0.097	0.068
2	0.118	0.104	0.073
3	0.127	0.111	0.077
4	0.134	0.117	0.081
5	0.140	0.121	0.084
6	0.154	0.129	0.089
7	0.167	0.136	0.093
8	0.184	0.146	0.098
9	0.198	0.158	0.102
10	0.211	0.168	0.105
11	0.221	0.175	0.105
12	0.238	0.184	0.104
13	0.252	0.196	0.106
14	0.285	0.222	0.102
15	0.100	0.089	0.062

Table 6-10- Maximum Displacement of Structure under the Manjil Earthquake

<i>Floor</i>	Without Damper	With MTMD	With SAMTMD
1	0.413	0.298	0.110
2	0.451	0.326	0.121
3	0.487	0.352	0.131
4	0.521	0.378	0.140
5	0.554	0.402	0.150
6	0.584	0.424	0.158
7	0.637	0.463	0.173
8	0.686	0.500	0.187
9	0.749	0.547	0.204
10	0.806	0.591	0.219
11	0.856	0.629	0.229
12	0.897	0.660	0.236
13	0.967	0.714	0.244
14	1.017	0.752	0.246
15	1.083	0.808	0.242

Table 6-11- Maximum Velocity of Structure under the Capemendocino Earthquake

<i>Floor</i>	Without Damper	With MTMD	With SAMTMD
1	0.487	0.458	0.413
2	0.528	0.496	0.450
3	0.560	0.524	0.479
4	0.582	0.542	0.501
5	0.595	0.551	0.522
6	0.600	0.554	0.536
7	0.596	0.550	0.556
8	0.586	0.538	0.561
9	0.591	0.540	0.552
10	0.615	0.621	0.577
11	0.677	0.688	0.551
12	0.711	0.717	0.539
13	0.736	0.709	0.504
14	0.842	0.678	0.461
15	0.994	0.873	0.481

Table 6-12- Maximum Velocity of Structure under the Duzce Earthquake

<i>Floor</i>	Without Damper	With MTMD	With SAMTMD
1	0.894	0.821	0.523
2	0.972	0.890	0.561
3	1.036	0.944	0.589
4	1.085	0.983	0.612
5	1.119	1.006	0.627
6	1.137	1.011	0.631
7	1.143	0.992	0.616
8	1.174	0.971	0.609
9	1.257	0.955	0.616
10	1.338	0.950	0.648
11	1.418	0.955	0.674
12	1.498	0.945	0.687
13	1.639	0.876	0.677

14	1.730	0.925	0.749
15	1.835	1.255	0.893

Table 6-13- Maximum Velocity of Structure under the Hector Mine Earthquake

<i>Floor</i>	Without Damper	With MTMD	With SAMTMD
1	0.257	0.234	0.178
2	0.279	0.252	0.188
3	0.300	0.267	0.194
4	0.317	0.278	0.197
5	0.333	0.286	0.206
6	0.345	0.289	0.216
7	0.365	0.290	0.235
8	0.379	0.295	0.254
9	0.392	0.313	0.276
10	0.406	0.326	0.285
11	0.426	0.333	0.297
12	0.441	0.332	0.310
13	0.470	0.387	0.317
14	0.562	0.454	0.302
15	0.792	0.571	0.302

Table 6-14- Maximum Velocity of Structure under the Imperial Valley Earthquake

<i>Floor</i>	Without Damper	With MTMD	With SAMTMD
1	0.568	0.342	0.170
2	0.619	0.375	0.183
3	0.668	0.407	0.192
4	0.713	0.438	0.199
5	0.755	0.468	0.206
6	0.792	0.497	0.215
7	0.854	0.549	0.230
8	0.908	0.598	0.245
9	0.975	0.663	0.268
10	1.036	0.723	0.292

11	1.103	0.772	0.304
12	1.161	0.814	0.305
13	1.264	0.890	0.290
14	1.344	0.949	0.319
15	1.464	1.050	0.398

Table 6-15- Maximum Velocity of Structure under the Kobe Earthquake

<i>Floor</i>	Without Damper	With MTMD	With SAMTMD
1	0.574	0.419	0.364
2	0.625	0.454	0.385
3	0.670	0.484	0.392
4	0.710	0.508	0.391
5	0.743	0.527	0.385
6	0.771	0.543	0.387
7	0.815	0.573	0.384
8	0.850	0.613	0.399
9	0.889	0.663	0.437
10	0.923	0.700	0.465
11	0.952	0.708	0.465
12	0.976	0.720	0.447
13	1.044	0.742	0.424
14	1.184	0.772	0.480
15	1.377	0.929	0.419

Table 6-16- Maximum Velocity of Structure under the Northridge Earthquake

<i>Floor</i>	Without Damper	With MTMD	With SAMTMD
1	0.847	0.547	0.410
2	0.921	0.596	0.450
3	0.984	0.640	0.490
4	1.037	0.679	0.527
5	1.077	0.715	0.565
6	1.105	0.749	0.602
7	1.135	0.806	0.675

8	1.142	0.857	0.743
9	1.123	0.916	0.819
10	1.079	0.968	0.863
11	1.109	1.000	0.858
12	1.129	1.024	0.849
13	1.266	1.044	0.806
14	1.446	1.011	0.724
15	1.728	1.080	0.711

Table 6-17- Maximum Velocity of Structure under the Chi-Chi Earthquake

<i>Floor</i>	Without Damper	With MTMD	With SAMTMD
1	0.760	0.342	0.171
2	0.831	0.373	0.186
3	0.899	0.403	0.199
4	0.963	0.430	0.211
5	1.025	0.456	0.220
6	1.083	0.479	0.229
7	1.185	0.519	0.243
8	1.279	0.554	0.256
9	1.401	0.610	0.278
10	1.512	0.672	0.297
11	1.609	0.727	0.309
12	1.689	0.775	0.315
13	1.827	0.866	0.327
14	1.925	0.940	0.337
15	2.056	1.067	0.334

Table 6-18- Maximum Velocity of Structure under the Kocaeli Earthquake

<i>Floor</i>	Without Damper	With MTMD	With SAMTMD
1	0.504	0.432	0.319
2	0.546	0.468	0.340

3	0.582	0.496	0.350
4	0.611	0.519	0.355
5	0.632	0.537	0.357
6	0.645	0.558	0.368
7	0.657	0.597	0.383
8	0.673	0.642	0.398
9	0.743	0.706	0.414
10	0.801	0.758	0.425
11	0.851	0.774	0.424
12	0.890	0.787	0.422
13	0.945	0.811	0.424
14	1.091	0.857	0.441
15	1.350	1.142	0.556

Table 6-19- Maximum Velocity of Structure under the Loma Prieta Earthquake

<i>Floor</i>	Without Damper	With MTMD	With SAMTMD
1	0.339	0.345	0.322
2	0.362	0.369	0.347
3	0.374	0.383	0.366
4	0.377	0.388	0.376
5	0.376	0.386	0.379
6	0.383	0.385	0.386
7	0.392	0.396	0.406
8	0.426	0.395	0.400
9	0.488	0.423	0.370
10	0.531	0.458	0.366
11	0.547	0.497	0.415
12	0.643	0.525	0.449
13	0.848	0.645	0.514
14	1.005	0.781	0.551
15	1.200	0.971	0.588

Table 6-20- Maximum Velocity of Structure under the Manjil Earthquake

<i>Floor</i>	Without Damper	With MTMD	With SAMTMD
--------------	-----------------------	------------------	--------------------

1	1.035	0.727	0.396
2	1.124	0.794	0.429
3	1.203	0.856	0.450
4	1.272	0.909	0.459
5	1.335	0.953	0.460
6	1.391	0.990	0.480
7	1.485	1.057	0.510
8	1.586	1.124	0.535
9	1.710	1.207	0.563
10	1.822	1.295	0.621
11	1.919	1.392	0.676
12	2.017	1.477	0.685
13	2.210	1.618	0.694
14	2.364	1.764	0.758
15	2.591	1.985	0.779

Table 6-21- Maximum Acceleration of Structure under the Capemendocino Earthquake

<i>Floor</i>	Without Damper	With MTMD	With SAMTMD
1	3.203	2.973	2.777
2	3.494	3.297	2.922
3	3.734	3.560	3.201
4	3.857	3.721	3.367
5	3.983	3.888	3.644
6	4.074	3.991	3.740
7	4.173	4.001	3.936
8	4.423	4.313	4.210
9	4.608	4.548	4.321
10	4.673	4.602	4.400
11	4.813	4.620	4.385
12	4.984	4.720	4.534
13	4.972	4.591	4.110
14	4.540	4.256	3.568
15	5.526	4.346	3.223

Table 6-22- Maximum Acceleration of Structure under the Duzce Earthquake

<i>Floor</i>	Without Damper	With MTMD	With SAMTMD
1	6.167	5.261	5.176
2	6.427	5.706	5.666
3	6.297	6.028	6.005
4	6.312	6.195	6.096
5	6.175	6.229	5.900
6	6.037	6.286	5.937
7	6.331	6.354	5.774
8	6.511	6.326	5.501
9	6.460	6.019	5.297
10	6.152	5.679	4.856
11	5.832	6.505	5.512
12	5.609	6.545	5.700
13	5.388	5.374	5.230
14	5.967	6.009	5.325
15	7.777	7.110	5.443

Table 6-23- Maximum Acceleration of Structure under the Hector Mine Earthquake

<i>Floor</i>	Without Damper	With MTMD	With SAMTMD
1	2.541	2.449	2.569
2	2.752	2.650	2.759
3	2.838	2.722	2.799
4	2.832	2.696	2.715
5	2.792	2.650	2.605
6	2.747	2.634	2.694
7	2.667	2.634	2.882
8	2.671	2.685	3.025
9	2.668	2.676	2.948
10	2.601	2.523	2.643
11	2.480	2.527	2.868
12	2.365	2.477	2.893
13	2.478	2.379	2.685

14	3.065	2.705	2.668
15	4.171	3.430	2.245

Table 6-24- Maximum Acceleration of Structure under the Imperial Valley Earthquake

<i>Floor</i>	Without Damper	With MTMD	With SAMTMD
1	2.398	2.846	3.203
2	2.596	3.062	3.472
3	2.656	3.104	3.569
4	2.625	3.020	3.510
5	2.577	2.898	3.308
6	2.536	2.835	3.225
7	2.481	2.670	3.009
8	2.558	2.411	2.647
9	2.735	2.298	2.647
10	2.896	2.375	2.509
11	3.038	2.468	2.540
12	3.165	2.390	2.370
13	3.448	2.222	2.915
14	3.672	2.564	3.162
15	4.114	3.370	2.444

Table 6-25- Maximum Acceleration of Structure under the Kobe Earthquake

<i>Floor</i>	Without Damper	With MTMD	With SAMTMD
1	5.281	5.531	5.807
2	5.659	5.872	6.050
3	5.807	5.946	5.907
4	5.814	5.835	5.610
5	5.712	5.685	5.296
6	5.553	5.611	5.428
7	5.323	5.572	5.801
8	5.315	5.612	5.877
9	5.572	5.596	5.414
10	5.639	5.279	4.686

11	5.495	5.365	5.337
12	5.448	5.446	5.818
13	5.965	5.635	5.418
14	5.867	5.636	5.549
15	5.487	5.530	4.837

Table 6-26- Maximum Acceleration of Structure under the Northridge Earthquake

<i>Floor</i>	Without Damper	With MTMD	With SAMTMD
1	3.621	3.362	3.385
2	3.913	3.628	3.662
3	4.167	3.784	3.920
4	4.324	3.845	3.950
5	4.472	3.841	3.774
6	4.558	3.826	3.718
7	4.593	3.673	3.674
8	4.502	3.497	3.720
9	4.247	3.393	3.692
10	3.856	3.635	4.265
11	3.844	3.714	4.084
12	3.889	3.602	3.652
13	4.644	3.753	3.289
14	5.718	3.673	3.651
15	7.200	6.176	4.347

Table 6-27- Maximum Acceleration of Structure under the Chi-Chi Earthquake

<i>Floor</i>	Without Damper	With MTMD	With SAMTMD
1	1.897	1.251	1.048
2	2.071	1.364	1.136
3	2.237	1.469	1.212
4	2.394	1.559	1.289
5	2.540	1.630	1.359
6	2.673	1.683	1.409
7	2.898	1.755	1.494

8	3.102	1.806	1.529
9	3.371	1.848	1.545
10	3.620	1.876	1.603
11	3.848	1.874	1.684
12	4.045	1.853	1.623
13	4.388	1.826	1.662
14	4.641	2.139	1.634
15	5.011	2.327	1.437

Table 6-28- Maximum Acceleration of Structure under the Kocaeli Earthquake

<i>Floor</i>	Without Damper	With MTMD	With SAMTMD
1	3.306	3.022	2.668
2	3.633	3.358	2.972
3	3.935	3.692	3.307
4	4.197	3.994	3.588
5	4.418	4.259	3.796
6	4.560	4.430	4.156
7	4.655	4.535	4.483
8	4.612	4.485	4.539
9	4.464	4.349	4.411
10	4.380	4.229	4.030
11	4.487	4.234	4.140
12	4.702	4.357	4.276
13	5.044	4.681	4.348
14	4.910	4.669	4.402
15	5.312	4.645	4.172

Table 6-29- Maximum Acceleration of Structure under the Loma Prieta Earthquake

<i>Floor</i>	Without Damper	With MTMD	With SAMTMD
1	5.046	4.855	5.642
2	5.501	5.180	5.860
3	5.842	5.370	5.834
4	6.036	5.637	5.774

5	6.160	5.839	5.743
6	6.213	6.004	6.025
7	6.086	6.060	6.156
8	5.893	5.956	5.894
9	5.425	5.483	5.745
10	5.077	5.283	5.285
11	5.426	5.813	5.575
12	5.540	5.911	5.840
13	5.744	5.672	6.139
14	6.583	6.487	6.440
15	6.685	5.836	4.934

Table 6-30- Maximum Acceleration of Structure under the Manjil Earthquake

<i>Floor</i>	Without Damper	With MTMD	With SAMTMD
<i>1</i>	5.004	4.510	4.705
<i>2</i>	5.228	4.790	4.832
<i>3</i>	5.258	5.059	4.847
<i>4</i>	5.258	5.106	5.171
<i>5</i>	5.272	4.976	5.283
<i>6</i>	5.459	5.082	5.295
<i>7</i>	5.683	5.325	5.525
<i>8</i>	5.866	5.367	5.573
<i>9</i>	6.485	5.571	5.475
<i>10</i>	6.917	5.744	5.573
<i>11</i>	7.239	6.113	5.897
<i>12</i>	7.654	6.530	6.314
<i>13</i>	8.517	6.603	6.296
<i>14</i>	9.234	6.407	5.962
<i>15</i>	10.719	7.344	6.186